CIC bioGUNE

MEMBER OF BASQUE RESEARCH & TECHNOLOGY ALLIANCE

Neddylation in Schwann cell myelination

Miguel Tamayo Caro

2022

UPV/EHU

Neddylation in Schwann cell myelination

Miguel Tamayo Caro

2022

Neddylation in Schwann cell myelination

Miguel Tamayo Caro

2022

eman ta zabal zazu

Universidad del País Vasco

Euskal Herriko Unibertsitatea

Neddylation in Schwann cell myelination

eman ta zabal zazu

Universidad del País Vasco
Euskal Herriko Unibertsitatea

Departamento de Neurociencias

Neddylation in Schwann cell myelination

MIGUEL TAMAYO CARO

Supervisors : Ashwin Woodhoo, Amanda Sierra

2022

The studies included in this PhD thesis were supported by the MCIU/AEI/FEDER, EU (Subprograma Ramon y Cajal RYC2010-06901; Proyectos Retos Investigacion RTI2018-097503-B-I00, SAF2015-65360-R; Proyectos Explora Ciencia SAF2015-72416-EXP; Proyectos Europa Excelencia SAF2015-62588-ERC), and the BBVA foundation.

Miguel Tamayo was supported by a FPI fellowship from the Spanish Ministry of Science and Innovation (MICINN) (BES-2016-078493)

TABLE OF CONTENTS

LIST OF FIGURES AND TABLES

FIGURES

TABLES

ABBREVIATIONS

- **4E-BP** Eukaryotic translation initiation factor 4E-Binding Protein 1
- **A/A** Antibiotic/Antimitotic
- **AA** Ascorbic Acid
- **Aβ** amyloid β
- **ACE** Angiotensin converting enzyme
- **AIDP** Acute Inflammatory Demyelinating Polyradiculoneuropathy
- **Akt** Protein Kinase B (**PKB**)
- **ALS** Amyotrophic Lateral Sclerosis
- **AMAN** Acute axonal motor neuropathy
- **AMP** Adenosin Mono Phosphate
- **AMPK** AMP-activated kinase
- **AMSAN** Acute motor sensory axonal polyneuropathy
- **APC/C** Anaphase Promoting Complex/Cyclosome
- **APP** Amyloid Precursor Protein
- **APP-BP1** Amyloid Precursor Protein
- binding protein 1
- **APP receptor** Amyloid Precursor Protein receptor
- **ASH1** Achaete-Scute Homologue
- **ATG12** Autophagy related 12
- **ATG8** Autophagy related 8
- **ATP** adenosine triphosphate
- **BACE** β-Site amyloid precursor protein cleaving enzyme 1
- **BCA3** breast cancer-associated gene 3
- **BFABP** Brain fatty acid-binding protein
- **BNDF** Brain Derived Neurotrophic Factor
- **BSA** Bovine Serum Albumin
- **c-CBL** casitas b-lineage lymphoma
- **Cadm3** Cell Adhesion Molecule 3
- **cAMP** cyclic Adenosine Monophosphate
- **CAND1** Cullin Associated And Neddylation Dissociated 1
- **c-CBL** casitas b-lineage lymphoma
- **CDC** Center for Disease Control and prevention.
- **Cdc53** Cyclin-Dependent Kinase 53
- **Cdkn1c** cyclin-dependent kinase inhibitor 1
- **cDNA** cyclic desoxirribonucleic acid
- **CHM** Charcot-Marie Tooth disease
- **CHX** Cycloheximide
- **CIPD** Chronic inflammatory demyelinating polyneuropathy
- **cKO** conditional Knock Out
- **CMAP** Compound Muscle Action Potentials
- **CMT1A** Charcot-Marie-Tooth disease 1A
- **CMT1B** Charcot-Marie-Tooth disease 1B
- **CMT1A** Charcot-Marie Tooth disease type 1 A
- **CNS** Central Nervous System
- **CNTF** Ciliary Neurotrophic Factor
- **COP9** Constitutive Photomorphogenesis 9, zinc metalloprotease
- **COX-2** cyclooxygenase-2
- **CREB** cAMP Response Element
- **CRLs** Cullin Ring Ligases
- **CSF** Cerebro Spinal Fluid
- **CSF-1** Colony Stimulating Factor-1
- **Cthrc1** Collagen Triple Helix Repeat Containing 1
- **Cx32**Connexin32
- **DAMPS** Damage-Associated Molecules Patterns
- ***Dhh*** Desert hedgehog
- **Dixdc1** DIX domain containing-1 protein
- **Dlg1** Disks Large Homolog 1
- DMEM
- **Dock7** Dedicator of Cytokinesis 7
- **DUBs** Deubiquitinating Enzymes
- **Dusp15** Dual specificity phosphatase 1
- **EDTA** Ethylenediaminetetraacetic acid
- **EdU** 5-ethynyl-2'-deoxyuridine
- **EGF** Epidermal Growth Factor
- **EGFR** Epidermal Growth Factor Receptor
- **EGR2** Early Growth Response 2 also know as **Krox-20**
- **EM** Electromicroscopy
- **ENS** Enteric Nervous System
- **EPAC** Exchange Protein Activated by cAMP

- **EPL** Experimental Paw Length
- **ER** Endoplasmic Reticulum
- **ERK** Extracellular signal-Regulated Kinases
- **ETS** Experimental Toe Spread
- **EZH2** Enhancer of zeste homolog 2
- **FA** Fatty Acid
- **FBS** Fetal Bovine Serum
- **FBXO1** Cyclin F
- **Fbxw7** F-Box And WD Repeat Domain Containing 7
- **Fig** Figure
- **fLAS** familiar Amyotrophic Lateral Sclerosis
- **FMR1** Fragile X Mental Retardation 1
- **FTD** frontotemporal dementia
- **FUS** Fused in Sarcoma
- **FXTAS** Fragile X associated tremor/ataxia syndrome
- **GalC** Galactosylceramidase
- **GAP43** Growth Associated Protein 43
- **GBS** Guillain-Barré-Strohl Syndrome
- **GDNF** Glial cell line Derived Neurotrophic Factor
- **GFAP** Glial Fibrillary Acidic Protein
- **GM1** Ganglioside type I
- **GD1a** Ganglioside type 1a
- **GPCRs** G protein-Coupled Receptors
- **gpr126** G protein-coupled receptor 126
- **HDAC1/2** Histone Deacetylases 1 and 2
- **HECK293T** Human embryonic kidney 293 cells expressing SV40 large T antigen
- **HECT** Homologous to E6-AP Carboxyl Terminus class, E3 ligases.
- **Hif1a** Hypoxia-inducible factor 1-alpha
- High levels of antibodies to GM1, GD1a, and other gangliosides
- **HIV** Human Immunodeficiency Virus
- **HMG-box** High Mobility Group Box. Family of proteins.
- **HMN** hereditary motor neuropathy
- **HNPP** Hereditary Neuropathy with Pressure Palsies
- **HuR** Human antigen R
- **IgG** Inmunoglobulin G
- **iHSCλ2** Immortalized normal human Schwann cell line λ2
- ***ic*KO** Inducible constitutive Knock Out
- **IL-6** Interleukin 6
- **IMCD3** Inner medullary collecting duct cell line 3
- **IPL** Interperiod Lines
- **ISC** Inmature Schwann cells
- **ISG15,**
- **IVIg** Intravenous immunoglobulin
- **LIF** Leukemia Inhibitory Factor
- **LIMK1** LIM domain kinase 1
- **LPA1** Lysophosphatidic Acid receptor 1
- **LTD** Long-Term Depression
- **LTP** Long-Term Potentiation
- **LXR** Liver X Receptor
- **MAG** Myelin associated glycoprotein
- **MAPK** mitogen-activated protein kinase. Family of proteins.
- **MBP** Myelin Basic Protein
- **MCP-1** Monocyte Chemoattractant Protein-
- **MDL** Mayor Dense Lines
- **Mdm2** Murine Double Minute 2
- **MEK** Mitogen-activated protein kinase kinase
- **MFN1** mitofusin 1
- **MIAT, CCDC163P, ZNF266, and GPR15. GPR15**
- **MIB1** ubiquitin Mind Bomb 1 ligase
- **MKK7** Dual specificity mitogen-activated protein kinase kinase 7
- **Mam** Mastermind
- **MMN** Multifocal Motor Neuropathy
- **MPZ** or **P0** Myelin Protein Zero
- **MTHFR** methylenetetrahydrofolate reductase
- **mTOR** mechanistic target of rapamycin
- **mTORC1** mTOR complex 1
- **mTORC2** mTOR complex 2
- **NB** New Born
- **N-CAM** Neural cell adhesion molecule
- **NADH and FADH2**
- **Nae1** Nedd8-activating enzyme 1
- **NCV** nerve conduction velocity
- **NTS** Normal Toe Spread
- **Nedd8** neural precursor cell-expressed, developmentally downregulated 8
- **Nedp1** Nedd8-specific Protease 1
- **NF-kB** Nuclear Factor kappa-light-chain-enhancer of activated B cells
- **NFATc4** Nuclear Factor Of Activated T Cells 4

- **NGF** Nerve Growth Factor
- **NGS** New Generation Sequencing
- **NPL** Normal Paw Length
- **NICD** Notch Intracellular Domain
- **NOS** Nitric Oxide Synthase
- **NRG1** Neuregulin1
- **NSAIDs** Non-steroidal anti-inflammatory drugs
- **NT3** Neurotrophin-3
- **OCT6** Pou3F1
- **olig 1** oligodendrocyte transcription factor
- **OTUs** ovarian tumor superfamily of ubiquitin isopeptidases.
- **OXPHOS** Mitochondrial Oxidative Phosphorylation System
- **P *(n)*** Postnatal day (*n)*
- **PDL** Poly-D-Lysine
- **p70S6K** ribosomal protein S6 kinase beta-1
- **p75 NTR**
- **PAMPS** Pathogen-Associated Molecular Patterns
- **PARC** Parkin E3 ubiquitin ligase
- **PBS** Phosphate Buffered Saline
- **PI3K** Phosphoinositide 3-Kinases
- **PKA** Protein inase A
- **PlGF** Placental Growth Factor
- **PLP** Proteolipid Protein
- **PMP22** peripheral myelin protein 22
- **PNS** peripeheral nervous system
- **PTLDS** Post Treatment Lyme Disease Syndrome
- **PTM** Post Translational Modification
- **pVHL** von Hippel landau
- **Rbx1** Ring-box protein 1
- **Rbx2** Ring-box protein 2
- **RGCs** Retinal Gnaglion Cells
- **RING** really interesting new gene finger domain-containing class, E3 ligases.
- **ROS** Reactive Oxygen Species
- **S6K1** Ribosomal protein S6 Kinase beta-1
- **sALS** sporadic Amyotrophic Lateral Sclerosis
- **Sam68** Src-associated in mitosis of 68 kD
- **SC** Schwann cells
- **SCF** Skp1-Cullin-F box protein
- **SCP** Schwann cell precursors
- **SFI** Sciatic Functional Index
- **SFN** Small Fiber Neuropathies
- ***Shh*** Sonic hedgehog
- **SLI** Schmidt-Lanterman Incisures
- **SMURF1** Smad ubiquitination regulatory factor.
- **SNRIs** Noradrenaline Reuptake Inhibitors
- **SOX2** (also know as SRY-Box2) Sex determining Region Y-box 2
- **SSeCKS** Src-suppressed Protein Kinase C Substrate
- **SSRIs** Serotonin Reuptake Inhibitors
- **SUMO** Small Ubiquitin-like Modifier
- **Sup** Supplementary
- **T1DM** Type 1 Diabetes Mellitus
- **T2DM** Type 2 Diabetes Mellitus
- **TACE** Tumor Necrosis Factor-α–converting, also known as ADAM17
- **TAZ** Tafazzin
- **TCA** tricarboxylic acid cycle
- **TCAs** Tricyclic Antidepressants
- **TDP1** Tyrosyl DNA Phosphodiesterase-1
- **TDP43** TAR-DNA binding protein 43
- **TEM** Transmission Electron Microscope
- **TGF ß** Transforming Growth Factor ß
- **TIMS** Time of flight Mass Spectrometer
- **TLR** Toll-like Receptor
- **TNF** Tumoral Necrosis Factor
- **TNF-α** Tumor Necrosis Factor-alpha
- **TRIF** TIR-domain-containing adapter-inducing interferon-β
- **uba3** ubiquitin-activating enzyme 3
- **UBE2M** NEDD8-conjugating enzyme, also called UBC12
- **UBLs** Ubiquitin-Like proteins
- **UCH** Ubiquitin C- terminal Hydrolases
- **UFM1**
- **ULPs** UBL-specific Proteases
- **URM1** Ubiquitin-related modifier-1
- **USP** Ubiquitin-Specific Proteases
- **UTR** Untranslated Region
- **VEGF** Vascular Endothelial Growth Factor
- **WD** Wallerian Degeneration
- **YAP** yes-associated protein 1
- **YY1** Ying Yang
- **Zeb2** Zinc finger E-box-binding homeobox 2
-

1 SUMMARY/RESUMEN

1 SUMMARY

Schwann cells (SCs) are the main glial cells in the peripheral nervous system. The main function of these glial cells is to produce the myelin sheets that isolate neurons and improve the nerve conduction velocity. This activity is vital for the correct functioning of the nervous system. Schwann cells also provide trophic and metabolic support to the neurons.

Over the last few years, there has been an explosion in studies aimed at identifying the signals and molecules that drive the Schwann cell phenotype during development and in disease situations. Thus, Schwann cell myelination has been shown to be regulated by several extrinsic and intrinsic signals, including neuregulin (NRG) type III, laminin, and mTOR amongst others. In addition, a complex transcriptional and epigenetic regulatory program has been uncovered, with key roles described for master transcription factors such Egr2, Sox10 and Zeb2 in positively regulating the myelinating phenotype. This process is opposed by negative regulators of myelination, including Notch, Sox2, mTOR and c-Jun signaling pathways that are downregulated during myelinogenesis.

Post-translational mechanisms, on the other hand, have barely been studied, even though these modifications can fine-tune the interactions, trafficking, stability, localization and activity of proteins, which could have a key role in the dynamic processes of myelin formation and breakdown. Neddylation, a ubiquitylation-like pathway that conjugates a ubiquitin-like protein NEDD8 to target proteins, has emerged as a critical regulatory process controlling ubiquitination, protein transcription and signaling transduction. Dysregulation of neddylation has been linked to a broad spectrum of pathological conditions ranging from tumorigenesis to neurodegeneration. So far, its role in Schwann cell development and function has not been examined.

In this thesis, we have found that neddylation is a critical regulator of Schwann cell myelination. We found that genetic ablation of Nae 1 (Nae1 cKO), a key enzyme in the neddylation pathway, in Schwann cells, led to striking defects in peripheral nerves that had all the hallmarks of a severe neuropathy. The conditional knockout mice developed gait abnormalities, muscle weakness, and hindlimb clasping, a typical presentation of neuromuscular dysfunction very early after birth, and most mice did not survive past three weeks of age. In neurophysiological tests, we recorded a severe reduction in nerve conduction velocity (NCV) in Nae1 cKO compared to control mice. Strikingly, electron microscopy (EM) revealed that Nae1-

deficient mice lacked peripheral myelination and exhibited active myelin breakdown of the few formed myelin sheaths. This lack of myelin was accompanied by an absence of the myelin structural proteins, and the master myelination transcriptional regulator Egr2.

We found widespread changes in the transcriptomic and proteomic profile of Nae1 cKO nerves. Notably, we found an upregulation of the negative regulator of myelination c-Jun, and that neddylation via regulation of the activity of Cullin Ring Ligases (CRL), E3 ubiquitin ligases that control the stability of numerous proteins, was responsible for regulating protein expression of c-Jun during myelination.

On the other hand, using a tamoxifen-inducible Nae1 knockout model, we did not find any robust role of neddylation for the maintenance of mature myelin sheaths, and in pilot studies, on the regeneration of nerves after nerve injury.

In summary, we found that neddylation is a critical regulator of the Schwann cell myelination and that one of the key mechanisms behind its biological function is the regulation of expression of negative regulators of myelination.

1 RESUMEN

Las células de Schwann son las celulares gliales más abundantes del sistema nervioso periférico. Su principal función es sintetizar y mantener las vainas de mielina que aíslan las neuronas y mejoran la velocidad de transmisión del impulso nervioso. Esta actividad es vital para el correcto funcionamiento del sistema nervioso pero no es la única función de las células de Schwann, ya que también dan soporte trófico y metabólico a las neuronas.

En el transcurso de los últimos años, ha habido un gran incremento en el número de investigaciones con el objetivo de identificar señales y moléculas que regulan el fenotipo de las células de Schwann durante el desarrollo embrionario y diferentes procesos patológicos. Se ha demostrado de esta forma que la mielinización de las células de Schwann es un proceso regulado por diferentes señales intrínsecas y extrínsecas, entre las que se incluyen Neuroregulina (NRG) tipo III, laminina y la ruta mTOR. Además, ha sido descubierta una compleja red de regulación transcripcional y epigenética, donde tienen un significativo papel reguladores transcripcionales como Egr2, Sox10 y Zeb2 que actúan regulando positivamente la mielinización. Por otro lado, reguladores como Notch, Sox2, mTOR y c-Jun, también llamados reguladores negativos de la mielinización, tienen un papel opuesto, des-regulando el proceso de mielinogenesis.

Por otra parte, las modificaciones postraduccionales, que a día de hoy aún han sido poco investigadas, pueden modificar minuciosamente interacciones, el tráfico celular, la estabilidad, la localización celular y la actividad de muchas proteínas que podrían participar en procesos celulares dinámicos como la síntesis y degradación de la mielina. La neddilación, una modificación postraduccional similar a la ubiquitina que conjuga la “ubiquitin like protein” (UBL) Nedd8 a proteínas diana, ha emergido como un importante mecanismo regulatorio que controla la ubiquitinación, traducción de proteínas y diferentes rutas de señalización. La desregulación de la neddilación ha sido vinculada con un amplio espectro de condiciones patológicas que van desde la tumorigenesis a la neurodegeneración. Hasta ahora, su papel en el desarrollo y función en las células de Schwann no ha sido descrito.

En esta tesis, hemos descrito que la neddilación participa en la regulación de la mielinización en células de Schwann. El silenciamiento genético específico de células de Schwann de la proteína Nae1 (Nae1 cKO), la enzima que inicia la cascada de neddilación, produjo sorprendentes defectos en los nervios periféricos similares a los observados en algunas neuropatías graves. Estos ratones “Knock Out” condicionales desarrollaron problemas de

movilidad, debilidad muscular y el comportamiento de “hindlimb clasping”, una manifestación de disfunción neuromuscular, en edades muy tempranas. Estas manifestaciones también iban acompañadas de una muerte prematura en torno a las 3-4 semanas de edad. Posteriormente realizamos un test neurofisiológico en el que registramos una gran reducción en la velocidad de conductividad nerviosa (NCV) en los ratones Nae1-cKO respecto a los ratones control. Sorprendentemente, las imágenes que tomamos de microscopía electrónica en muestras de ratones Nae1 cKO mostraban la ausencia de axones mielinizados en los nervios periféricos y multitud de anomalías en la mielinización. Además, el reducido número de vainas de mielina presentes en los nervios periféricos se encontraban en proceso de degradación. Esta carencia casi total de mielina estaba acompañada de la ausencia de proteína básica de mielina (MPZ) y del regulador transcripcional de la mielinización Egr2 (también llamado Krox-20).

Para profundizar en el análisis del fenotipo de nuestros ratones Nae1 cKO realizamos un estudio transcriptómico y proteómico en el que encontramos profundos cambios en comparación con los ratones control. Sorprendentemente, encontramos una sobrexpresión del regulador negativo de la mielinización c-Jun. También pudimos describir que la neddilación a través de la regulación de la actividad de las Cullin Ring Ligasas (CRL), es capaz de actuar sobre la estabilidad de numerosas proteínas, así como regular la expresión de c-Jun durante la mielinización.

En resumen, hemos determinado que la neddilación es clave en la regulación de la mielinización en las células de Schwann y que uno de los mecanismos clave detrás de este proceso es la regulación de la expresión de reguladores negativos de la mielinización.

2 INTRODUCTION

2 INTRODUCTION

2.1 PERIPHERAL NERVOUS SYSTEM

The vertebrate nervous system consists of the peripheral nervous system (PNS) and central nervous system (CNS), which in turn, is formed by the brain and spinal cord. The PNS connects the CNS to the rest of organs and limbs, coordinating body functions. It is composed of several components, including motor, sensory, and autonomic neurons, their afferent and efferent axons and connective tissue components (endoneurium, perineurium, epineurium, blood and lymphatic vessels)[1] . Nerves contain different types of cells including neurons and non-neuronal cells, named glial cells, constituting the vast majority of PNS cells, in addition of macrophages and fibroblast, among other cell types.

Schwann cells, named after the physiologist Theodor Schwann, are the main glial cells in the PNS. Two different types of mature Schwann cells exist in adult nerves: non-myelin Schwann cells, also known as Remak Schwann cells (named after embryologist Robert Remak) and myelinating Schwann cells. Schwann cells play key roles in the peripheral nervous system, including the elaboration of myelin sheaths that allow saltatory nerve impulse transmission. They are also important for axonal trophic and metabolic support, and can support axonal regeneration after a nerve insult[2].

In addition to myelinating and non-myelinating Schwann cells, there are different types of glial cells in the PNS [3,4]:

Satellite glia. They are associated directly with neuronal cell bodies in sympathetic, parasympathetic and sensory ganglia

Boundary cap cells participate in the formation of the boundary between the central nervous system and the peripheral nervous system[5].

Terminal (or perisynaptic) **Schwann cells**. They maintain the stability of neuromuscular junction and help reinnervation after injury

Enteric glial cells. They can be found in the autonomic ganglia in the gut.

Olfactory ensheathing cells. They are called olfactory Schwann cells, because they ensheath the non-myelinated axons of olfactory neurons, similar to Remak cells in PNS.

2.1.1 The Schwann cell lineage

2.1.1.1 Schwann cell precursors

Adult differentiated Schwann cells are derived from neural crest cells, a group of multipotent cells that arise from neural tube dorsal side. The first stage in Schwann cell development is the differentiation of neural crest cells into Schwann cell precursors (SCPs) between day E12/E13 of embryo development in mice (E14/E15 in rats) [6]. The regulation of this transition is still poorly known. SCPs are highly multipotent and can differentiate into many different cell types, including neurons, fibroblast, chromaffin cells, melanoblast, odontoblast and immature Schwann cells (ISCs).

SCPs are strictly dependent on axonal signals for their survival and further differentiation. Thus, when SCPs are isolated from embryonic nerves and cultured in vitro in the absence of axons, they survive poorly. Nonetheless, addition of growth factors to the culture medium, such as neuregulin1 (NRG1) can promote SCP survival, as well as promoting differentiation to iSCs [7].

The differentiation of neural crest cells to SCP leads to a profound change in gene expression profile with downregulation of some genes in SCP and a simultaneous upregulation of a three-fold number of genes[6]. Several genes such as the ones encoding for myelin basic protein (MBP), *Plp22*, *BFABP* and desert Hedgehog (*Dhh*) persist or are even up-regulated during the subsequent Schwann cell developmental stages[8].

2.1.1.2 Second embryonic stage: Immature Schwann cells (iSCs)

SCPs at embryo day E15/E16 mice (E17/E18) give rise to iSCs, which then differentiate to mature non-myelin (Remak) or myelinating Schwann cells after birth. ISCs associate with connective tissue and basal lamina, and do not depend on axons for survival, although axonal signals are required for their generation from SCP, as explained above. The transition of SCP to iSC is characterized by an upregulation of several genes, such as S100 and glial fibrillary acidic protein (GFAP), and the downregulation of SCP markers, including AP2, α4 integrin and N-cadherin[6]. The differentiation of SCP to iSCs is promoted by the Notch signaling pathway and negatively regulated by endothelins [9].

ISCs show a reduced migration capacity in comparison with SCPs but are more proliferative, reaching a peak in DNA synthesis just before birth. Proliferation of ISCs is controlled by a wide range of factors: axonal contact, NRG1, Notch, laminins expressed in basal lamina and transforming growth factorß (TGFß), among other signals[10]. Hippo and cAMP

pathways also contribute to the regulation of Schwann cell proliferation in developing nerves *in vivo*[11].

Supernumerary Schwann cells can undergo apoptosis during development, which is controlled mainly by TGF-β through interacts with TGF-β type II receptors. Nerve growth factor (NGF), acting through p75 ^{NTR} receptor, is not implicated in Schwann cell survival during development, although in injured nerves, NGF signaling can control Schwann cell death[12]. Apoptosis during development or during a nerve injury response can be inhibited by exogenous NRG1 addition[7].

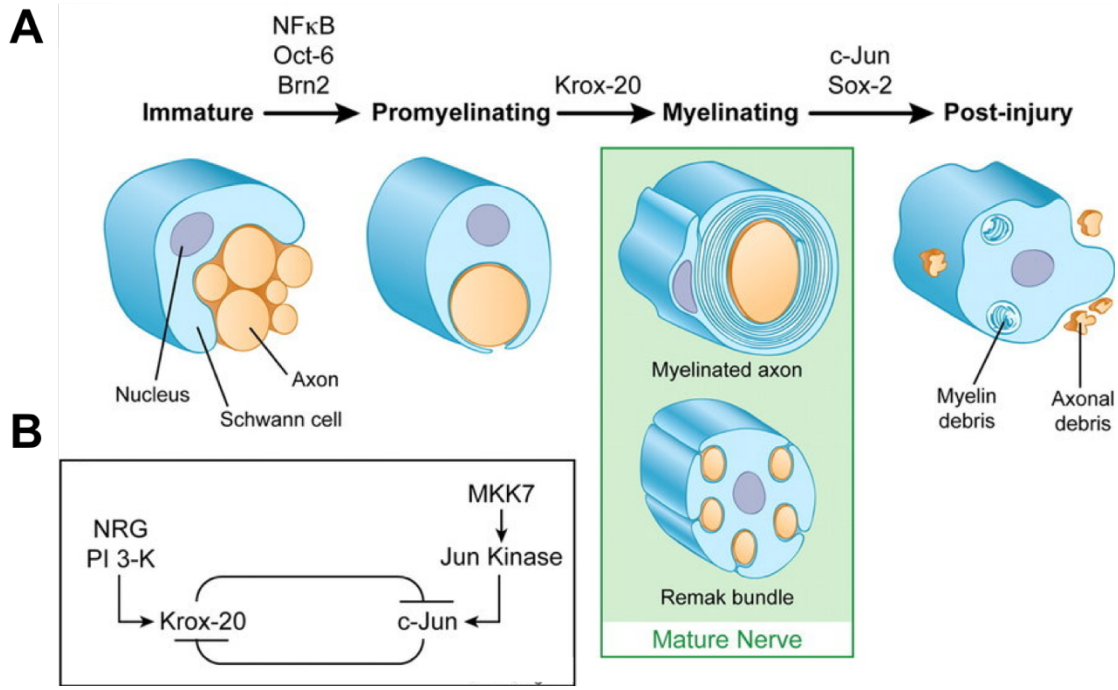

Figure 1. **Regulation of Schwann cell myelination and dedifferentiation**. **(A)** Schwann cell differentiation is regulated by expression of specific transcription factors including neuregulin 1 (NRG), NFκB, Oct-6, and Brn2. These transcription factors promote differentiation to the promyelinating stage, in which Schwann cells express early myelin markers. Krox-20 up-regulation is an essential requirement to form myelin sheaths and express myelin-specific proteins. After a peripheral nerve insult, c-Jun and Sox-2 are up-regulated and the differentiation of Schwann cells to repair Schwann cells, and the subsequent axonal regeneration. **(B)** Cross-inhibition of Krox-20 and c-Jun promotes a switch in transcriptional complexes. Promyelinating signals stimulate Krox-20 expression via the phosphatidylinositol 3-kinase pathway. JNK pathway is activated after a nerve injury promoting c-Jun expression. Salzer et al, 2008.

After birth, iSCs segregate larger diameter axons in a process commonly known as radial sorting and establish a 1:1 relationship with the large diameter axon. After radial sorting, these pro-myelinating Schwann cells differentiate to myelinating Schwann cells. Remak cells differentiate from iSCs and they can surround more than one small diameter axon (< 1µm). In

contrast to myelinating Schwann cells, Remak cells do not produce myelin sheets around the axons. The extracellular signals that control fate choice at this lineage stage are not well understood, although if a Remak Schwann cell is placed in contact with a large diameter axon rather than a smaller one, it would differentiate to a myelinating Schwann cell instead of a Remak Schwann cell[13].

Differentiated mature Schwann cell and iSCs are characterized by different antigenic profiles. iSCs destined to form myelin start to express Galactosylceramidase (GalC) shortly after iSC differentiation into mature Remak Schwann cells at around the third postnatal week. Furthermore, iSCs that differentiate to myelinating Schwann cells downregulate expression of GFAP, N-CAM and $p75^{NTR}$, among others[14].

Around the fifth week after birth in mice, mature Schwann cells become quiescent. However, Remak and myelinating Schwann cells are highly plastic cells[15]. They can undergo a switch in their phenotypic identity after injury, to convert to "repair Schwann cells", a specific Schwann cell phenotype essential for axonal regeneration[2].

2.2 REPAIR SCHWANN CELLS IN WALLERIAN DEGENERATION

After peripheral nerve injury, mature Schwann cells that lose axonal contact and transdifferentiate to give rise to repair Schwann cells (as mentioned above), also known as Bungner cells, in a process referred to as Wallerian degeneration[16]. Although axonal degeneration after a nerve injury is observed after 2-4 days, activation of Schwann cells can be observed earlier, even hours after injury, through mechanism that are still poorly known.

The conversion to repair Schwann cells was commonly described as a dedifferentiation process where the adult denervated cells revert to an earlier stage similar to those of iSCs, re-expressing genes of iSC phenotype. However, it was recently demonstrated that repair Schwann cells are different in structure, molecular profile and function than iSC[17]. Furthermore, oligodendrocyte transcription factor 1 (*Olig 1*) and sonic hedgehog (*Shh*) genes, which are upregulated in repair Schwann cells distinguishes them from other cells of the Schwann cell lineage, which do not express them[13]. These results suggest that repair Schwann cell phenotype is a specific and transitory stage. This repair response after a nerve insult is controlled by several factors, such as the Notch signaling pathway and the c-Jun transcription factor [18,19].

During this process of Wallerian degeneration, Schwann cells are able to digest themselves part of their myelin sheaths, by a specialized form of autophagy, called myelinophagy[20]. The denervated cells stimulate cytokines expression, including Tumoral Necrosis Factor (TNF), IL-6 and IL-1ß, which promote the recruitment and activation of macrophages[21] to help Schwann cells in myelin breakdown. Schwann cells digest around 40% of the myelin while macrophages deal with the 60%[20]. Some cytokines secreted [Interleukin 1ß (IL-1ß), Ciliary Neurotrophic Factor (CNTF), Leukemia Inhibitory Factor (LIF) and Interleukin 6 (IL-6)] can also act directly on neurons, promoting axonal regeneration[22].

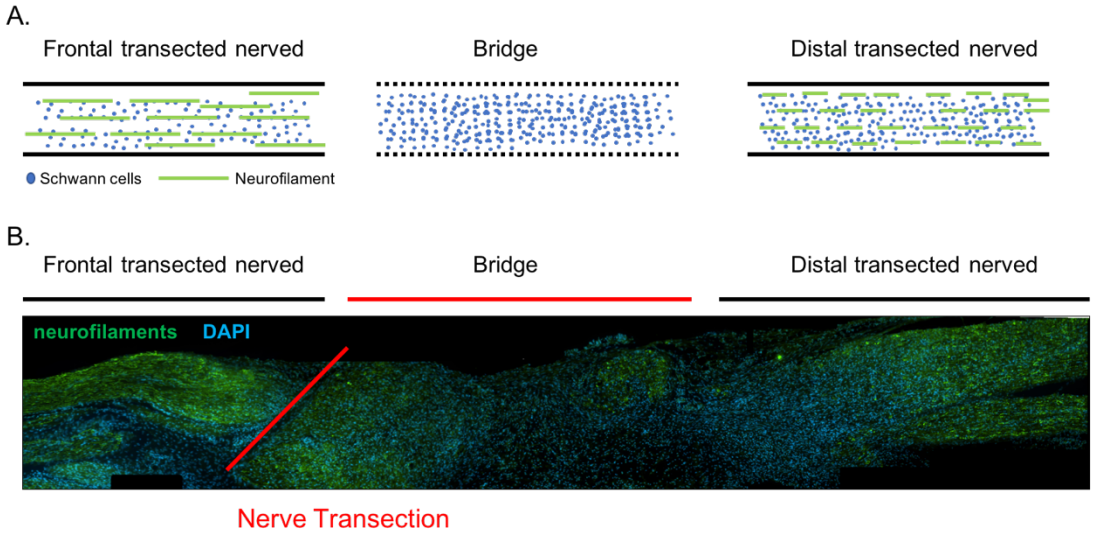

Figure 2. Bridge formation after a nerve injury. **A)** Schematic diagram depicting neurofilament structure in the frontal and distal sections of a transected nerve. **B)** Picture of a transected sciatic nerve from a WT mouse showing how Schwann cells proliferate in the bridge to repair the injury and help proximal axons to reach the distal section of the nerve. Proliferation is increased in the bridge and distal nerve. Neurofilaments in the proximal section maintain their structure but are degraded in the distal section.

Once the axons regrow through the distal injured nerve and reconnect to their target organs (**Figure 2**), the repair Schwann cells associate with these axons and undergo remyelination, which is needed for a complete axonal regeneration. Several factors regulate this process, including extracellular matrix molecules (laminins, dystroglycans), cell adhesion molecules (N-cadherin, NCAM)[23], neurotrophic factors and receptors [BNDF, p75 NTR, Tropomyosin receptor kinase B (trkB)][24,25] intracellular regulators (e.g. P13K/AKT signaling pathway), hormones (progesterone, thyroid hormone)[26] and diverse microRNAs[27]. The success of remyelination after a nerve injury depends on transcription factors which are activated during the early steps of the regeneration and then downregulated to initiate remyelination[13]. Transcription factors, such as c-Jun and Sox2, which are negative regulators of myelination, can

impair the full recovery of the injury if their levels are maintained for a prolonged time during this process[28].

Repair and mature Schwann cells differ not only in their gene expression profile, but also in morphology. Repair Schwann cells are more elongated than myelin or Remak Schwann cells[29], and produce the regeneration tracks that connect the proximal stump with the distal part of the injured nerve. After reinnervation of target organs, Schwann cells re-establish a 1:1 relationship with the axons and remyelinate them. However, the newly synthetized myelin sheaths are thinner and the internodes are usually shorter than in normal nerves [29]. During Wallerian degeneration, the number of Schwann cells is increased due the activation of proliferation although inhibition of proliferation does not affect nerve regeneration, suggesting proliferation is not essential for axonal regeneration[30].

2.3 MYELINATION

2.3.1 Role of Myelination

Myelination is an indispensable process that takes place in both central and peripheral nervous system after birth and continue during the rest of the life. Myelin sheaths are important not only for accelerating action potential conduction but also because they provide trophic and metabolic support to axons[31].

Myelinating Schwann cells insulate a unique axon, extending around the axonal segment and leaving a non-myelinated space from one myelin sheath to another, regions known as Nodes of Ranvier nodes (named after their discovery in 1877 by Louis-Antonie Ranvier. In myelinated axons, the nerve impulses travel through one ranvier node to the next, which is essential for the rapid saltatory impulse of action potential, discovered in 1939 by Tasaki[32].

Myelin formation starts with the radial sorting of large diameter axons (>1µm) by iSCs to give rise to pro-myelinating Schwann cells, which then differentiate to myelinating Schwann cells. Axonal signals, such as NRG1 type III which is associated with axonal membranes [33], promote axonal wrapping (Figure 1). This process is characterized by the nuclear circumnavigation of the axon by the Schwann cells, with the plasma membrane expanding about 20 mm^2 in order to form the myelin sheath[34].

Profound gene expression changes occur during the myelination process, characterized by an upregulation of myelin related genes (MBP, MPZ, periaxin, MAG, etc.) together with the downregulation of some iSC markers, including NCAM, GFAP and $p75^{NTR}$. Several pro-myelinating transcription factors regulate myelination, including NF-KB, Pou3f1 (Oct6), Pou3f2

(BRN2), NFATc4, YY1 (Ying Yang), and Krox-20 (EGR2)[35–37]. Moreover, sterol regulation element binding proteins (SREBP) induce lipid biosynthesis necessary for myelin sheath[38].

Myelination is also regulated by epigenetic modifications, including DNA methylation, posttranslational modification of nucleosomal histones[39], and noncoding RNAs, including micro RNAs (miRNAs)[27,40].

2.3.2 Myelinated fiber structure

Myelinating Schwann cells are longitudinally and radially polarized cells, organized into distinct domains. Longitudinal polarity is demonstrated by the organization into nodal, paranodal, juxtaparanodal, and internodal compartments of myelinated axon[41]. Radial polarity is confirmed by the presence of different membranes, which are present at each end of the cell on opposite sides: the inner membrane is the adaxonal and the outer membrane is called abaxonal. The compact part of the myelin sheath is found between these membranes surfaces[34]. Initially, Schwann cells start surrounding axons and bring together the two sides of its plasma membrane, a region known as inner mesaxon. The mesaxon elongates to create a spiral around the axon that continues winding to increase the number of spiral layers (myelin lamellae) (Figure 3).

While myelin lamellae are being formed, the mesaxon starts condensating due the interaction between myelin related proteins, such as MPZ, forming compact myelin. The adaxonal membrane is separated from the plasma membrane (axolemma) by a space about 15 nm. It is enriched in adhesion molecules and receptors that mediate interaction with axonal ligands. The abaxonal membrane interacts with laminin from basal lamina via integrins, such as a6ß1-integrin, a6ß4-integrin and ß dystroglycan. This outer surface is interrupted by periodic appositions that delineate several cytoplasmic channels called Cajal Bands[34]. These channels provide a conduit to transport the RNA and proteins formed in cell soma. Basal lamina wraps around the Schwann cell plasma membrane, surrounding the whole axon-Schwann cell unit.

Myelin sheaths are composed of around 40 or more lamellae. The internode, located between two nodes of Ranvier, is the largest longitudinal part of the Schwann cell (about 99% of the total Schwann cell length) extending out to 2mm. It consists of compact and non-compact myelin, name proposed by German pathologist Rudolf Ludwig Virchow. Electron micrographs show compact myelin as a structure with light and dark lines. Mayor dense lines (MDL) are about 2.5nm thick and are formed by two cytoplasmic lipid bilayers that are separated from each other by extracellular light interperiod lines (IPL)[34].

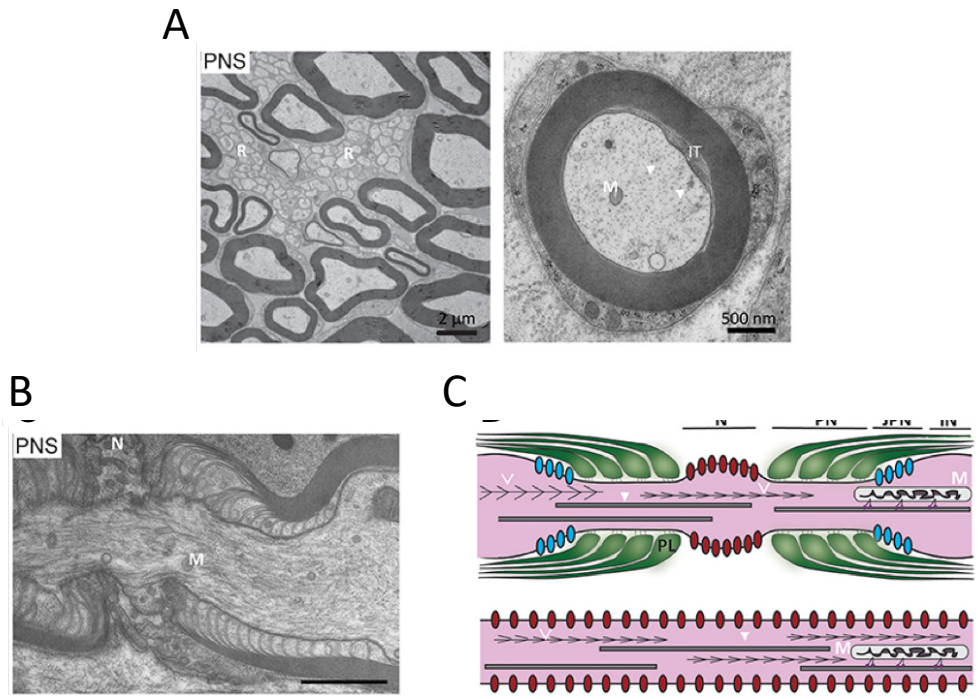

Figure 3. Ultrastructure of PNS myelinated axons. (**A**) EM pictures showing the ultrastructure of a peripheral nerve (PNS). Some axonal cytoskeletal elements and organelles are visible at high magnification: microtubules (arrows) and neurofilaments (arrow heads), mitochondria (M). In the PNS, myelinated fibers are separated by connective tissue. Schwann cells plasma membrane is covered by a basal lamina and small diameter axons, which are not myelinated, are surrounded by Remak cells and organized in Remak bundles (R). (**B**) Electron micrograph showing a node of Ranvier in the PNS. (**C**) Schematic representation of the different elements that can be found in a Ranvier node: paranodal loops of the myelin sheath (green), mitochondria (M), Nav1.6 channels (red), Kv1 channels (blue), microtubules (open arrow heads) and neurofilaments (arrowheads). The node of Ranvier includes different regions: Node (N), paranode (PN), juxtaparanode (JPN) and internode (IN). The picture below represents a non-myelinated axon, showing a uniform distribution of Nav1.6 channels along the axolemma characteristic of these fibers. Adapted from Stassart et al.[43].

Compact myelin is interrupted by Schmidt-Lanterman incisures (SLI) from the adaxonal to the abaxonal membrane, which form non-compact myelin[42]. SLI generate a Schwann cell cytoplasm network throughout the compact myelin allowing intracellular communication. SLI are observed once myelin is formed, so its late origin suggest that they are not essential for myelin formation but may serve in myelin maintenance. Adherens, gap and tight junctions are found in SLI and they also contribute to connect the different parts of the Schwann cell[43,44]. Cajal bands are located perpendicular to SLI. Axons and Schwann cells contact directly at the paranodal regions in nodes of Ranvier through septate-like junctions. The juxtaparanodes are small areas located between the paranodal junction and the internode that contain voltage-sensitive potassium channels, which play a role in repolarization, maintenance of resting potential and prevention of ectopic impulses[45].

In unmyelinated axons, nerve impulse is propagated by local circuits of ion current channels from the active region of axonal membranes throughout the axon to the adjacent sections[46]. On the other hand, in myelinated fibers, the action potential flows from an excitable part of the membrane, which correspond to the node of Ranvier, to the next node of Ranvier, in a high saltatory velocity.

2.3.3 Myelin composition

Myelin content is divided into a liquid part of about 40 % of water and 60 % of dry mass, which it´s composed of 75% lipids and a low proportion of proteins (about 20%). The main lipids found in myelin are glycosphingolipid, saturated long chain fatty acids and cholesterol. One of the biochemical characteristics that distinguish myelin from other biological membranes is its high lipid content, 2 to 5 times higher than the protein content, which contributes to the insulating properties of the myelin internode. Although there are no myelin specific lipids, the ratio of cholesterol, phospholipids and glycosphingolipids in most membranes is about 25%:65%:10%, whereas in the myelin sheath it represents a range of 40%:40%:20%. This PNS lipid content varies quantitatively from one species to another[47]. Furthermore, PNS and CNS myelin present similar lipid content with quantitative differences. PNS myelin has considerably more sphingomyelin, accounting for 10-35% of the total lipids, but less cerebroside and sulfatide than CNS myelin. A characteristic difference between PNS and CNS myelin is the presence of sialyl-lactone tetrosyl ceramide also known as ganglioside LM1. Cholesterol is essential for the formation and maintenance of myelin and represents about 28% of myelin dry mass. The glycolipids GalC and galactosulfatide are involved in myelin stability and are required for node and paranode formation[48]. Oleic acid is the major fatty acid of PNS, representing about 30-40% of fatty acids in sciatic nerves.

Some proteins of PNS are shared with CNS, whereas others are unique. Myelin Protein Zero (MPZ or P_0) is the major protein in PNS, accounting for more that the half of the myelin protein composition. It is exclusively synthetized by Schwann cells. In addition to MPZ glycoprotein, compact myelin also contains PMP22, which represents about 5% of total protein amount and it is thought to control myelin thickness. MBP accounts for 5 to 18% of the protein content (in contrast to CNS, where it accounts for about 30% of total proteins)[49]. Moreover, four different isoforms have been found in either CNS or PNS. MBP, together with MPZ, contribute to the formation and compaction of Mayor Dense lines (MDL). Myelin associated glycoprotein (MAG) is found in non-compact myelin, including SLI. P_2 is a protein found in the PNS which seems to be involved in lipid assembly or turnover in myelin sheath[50]. Other proteins expressed in PNS myelin include proteolipid protein (PLP)[51], which is the major protein in CNS.

2.3.4 Regulation of myelination

Myelination is a process tightly regulated by major signaling pathways, including mTOR, Wnt or MAP kinases, transcription factors, including EGR2 or Zeb2 and receptors associated to G proteins, such as GPR136, and ErbB2/3. Below, the role of different regulators of myelination will be described, classified as: receptors, transcription factors, signaling pathways and other regulators, and their specific roles during development and during the response to a nerve insult discussed.

2.3.4.1 Receptors

2.3.4.1.1 NRG1/ErbB2/3 – Development

One of most important signaling pathways that regulate the interaction of axons with Schwann cells is the NRG1/ErbB2/3 pathway. NRG1 comprises a family of transmembrane and secreted proteins that are encoded by four genes (NRG1-4), in which NRG1 is the best characterized. Six different proteins of NRG1 have been described (types I-VI) with at least 31 isoforms[7], which differ in the amino-terminal region. Each NRG1 has an extracellular domain containing two extracellular cysteine-rich regions, a transmembrane domain, a short intracellular juxtamembrane region, a tyrosine kinase domain and a carboxy-terminal tail. All of them share an epidermal growth factor (EGF)-like signaling domain located in the extracellular region.

The expression pattern of the isoforms differs in different tissues. Types I–III are the most common NRG1, with type III being the most abundant in peripheral axons. NRG1 stimulates transmembrane tyrosine kinases called ErbB receptors. NRG1 promotes ErbB dimerization and activates the ErbB kinase domain, which results in auto- and trans-phosphorylation of the intracellular domains. This ErbB activation results in the activation of several pathways, including Raf-MEK-ERK and PI3K-AKT-S6K and an increase of the intracellular Ca^{+2} [7].

NRG1 type III plays an important role in the regulation of PNS myelination by activating ErbB2-ErbB3 in Schwann cells (Figure 4). Importantly, inactivation of NRG1 receptors and reduced levels of NRG1 lead to hypomyelination of peripheral nerves, while overexpression of NRG1 promotes hypermyelination[36]. Moreover, increased levels of NRG1 promotes a higher number of Schwann cells required for myelination, but once myelination is complete, axonal NRG1/ErbB signals is no longer required to maintain myelination. Fricker's group demonstrated

that NRG1/ErbB signaling seems dispensable for the maintenance of the myelin sheaths, as their knockout models showed no impairment in myelin sheath integrity [53].

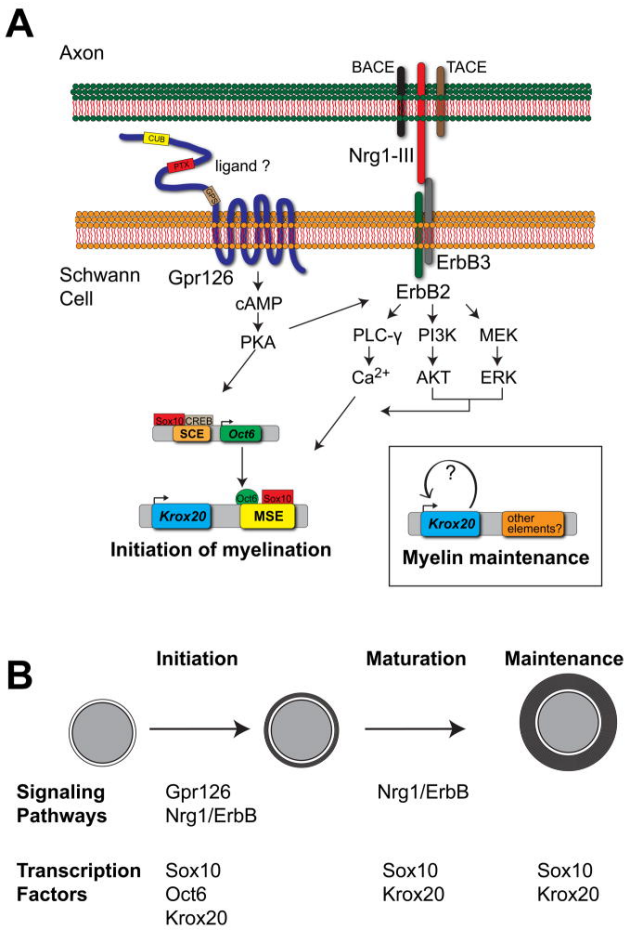

Figure 4. A simplified representation of the different signaling pathways and transcription factors involved in the initiation, maturation, and maintenance of myelin in Schwann cells. (**A**) Gpr126 and Nrg1-III/ErbB stimulate Oct6 and Krox20 upregulation to initiate myelination. PKA functions downstream of Gpr126, and Sox10 and CREB binding sites are present in the SCE. Krox20 levels can be maintained independently once initiated by Gpr126. (**B**) Representation showing the regulation of the stages of myelination by the myelination regulators in (**A**). Adapted from Glenn et al, 2013.[52]

Regeneration

Numerous studies have examined the role of this pathway during nerve repair after injury. Ronchi et al found reduced levels of NRG1 and negative regulators of myelination after chronic denervation in rats[54,55]. Guertin et al., observed a blockade in demyelination after nerve transection when treating rats with an ErbB2 inhibitor, highlighting the relevance of this pathway just after the nerve damaged is produced[56].

Haesun Kim's group determined that NRG1 type II and III can stimulate or block myelination depending of their concentration in the medium in Schwann cell-neuron co-

cultures. High concentrations of NRG1 type II and III induced an overactivation of ERK signaling pathway causing demyelination and de-differentiation in Schwann cells[57]. ErbB receptors can also interact and activate Dock7, which is a negative regulator of myelination upstream of Rac/JNK. When Dock7 is inhibited in cultured Schwann cells, the de-differentiation induced by NRG1 is reduced[58]. As mentioned before, *in vivo* studies have shown that ErbB2 inhibition or silencing of NRG1 in axons after a nerve injury do not compromise proliferation or survival of Schwann cells[59].

The effect of NRG1 in the myelination in development and remyelination following nerve injury has been well established. Myelin thickness is determined during development and after nerve injury by the interaction of axonal NRG1 type III interacting with Schwann cell ErbB2/3 receptors[53].

NRG1 has a vital role during development in Schwann cell myelination but it is not essential for nerve repair[60]. Autocrine and paracrine secretion of soluble NRG1 type I from Schwann cells stimulate their own survival and remyelination. However, this secretion is later inhibited when axons re-grow and express their own NRG1[61]. NRG1 function could be related with Rac/JNK activation, as ErbbB2 silencing led to a downregulation of MKK7 and c-Jun, which are activated by Rac/JNK, after a nerve injury[62].

ErbB activation can be modulated by two proteases that cleavage NRG1[63,64]. β-Site amyloid precursor protein cleaving enzyme 1 (BACE1) inhibition accelerates myelin degradation and the reinnervation of neuromuscular junctions. BACE1 protease regulates myelination during development by cleaving Notch's ligands Jagged and Delta[65].On the other hand, Tumor necrosis factor-α–converting enzyme (TACE, also known as ADAM17) negatively regulates myelination by cleaving NRG1-III in neurons , preventing the activation of PI3K and its activation of myelination[66]. Overactivation of NRG1/ErbB can increase the risk of suffering neuropathies or peripheral nerves tumors[67,68].

2.3.4.1.2 Toll-like receptors (TLRs)

Toll like receptors belong to the family of pattern-recognition receptors that detect pathogen-associated molecular patterns (PAMPs) present in microbes and self-derived molecules from damaged cells called damage-associated molecules patterns (DAMPs). These receptors are important for the initiation of the inflammatory and immune response, especially for the innate immune signaling pathways. The family of toll like receptors is composed of 10 different receptors in human (TLR1–TLR10) and 12 in mice (TLR1–TLR9, TLR11–TLR13), with each one of them activated by the binding of different ligands. Some TLRs are found on the cell

surface (TLR1, TLR2 , TLR4, TLR5, TLR6, TLR10) while others are located in endosomes (TLR3. TLR7 , TLR8, TLR9, TLR11, TLR12 and TLR13)[69].

The interaction with PAMP and DAMPs allows the TLR to recruit adaptor proteins containing TLR domains such as MyD88 and TRIF. These proteins trigger the signaling pathway that activates NF-κB, IRFs or MAP kinases to induce the synthesis and secretion of cytokines, type I interferon and chemokines. These molecules stimulate inflammation, immune cells recruitment and proliferation, and protect the host from pathogens[70].

Regeneration

TLRs participate in the response against nerve damage, interacting with PAMPs and ligands present in the injury microenvironment, including the molecules released by damaged cells. Not all the TLRs can be found in Schwann cells, but they constitutively express TLR3, TLR4 and TLR7. TLR1 is expressed after nerve injury, which suggests the relevance that these receptors have in the response to nerve damage in the Schwann cells. The direct activation of TLR2 and TLR4 by addition of their ligands to the injury site, accelerates the recovery of the animals[71]. Inhibition of TLR3 reduces the expression of tumor necrosis factor-alpha (TNF-α) or monocyte chemoattractant protein-1 (MCP-1), when the inflammatory response is activated in Schwann cells.

In vitro, the addition of necrotic neurons to Schwann cells activates their inflammatory response through TLR signaling. It increases their gene expression of inflammatory mediators such as TNF-α or MCP-1, and this effect is reduced in Schwann cells from mice lacking TLR3[72]. Boivin and collaborators provided in vivo evidence that TLR signaling is involved in WD and nerve regeneration following nerve injury, possibly through NF-κB activation[71]. The early expression of inflammatory modulators such as MCP-1, macrophage recruitment and activation, axonal regeneration and functional recovery are impaired in the mice deficient in TLR signaling. The results are indeed similar in mice lacking TLR2, TLR4 (which activates NF-κB) or their adaptor myeloid differentiation primary response gene 88 (MyD88). Besides its likely role in Schwann cells response to nerve injury, TLR signaling has also been linked to the development of neuropathic pain, making TLRs promising therapeutic targets[73].

2.3.4.1.3 GPCR Signaling

Recent studies have elucidated the role of G protein-coupled receptors (GPCRs) in the regulation of myelination, with 3 different GPCRs identified so far: Gpr126, Gpr44, and lysophosphatidic acid receptor 1 (LPA1)[74].

Gpr126 is proteolytically cleaved into N terminal and C terminal fragments during development. These two fragments have specific functions but both interact with Laminin-211, which is a recently discovered ligand of Gpr126, that mediates its regulation of cAMP levels during early and late stages of Schwann cell development[75]. N terminal fragments interact with Laminin 211 to regulate radial sorting, and C terminal domain interacts with this component of the basal lamina to increase cAMP levels in Schwann cells. Gpr126 participates in the initiation of Schwann cells myelination[76] and its downregulation after nerve injury impairs remyelination, regeneration and macrophage recruitment[74]. Consequently, when Gpr126 is silenced in mice, the levels of MPZ, MBP are reduced, Schwann cell markers including Pou3f1 and Krox-20 are downregulated, and hypomyelinating peripheral neuropathy is observed[77].

Gpr56 regulates RhoA, an actin reorganization modulator[78], during development to promote a correct radial sorting of the axons and is involved in the regulation of myelin thickness and organization of the myelin sheath[79], whereas LPA1 regulates Schwann cell migration, axonal sorting and myelination [80].

Finally, Gpr44 and its ligand the prostaglandin D2 synthase impair myelination when they are inhibited, suggesting that they are components of an axo-glial interaction that controls PNS myelination[81].

2.3.4.2. cAMP

Myelin formation is partially regulated by cyclic adenosine monophosphate (cAMP). Upon ligand binding, Gpr126 activates adenylyl cyclase, converting ATP into the secondary messenger cAMP. This secondary messenger activates protein kinase A (PKA) that induces the cAMP response element (CREB) signal transduction pathway, which then stimulates krox-20 upregulation and c-Jun downregulation. Moreover, the CREB signaling pathway also upregulates the exchange protein activated by cAMP (EPAC), which is required for Schwann cell differentiation and myelin formation[82]. Strikingly, Grp126 is the only receptor identified that drives Schwann cells differentiation by elevating cAMP levels.

Elevation of intracellular cAMP levels in Schwann cell cultures with cell-permeable and non-hydrolysable cAMP analogues (db cAMP) together with exogenous NRG1 addition, can upregulate expression of myelin-related genes including: *MPZ*, *MBP*, *Periaxin* and *Krox-20*[83]. Conversely, negative regulators of myelination are downregulated, including c-Jun and Sox-2 transcription factors, and markers of iSC or Remak Schwann cells such as $p75^{NTR}$ and GFAP[14]. cAMP promotes the switch from survival and proliferation to the differentiation and myelination response of NRG1 in Schwann cell cultures. Once myelination is initiated, elevation of gpr126 and cAMP levels are no longer required for myelin maintenance[84].

2.3.4.3 Transcription factors

Decades of research have identified a vast complex of signaling pathways that converge on a network of transcription factors that regulate the proliferation of Schwann cell precursors, the differentiation, myelination and the response to nerve damage in the Schwann cells.

2.3.4.3.1. Notch

Notch is a transmembrane receptor protein that can act as a transcriptional regulator. After binding to its ligand Delta, Serrate (called Jagged in vertebrates) or Lag2, the Notch receptor is cleaved and the Notch intracellular domain (NICD) is released from the receptor and imported to the nucleus[9]. Once in the nucleus, NICD form a regulatory complex with CSL (CBF1 in humans) and Mastermind (Mam)/Lag3 co-activators to bind specific regulatory DNA sequences and switching them from repression to activation[85].

During development, Notch signaling promotes Schwann cell proliferation, regulates the differentiation of Schwann cell precursors to immature Schwann cells and act as a negative regulator of myelination[9]. Notch signaling is inhibited during myelination and when Notch is artificially activated in Schwann cells in vivo, myelination is transiently impaired [9].

Similar to c-Jun, Notch is activated after nerve injury and contributes to nerve repair. Inhibition of the Notch signaling pathway in injured nerves in vivo delays myelin breakdown[9]. On the other hand, the activation of the Notch pathway after nerve axotomy in rats by addition of recombinant Jagged 1 (Notch activator) improves the recovery and nerve regeneration[86]

2.3.4.3.2. Zeb2

Zeb2 is a transcriptional repressor and plays a critical role in Schwann cell myelination and remyelination. Zeb2 ablation in Schwann cells in vivo leads to a block of myelination and induces a severe peripheral neuropathy during development, and perturbs nerve repair and remyelination after nerve injury [8,87]. Zeb2 performs these functions by recruiting histone deacetylases HDAC 1 and 2 (HDAC1/2) and nucleosome remodeling and deacetylase complex (NuRD) co-repressor complexes and participating in the downregulation of negative regulators of myelination, including Notch and Sox2 (SRY-related HMG-box gene 2).

2.3.4.3.3. NF-κB

The nuclear factor κB (NF-κB) is key transcriptional regulator for many signaling pathways that mediate inflammatory responses in different cell types and diseases. It is dispensable for myelination in vivo, as demonstrated by Morton and colleagues, although its inhibition during nerve regeneration delays nerve repair and remyelination[88].

NF-κB stimulates the transcription of different targets like placental growth factor (PlGF), which regulates proliferation, myelin degradation and increases the macrophages invasion during the response to nerve injury[89].

2.3.4.3.4. Sox-2, Pax-3 and Id2

These transcription factors regulate the nerve damage response by collaborating with c-Jun and Notch. Their basal levels are low during myelination and they are overexpressed during the early events of the nerve damage response [89]. Sox-2 also regulates the formation of the bridge between the sectioned nerve and the distal stump. During this process, repair Schwann cells migrate to the distal stump and help the proximal axons to reach it. This migration and cell sorting is regulated by an ephrin-B/EphB2 in Schwann cells and Fibroblast [90].

2.3.4.3.5. EGR2 (Krox-20)

EGR2 (Krox-20), a zinc-finger transcription factor, is a master regulator of Schwann cells myelination. Krox-20 is regulated by Oct6 and Brn2. Krox-20 is a cross-antagonist of c-Jun transcription factor, one of the main negative regulators of myelination. Moreover, the expression of c-Jun and Krox-20 is mutually exclusive, with c-Jun levels high in immature Schwann cells while Krox-20 levels are low. However, myelinating cells upregulate Krox-20 levels and downregulate c-Jun[10,91]. Krox-20 regulates the expression of myelin proteins like P0 (MPZ) and Periaxin, whose expression are largely confined to myelinating Schwann cells in the PNS.

Mutations in Krox-20 gene in humans has been related with diseases including Charcot-Marie-Tooth, Dejerine-Sottas, and other neuropathies[10].

2.3.5.4. Ras/Raf/MEK/ERK

ERK1 and ERK2 are protein-serine/threonine kinases that participate in the Ras-Raf-MEK-ERK signal transduction cascade. This is one of the main signaling cascades in the cell regulating different processes including cell adhesion, cell migration, cell survival, cell cycle progression, , differentiation, metabolism[92] and proliferation. When Ras is activated by different receptors, adaptor protein of these or exchange factors, it activates protein kinases from Raf family (Raf-1, B-Raf, and A-Raf know as Rafs)[93]. Following its activation, Rafs proteins phosphorylate MAPK/ERK kinases (MEK) which then activate ERK1/2 by phosphorylating it in Tyr204/187 and Thr202/185 residues.

Raf pathway activation induces adult Schwann cell to dedifferentiate and demyelinate. Raf activation in cultured Schwann cells, under myelinogenic conditions, drives their dedifferentiation. Dual specificity phosphatase 15 (Dusp15) is necessary to activate ERK and this

activation is able to shut down the expression of myelin genes[94] . Raf-kinase participates in the induction of an inflammatory cascade in response to nerve damage allowing the breakdown of the blood-nerve barrier and the influx of inflammatory cells to the injury to improve nerve regeneration[95].

2.3.5.5. MAPK pathway.

ERK/MAPK pathway has a critical role in PNS development regulating Schwann cells differentiation and myelination. However, a sustained activation of ERK/MAPK in adult Schwann cells has detrimental consequences in development and during the nerve repair. This overactivation can causes demyelination and de-differentiation in adult Schwann cells and a delay in the regeneration after nerve damage[96].

2.3.5.6 Rac/JNK

JNK, the MAPK that activates c-Jun, has a key role during Schwann cell response to nerve damage[97]. JNK is phosphorylated by MMK7 and this kinase is regulated by rac1 GTPase (Rac)[98]. In Schwann cell cultures, Rac regulates JNK pathway, increasing the levels of c-Jun and down regulating Krox-20. Inhibiting Rac activation after nerve injury blocks the activation of c-Jun and MKK7. Rac can be activated by atypical guanine-nucleotide exchange factor dedicator of cytokinesis protein 7 (Dock7) and collagen triple helix repeat containing 1 (Cthrc1). Rac activation by those proteins stimulates the proliferation and the migration of Schwann cells in vitro and in vivo. The inhibition of Dock7 causes reduced Rac activity and increases SCs myelination. [99–101]

2.3.5.7. P38 MAPK

p38 MAPK is a key regulator of Schwann cell reprogramming. Mice lacking p38 MAPK exhibit a blockage in myelin degradation and dedifferentiation after nerve injury. This impairment in myelin breakdown was regulated by NRG1 in Schwann cell DRG co-cultures[102]. Moreover, when p38 MAPK is ectopically activated, it can induce myelin breakdown and induce Schwann cell dedifferentiation to a phenotype similar to immature Schwann cells.

2.3.5.8. C-Jun

C-Jun is a transcription factor that homodimerizes or heterodimerizes with members from the Jun family (JunB or JunD) or Fos Family (FOS, FOSB, FOSL1 and FOSL2) to form the AP-1 transcription factor. These proteins are characterized by their Zinc finger domains that allows them to bind DNA and their domains that activates the transcription of target genes[103]. c-Jun

inhibits the expression of myelin proteins when it is overexpressed, and the expression of these proteins is increased when cells lack c-Jun in cultured Schwann cells[10]. C-Jun is highly expressed in immature Schwann cells and their levels go down as the Schwann cells differentiate to myelinating Schwann cells. Mice lacking c-Jun display no differences in Schwann cell myelination[91]. However, overexpression of c-Jun *in vivo* in Schwann cells strikingly blocks Schwann cell myelination[104] showing that the downregulation of c-Jun during development is necessary for myelination to proceed normally

In contrast to development, c-Jun levels are elevated in Schwann cells after nerve injury as well as in demyelinating diseases such as Amyotrophic Lateral Aclerosis (ALS)[105] and Charcot-Marie Tooth disease (CMT)[106]. During Schwann cell reprogramming after nerve injury, c-Jun stimulates myelin degradation, the formation of the Büngner bands, cytokine production and the synthesis of trophic factors to improve the survival of the neurons[107].

2.3.5.9. Cyclin-dependent kinase inhibitor 1 (Cdkn1c).

Cdkn1c, also known as p57Kip2 is a downstream effector of Rac/cdc42/rho that blocks G1/S transition during cell cycle[108]. It can also regulate actin filament dynamics by interacting and translocating LIM domain kinase 1 (LIMK1)[89]. p57kip2 depletion stimulates upregulation of myelin genes in Schwann cell cultures and SC-DRG co-cultures, suggesting that Cdkn1c is a negative regulator of myelination[109].

Enhancer of zeste homolog 2 (EZH2) interacts with the Cdkn1c promoter, inducing a decrease in histone H3K27 trimethylation of Cdkn1c that leads to an increase in the expression of the gene and reducing the activation of myelin proteins in Schwann cell culture[110].

2.3.5.10. PI3K/Akt/mTOR

Activation of PI3K/Akt by different transcriptions factors or molecules like Src-associated in mitosis of 68 kD (Sam68), DIX domain containing-1 (Dixdc1) or 17β-estradiol promotes Schwann cell proliferation and myelination[111,112]. Conversely, the inhibition of this pathway by Src-suppressed protein kinase C substrate (SSeCKS)[113], cell adhesion molecule 3 (Cadm3) [114] and the mammalian disks large homolog 1 (Dlg1) blocks Schwann cells differentiation and myelination[115]. Dlg1-mediated effects include regulation of myelin thickness and its downregulation could lead to myelin outfoldings, over myelination and later a pathologic demyelination[115]. PI3K/Akt regulates proliferation through different transcription factors like NF-kß and Hif1α; stimulates survival inhibiting p53; controls the synthesis of proteins regulating ribosomal protein S6 kinase beta-1(p70S6K) and eukaryotic translation initiation factor 4E-binding protein 1(4E-BP) among others[116].

Mammalian target of rapamycin or mTOR is serine/threonine protein kinase encoded by the gene *mTOR*. mTOR belongs to phosphatydilinositol 3-kinase-related kinase (PI3K) family of proteins. mTOR is one of the main constituent of mTOR complex 1 (mTORC1) and mTOR complex 2 (mTORC2)[117]. The main role of mTORC1 is mRNA translation regulation through its targets 4EBPs and S6Ks. Upon phosphorylation by mTORC1, 4EBP1 is released form eIF4E in the cap-binding complex, promoting translation[118]. Additionally, S6K1 phosphorylation allows eIF4A helicase activity[119]. Furthermore, mTORC1 regulates the activation of SREBP transcription factors SCREBP1a, SREBP1 and SREBP2, which induce the expression of different enzymes that regulate cholesterol and fatty acids biosynthesis[120] (Figure 5). Endogenous fatty acid (FA) synthesis is a critical process in Schwann cells that is require for a correct myelination of peripheral nerves[121]. Thus, mTOR downregulation blocks the myelination cascade in Schwann cells[122].

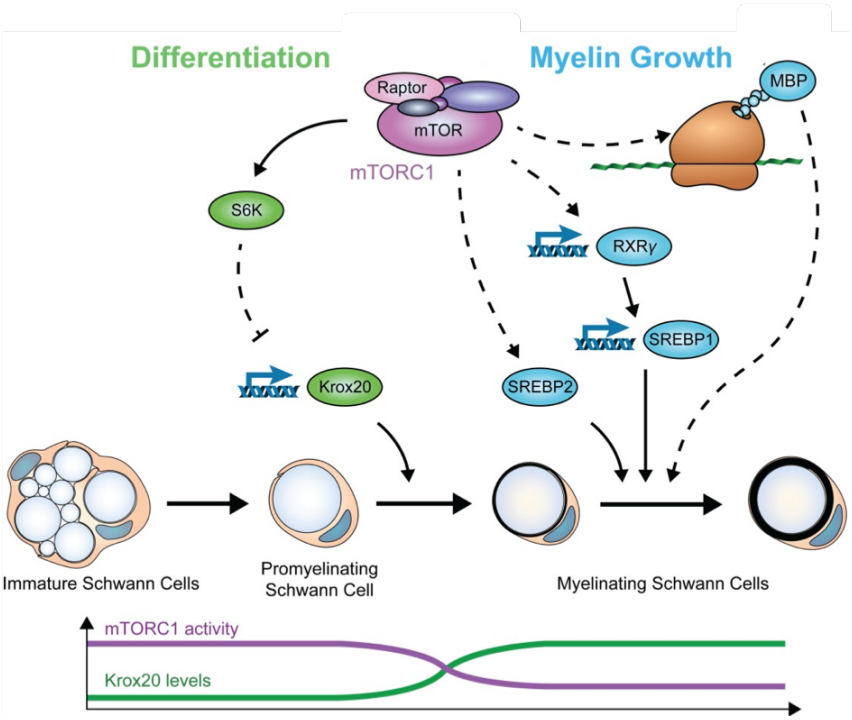

Figure 5. MTOR signaling pathway in Schwann cells differentiation and myelination.
mTORC1 suppresses Krox20 expression during Schwann cell development via S6K allowing the transition from immature to promyelinating Schwann cell. When mTORC1 activity decreases Krox20 levels start to increase allowing myelination to begin. Adapted from Figlia et al. 2017.

Recently it has been demonstrated that the conditional ablation of raptor, an essential component of the mTORC1 complex, in Schwann cells leads to hypomyelination and abnormal lipid biosynthesis[38]. Disruption or inhibition of mTORC1 affects myelin protein levels, specially MBP translation, indicating that mTORC1 could potentially regulate myelin protein translation[123].

AMPK is a key energy sensor that regulates the maintenance of the energy homeostasis in cells. It is a negative regulator of myelination that inhibits mTOR and upregulates c-Jun expression[124]. AMPK inhibition down regulates c-Jun, which triggers myelination, up regulating myelin genes and increasing myelin thickness.

2.3.5.11. Wnt Signaling

The Wnt/β-catenin pathway is essential for Schwann cell lineage progression, proliferation and myelination[125]. A cross-talk between Wnt pathway and liver X receptors (LXR) have been shown to precisely regulate myelin gene expression[126]. LXR are oxysterols (reactive molecules derived from oxidated cholesterol) receptors in the nucleus that participate in cholesterol homeostasis and have been related with neurodegenerative diseases. The group of Charbel Massaad demonstrated that Paraquat, a redox-active herbicide, increases the oxidative stress in nerves and activates LXR, preventing the interaction of ß catenin with myelin genes promoters, and thus blocking the regulation of myelin genes expression by the Wnt/ß catenin cascade[127]. This block affects PNS myelination, causing an aggregation of myelin proteins, a disorganization of myelin sheaths and locomotor deficits. The oxidative stress caused by Paraquat could be reduced by using LiCl, which inhibits GSK3 activation of Wnt signaling. When LiCl was added to an injured nerve, myelin degradation was improved.

2.4 NERVE DISORDERS

There are many different pathologies related with dysfunctions in the peripheral nervous system, several of which are related with myelination defects.

Neuropathies can be classified by cellular location in the PNS as axonal, where the pathological dysfunction is originated in the axons; and demyelinating, when the pathology is related with the Schwann cell function. Since the integrity and maintenance of axonal myelination depend on signals secreted by both the axon and the Schwann cells, axonal neuropathies can progress to demyelination.

Some examples of the most studied demyelinating neuropathies are the Charcot-Marie-Tooth (CMT) disease, Guillian-Barre's syndrome (GBS), diabetic neuropathies, Amyotrophic Lateral Sclerosis (ALS), Lyme disease and small fiber neuropathy.

2.4.1 Charcot-Marie-Tooth disease (CMT)

CMT disease is group of neurodegenerative pathologies that affect the PNS. It is the most frequent inherited neuropathy affecting PNS, and its incidence is around 1:2500[128]. There are different mutations and sub types of this disease. The most relevant sub-types are CMT1 (characterized by the demyelination of the axons and the most common cause of CMT disease), CMT2 (characterized by axonal pathologies), hereditary motor neuropathy (HMN) and hereditary sensory neuropathy (HSN). New sequencing technologies, including Next Generation Sequencing (NGS), have considerably helped to relate more than 100 genes to CMT disease[129].

DNA duplication in the chromosome 17 p11.2 region containing the PMP22 gene is the main cause of CMT1A disease, while its deletion causes hereditary neuropathy with pressure palsies (HNPP). Together with the mutations in the genes GJB1 (CMTX1), MFN2 (CMT2A) and MPZ (CMT1B), these five subtypes are the main causes of CMT disease in more than the 90% of genetically diagnosed patients of CMT[130]. The overexpression of PMP22 has been related with anomalies of demyelination and remyelination in the nerves, causing an impairment of nerve conduction velocities.

Some of the related symptoms with Charcot-Marie-Tooth disease are weakness of the feet and lower leg muscles, the presence of foot deformities, like high arch foot and bent toes (hammer toes), difficulties lifting the feet while walking (foot drop), loss of the muscle around the hands and feet and feelings of numbness, burning, or loss of temperature sensation in the hands and feet.

During the last decades, different treatments have been tested for CMT disease. Ascorbic acid (vitamin C) treatment has been successfully used to improve myelination in CMT1A mice models. The treatment improved the performance of the animals in rotarod test and grip

test. Furthermore, it was determined that AA stopped the demyelination[131]. The treatment with high doses of ascorbic acid modifies the cyclic AMP pool, since it is a mild inhibitor of adenylate cyclases in the cells. This approach reduces PMP22 expression, promoting Schwann cell myelination. Different trials have been developed to test the effects of AA treatment in humans, but despite the treatment being safe, the symptoms were improved only slightly[132]. PXT3003 is a mix of three molecules that act on PMP22 expression: sorbitol, naltrexone, and baclofen. It has been tested on mice and rats and it reduced the clinical phenotypes and improved myelination and nerve conduction velocities. Phase III clinical trials were performed in 2021 to validate the safety and effectivity of PXT3003 after a previous Phase III trial failed to confirm the efficacy of the treatment in 2017[133]. Curcumin has been tested as potential treatment for CMT1A in a formulation of cyclodextrin/cellulose nanocrystals to improve its pharmacokinetics. Preliminary tests were performed in CMT1A rats and promising results were obtained, including increased sensory and motor nerve conduction, grip test and balance performance. Myelin thickness was increased in treated rats and the expression of MPZ and PMP was higher after the treatment[134].

As mentioned previously, the cause of some of the different CMT diseases are mutations or dysregulation of myelin proteins like PMP22, MPZ, and Connexin32 (Cx32). Some mutations directly impair the normal maturation and trafficking of these proteins, affecting their final destination in the cell, and become accumulated in the ER or Golgi apparatus. This accumulation of unstructured proteins triggers the response to unfolded proteins, a pathway that mediates the degradation of proteins that can generate cellular stress. Thus, targeting the ER quality control pathway to reduce the accumulation of these proteins has been proposed as an effective therapeutic approach for CMT. One treatment that has been tested targeting this pathway is the pharmacological inhibition of PP1c/PPP1R15A phosphatase complex. Using the IFB-088 (Sephin1, InFlectis BioScience) small molecule to inhibit this complex, the group of Dr Bertolotti was able to prevent the morphological and molecular defects found in S63del mice, a CMT model[135,136].

Another approach to treat these diseases has been directed at reducing the inflammation associated with the aggregated proteins to improve the survival of the neurons. Macrophages and other cell types from the innate and adaptive immune system are likely to be the main source of this inflammation. The group of R. Martini demonstrated the effect of macrophages and endogenous antibodies in the demyelination observed in CMT1B mice models. When they reduced the amount of antibodies and B lymphocytes, the myelination of peripheral nerves was partially recovered[137]. Another interesting therapeutical approach is the inhibition of cytokine colony stimulating factor-1 (CSF-1), which is expressed by fibroblast and

its key in the regulation of macrophage related disease mechanisms in peripheral nerves[138]. Its inhibition reduced the damage of peripheral nerves in mutant mice[139].

Finally, the group of M. Sereda showed that addition of phosphatidylcholine and phosphatidylethanolamine to the diet increased the amount of myelinated fibers in the Pmp22-transgenic rat model of CMT and reduced the neuropathic phenotype[140], suggesting another potential therapeutic option.

2.4.2 Lyme disease

Lyme disease is an emerging infectious disease caused by three different spirochaete genospecies of *Borrelia burgdorferi*: *B. burgdorferi*, *B. afzelii* and *B. garinii*. These bacteria are transmitted to humans by the ticks *Ixodes scapularis* (mostly in north America) and *Ixodes ricinus* (in Europe)[141]. This disease is mainly reported in North America and Europe. Around 30,000 cases are reported each year in USA but CDC estimates that the number of cases could be even 10 times higher. In Europe, countries like Netherlands, Belgium, Austria, Slovenia, Lithuania and Estonia have the higher incidence (around 80 cases per 100,000 individuals).

The first manifestation after the tick's bite is the erytrema migrans that could be accompanied (if the bacteria was *B. Burgdorferi*) by other symptoms such as fatigue, headache, arthralgias, myalgias, fever and regional lymphadenopathy[141]. The infection by the other genoespecies of B burgdorferi in Europe does not usually produce any other symptoms other than the eritrema migrans. The bacteria disseminate from the zone where the patient was bitten by the tick within days or weeks, reaching different organs in the body. B. Burgdorferi can infect by this way the peripheral and central nervous systems, leading to neuroborreliosis, a demyelinating disease[142].

The presence of borrelia in the brain triggers changes in gene expression programs in the host immune system. Around 2200 different genes were unregulated or downregulated in a short term infection study performed with macaque rhesus monkeys[143]. In fact, most genes were related with inflammatory responses, increasing the synthesis of pro inflammatory cytokines, including IL6.

Nowadays, the only approved treatment for Lyme borreliosis is long-term antibiotic treatment. Some patients still suffer from persistent Lyme disease-like symptoms for long periods after the treatment[144].

2.4.3 Diabetic Neuropathy

Diabetic neuropathy is a complication developed by at least 50 % of diabetic patients. Distal symmetric polyneuropathy is the most common diabetic neuropathy, and it is characterized by a loss of sensory function (heat, touch) in the hands and lower limbs, and it could also be accompanied by neuropathic pain. The number of diabetic patients has been estimated to be around 400 million people and the prediabetic patients to reach the 600 million (data by Diabetic International Federation)[145].

Diabetic neuropathy affects mainly to the sensory axons, which differentiates this pathology from other types of neuropathies. However, in the later stages of the illness, autonomic and motor axons can be also affected. The progression of this neuropathy is characterized by the retraction of the terminal part of the sensory axons, with a greater effect in longer axons, explaining why the first symptoms are detected in the distal limbs.

Two gene polymorphisms have been related with higher risk of diabetic neuropathy: *ACE* (encoding angiotensin converting enzyme) and *MTHFR* (encoding methylenetetrahydrofolate reductase)[146]. Little is known about the effect of those genes in the pathology, and future experiments will be needed to understand better their role in the diabetic neuropathy. Although diabetic neuropathy is not a primarily demyelinating disease, the stress and damage from hyperglycemia can affect Schwann cells and lead them to demyelination in some patients.

Recent studies have related the Schwann damage with severe reticulum stress caused by diabetes. Hyperglycemia could affect the expression of heat shock proteins (HSPs), growth associated protein 43 (GAP43) , β-tubulin and poly(ADP-ribose) polymerase (PARP)[147]. Hyperglycemia is characterized by a substrate overload of glucose and fatty acids that saturate the main metabolic pathways that use them as energy source (TCA and Beta oxidation). The fatty acids are beta oxidated in Schwann cells generating acetyl-CoA, that is used in the TCA cycle to produce NADH and FADH2. The excess of acetyl coA molecules during hyperglycemia saturates the transporter routes, causing the accumulation of acetyl-CoA[146] . To deal with this stress, Schwann cells convert acetyl-CoA in acylcarnitines, molecules that are toxic for both Schwann cells and neurons. Schwann cells release these molecules to avoid mitochondrial dysfunction, likely causing axonal degeneration[146]. Moreover, the excess of glucose and fatty acids causes an accumulation of ROS in the cells, causing mitochondrial dysfunction and reducing the energy production needed for the normal activity of the Schwann cells and neurons.[148]

As the main cause of the diabetic neuropathy is hyperglycemia, glucose control and intense insulin treatment are two promising therapies to prevent the development of diabetic

neuropathy in T1DM patients[149,150]. However, those approaches have proved less effective for T2DM patients. In these cases, lifestyle changes, including a personalized diet, exercise and periodical lipid and blood pressure controls, are warranted. A study showed an improved nerve regenerative capacity in patients with diabetes and/or metabolic syndrome after 4 months of lifestyle intervention with diet and exercise[151].

2.4.4 Amyotrophic lateral sclerosis (ALS)

ALS is a neurodegenerative disorder where motor neurons from spinal cord, brainstem and motor cortex suffer cell death as result of an intracellular accumulation of aggregated proteins. Most ALS cases are sporadic (sALS) (around 80-90%), whereas familiar ALS (fLAS) accounts for only in 10-20% of the patients[152]. ALS is a complex genetic disorder and many different mutations have been related with the disease in the last decade. Mutations in SOD1, TAR-DNA binding protein 43 (TDP43), Fused in Sarcoma (FUS) and an hexanucleotide repeat expansion in C9orf72 are the most common causes of ALS[153]. These mutations affect directly or indirectly the protein degradation cascade, disrupting cellular homeostasis and thus promoting the accumulation of proteins in the cell. It was recently proposed that high molecular weight complexes that appear before the accumulation of aggregates in ALS, could be the primary cause of the toxicity found in motor neurons [152]. Although the mechanisms causing the toxicity remain obscure, the result of ALS is the loss of axonal projections in the motor neurons, a retraction of the axon and the denervation of the target cell (e.g. muscle).

There are only two treatments approved to specifically treat the disease, Riluzole, a drug which targets voltage-gated sodium channels, and Edaravone, which act as antioxidant, reducing the progression of the disease[152]. Dextromethorphan hydrobromide and quinidine sulfate have been used to improve the bulbar function impaired by the disease, while Baclofen and Tizanidine (muscle relaxants) are used to alleviate the spasticity of patients. Cannabinoids are not approved as official treatment for the disease but are used off label to alleviate the spasticity and neuropathic pain. Furthermore, atropine, hyoscine, amitriptyline and glycopyrrolate have been used to treat sialorrhea (hypersalivation), one of the most troublesome symptoms that suffer ALS patients[154].

The drugs used to treat the nociceptive and neuropathic pain are abapentin, pregabalin and tricyclic antidepressants (for neuropathic pain) and non-steroidal anti-inflammatory drugs (NSAIDs), opioids as well as the cannabinoids previously mentioned. The instability of the motor units observed in 25 % of ALS patients develops into muscle cramps, a common pain symptom which is treated with quinine sulfate, levetiracetam and mexiletine[152].

2.4.5. Other peripheral disorders:

Guillain-Barré-Strohl Syndrome (GBS) is a group of autoimmune disorders that could differ in their pathogenesis but have a common consequence, an acute poly-radiculoneuropathy with fast progression. These disorders are: acute inflammatory demyelinating polyradiculoneuropathy (AIDP), which is the most common variant and it has the best prognosis in comparison with the others; acute axonal motor neuropathy (AMAN), which has a worse prognosis but is less common than AIDP, and acute motor sensory axonal polyneuropathy (AMSAN)[155].

The pathogenesis of this syndrome is not well understood but the most reasonable hypothesis is that an aberrant immune response to a pathogen causes damage to peripheral nerves. This immune response could include the production of antibodies against lipo-oligosaccharides from different bacteria or viruses that are similar to human gangliosides (causing self-reactive antibodies), activation of the complement and the macrophages infiltration in peripheral nerves. High levels of antibodies to GM1, GD1a, and other gangliosides were found in patients who developed GBS after *C.jejuni* infection, which is explained by the molecular mimicry between the *C jejuni* lipo-oligosaccharides and human gangliosides[156].

The main symptom is weakness and sensory impairment in the legs with a rapid progression, affecting later to arms and cranial muscles. Some patients (around 20%) can suffer from respiratory failure, blood pressure instability and cardiac arrhythmias when the autonomic nervous system is affected. Up to 2/3 of the patients also report pain. All the symptoms can vary due the different variants of the GBS. Due to the high possibilities that GBS patients have of suffering complications related with breathing and cardiovascular problems, close monitoring and the patient transfer to critical care units (if needed) can reduce effectively the mortality of the syndrome. Intravenous immunoglobulin (IVIg) and plasma exchange can be quite useful if administered in the early moments of the syndrome.[157]

Chronic inflammatory demyelinating polyneuropathy (CIPD) is an autoimmune disease where both humoral and cellular immune responses target peripheral myelin sheets, producing demyelination that causes a neuronal degeneration later on[158].

Acquired demyelinating sensory neuropathy is characterized by having mainly sensory symptoms although some patients also report distal weakness. The nerve conduction velocity in motor fibers is reduced. Presence of self-reactive IgM antibodies against MAG protein. Patients are usually treated with rituximab because most of them do not respond to IVIG treatment[155].

Multifocal motor neuropathy (MMN) is a demyelinating neuropathy caused by IgM antibodies against GM1. Moreover, these antibodies are present in serum of almost 50% of the patients and produce distal arm weakness. MMN is slowly progressive and can be treated with Rituximab or IVIG treatment[155,158]

Small fiber neuropathies (SFN) has been related with different illness such as diabetes mellitus, connective tissue diseases, B12 deficiency, human immunodeficiency virus (HIV), metabolic syndrome among others[159]. It impairs the quality of life of the patients because of the autonomic symptoms and neuropathic pain it produces. This disease affects small-diameter peripheral nerve fibers and the main treatment are lifestyle modification and pain relief[160].

2.5. UBIQUITIN, UBLS AND THE NEDD8 PATHWAY

As described above, the transcriptional and post-transcriptional program regulating Schwann cell myelination has been intensely studied over the past decades. The role of translational mechanisms and post-translational modifications (PTMs) have, however, been barely studied. A notabtle exception is glycosylation, which was shown to be essential for Schwann cell myelination. In the study, the authors found that Schwann cell-specific deletion of OGT protein O-GlcNAc transferase (OGT), which mediates post-translational O-linked N-acetylglucosamine (GlcNAc) modification, causes a tomaculous demyelinating neuropathy accompanied with progressive axon degeneration and motor and sensory nerve dysfunction[161]. Other PTMs, however, have not been studied.

2.5.1. Ubiquitylation and UBLs conjugation cascades

Ubiquitin and ubiquitin-like proteins (UBLs) are small proteins that are conjugated to substrates as posttranslational modifications. The UBLs have a high similarity with the ubiquitin protein and in some cases they share proteins in their routes[162–164]. Most of these proteins have to be processed in their C termini and activated to be able to be conjugated to target proteins because they are synthesized as inactive precursors. Deubiquitinating enzymes (DUBs) are the proteases responsible of processing ubiquitin while the UBLs have their own UBL-specific proteases (ULPs)[165]. After processing, they have to be activated by a specific activating enzyme (named E1 or E1-like enzyme)[166]. This is the first step of the cascade. Using ATP, the activating enzyme adenylates the UBL at its C terminus. This anhydride bond is quickly attached to the active site of the E1 expelling AMP. Later the Ubiquitin or UBL is passed to the active site cysteine of the

second enzyme of the cascade, the UB-conjugating or UBL conjugating enzyme, usually called E2 or E2-like enzyme[167]. The last step consists in the conjugation of the modifier to a specific substrate using an E3 protein ligase that binds both the E2 enzyme and the target protein (Figure 6). A covalent isopeptide linkage is formed between the ε-amino group of a lysine in the target substrate and the C terminus of the ubiquitin or UBL. The E1-E2 and E2-E3 interactions are mutually exclusive because of a structural overlap in E1 and E3 binding sites present in the E2. In this way, a unidirectional progression of the E1-E2-E3 cascade is ensured[168].

Ubiquitination has different roles in the cell depending on the number of ubiquitins conjugated (or the chain type) to target proteins and the residues where they are covalently attached. The best studied type of ubiquitination is the polyubiquitin chains conjugated to lysine 48 (K48) in substrate proteins, which is involved in degradation of the target protein by the 26S proteasome[169]. Other types of ubiquitination like mono-, oligo- or poly-ubiquination in alternative residues have different cellular functions, such as intracellular targeting, endocytosis or DNA repair [170–172]. The process of polyubiquitination is yet not completely understood in vivo and alternative K63-linked polyubiquitin chains have been related to degradation by the 26S proteasome as well[173].

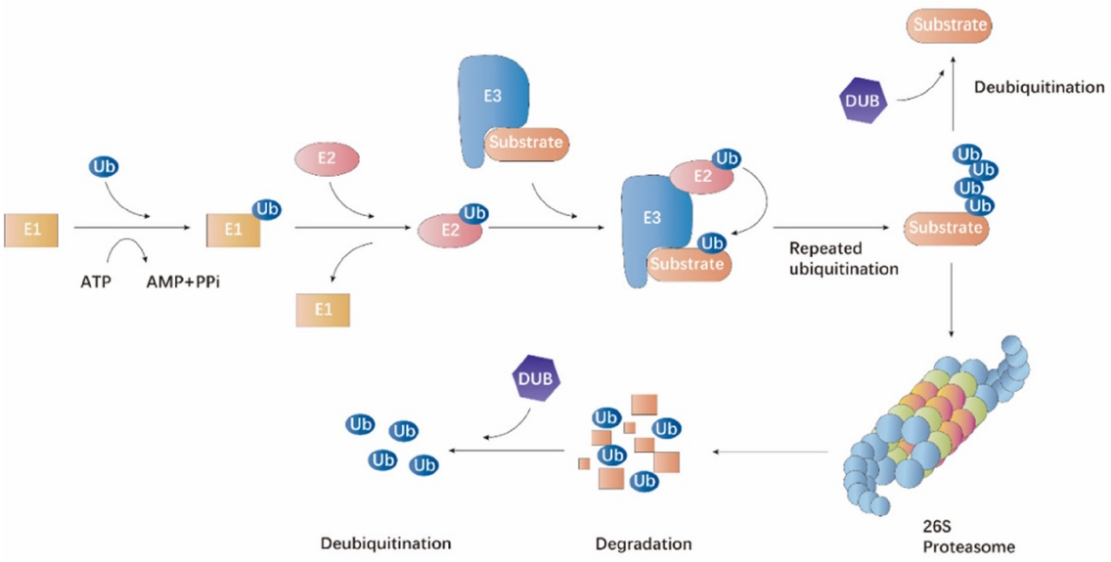

Figure 6. Ubiquitin-proteasome proteolytic pathway. Ubiquitin is activated by the E1 enzyme, later conjugated to and E2 to be finally used to modify a target protein by the E3 ubiquitin ligase. One of the main functions of the ubiquitin is to target proteins to degradation in the 26S proteasome. The process of protein degradation via the ubiquitin-proteasome complex. Ubiquitin molecules can be removed from target proteins by de-ubiquitinating enzymes action (DUBS). enzymes. (Adapted from Meng et al., 2021)

The E3 ubiquitin ligases can be divided in the really interesting new gene (RING) finger domain-containing class and the homologous to E6-AP carboxyl terminus (HECT) class. Cullin RING ligases (CRLs) is the largest family of RING E3 ligases. Those ligases are composed of a Cullin scaffold protein, a subunit or domain that contains the RING motif and one or more subunit(s), which act as adaptors or participate in the recognition of substrates. A key step for the activation of the CRLs is the neddylation of the Cullins, which is a necessary modification for the transfer of the ubiquitin between the E2 and the target protein once both are bonded to the CRL.

On the other hand, the mechanism of catalysis which is used by the HECT E3s is different compared with the one used by the Cullin Ring ligases[174]. The ubiquitin is transferred from the E2 to a conserved cysteine located in the active site of the HECT domain in the E3 ligase. Right after this, the ubiquitin is transferred again to the substrate protein [175,176]. The degradation of proteins by the Ubiquitin Proteasome system is highly specific and regulated. This is reflected by the high number of different E3s that are found in eukaryotic genomes (in humans, more than 700 putative E3 ligases have been predicted)[177].

Ubiquitination is a reversible posttranslational modification which can be removed from target proteins. This process is performed by the deubiquitinating enzymes (DUBs), which are proteases capable of remodelling polyubiquitins (or ubiquitin like) or reverse single ubiquitinations (or UBLs)[178]. There are five families of DUBs with specificity for ubiquitin that include nearly 100 enzymes in the human genome. This families are: ubiquitin-specific proteases (USPs), ubiquitin C- terminal hydrolases (UCHs), Machado-Josephin domain-containing ubiquitin peptidases, ovarian tumor superfamily of ubiquitin isopeptidases (OTUs) and the JAMM family of proteases[179–181]**.** The last one is quite different from the first four families because it is composed by zinc metalloproteases instead of cysteine proteases[179].

2.5.2 The NEDD8 conjugation pathway

NEDD8 (neural precursor cell-expressed, developmentally downregulated 8) was identified for the first time in a cDNA library screen in 1992[182]. It is the UBL with highest identity to ubiquitin (60%) and the neddylation cascade resembles the three-step reaction of the ubiquitination pathway[183,184].NEDD8 has a conjugation cascade with a unique and specific E1, two E2 and a great variety of E3s, some of them shared with the ubiquitin pathway. NEDD8 is synthesized as an 81aa precursor that has to be processed to be active. De-neddylating enzymes are responsible of this process[185]. They expose the glycine-glycine motif present in NEDD8, allowing it to be adenylated by the heterodimeric E1 NEDD8-activating enzyme (Nae1), which has too subunits: Nae1 and ubiquitin-activating enzyme 3 (uba3). Once adenylated, NEDD8 is transferred to Uba3, via a thyolested linkage which allows it to be transferred to the E2 NEDD8-

conjugating enzyme Ubc12 or the NEDD8 E2 Ube2f[186]. This E2 can interact with a E3 nedd8 ligase that will help to transfer NEDD8 to the ε-amino group of lysine residues forming a isopeptide bond on the substrates .

Only a few NEDD8 E3 ligases have been described and all of them contain a really interesting novel gene (RING) finger domains except defective in Cullin neddylation 1 (Dcn1) protein[187,188]. Examples of NEDD8 E3 ligases are Ring-box protein 1 and 2 (Rbx1 and Rbx2)**,** casitas b-lineage lymphoma (c-CBL) protein, murine double minute 2 (Mdm2) and Skp1-Cullin-F box protein (SCF)[183,189]. Moreover, Dcn1 interacts with yeast rbx1 homolog (Hrt1), not requiring any cysteines for its catalytic activity. After their interaction they promote together the ligation to cyclin-dependent kinase 53 (Cdc53), a yeast Cullin RING ligase[190].

In humans, Dcn1-like proteins are named Dcnl1-5 and they mediate Cullin neddylation. For that purpose, they form complexes with Cullin Associated And Neddylation Dissociated 1 (CAND1, a Cullin inhibitor) and Cullins, waiting for the bindings of adaptors to neddylate the Cullins and release CAND1[191,192] (Figure 7). Neddylation is a reversible modification (as ubiquitination) and the proteins that carry out this process are the de-neddylating enzymes.

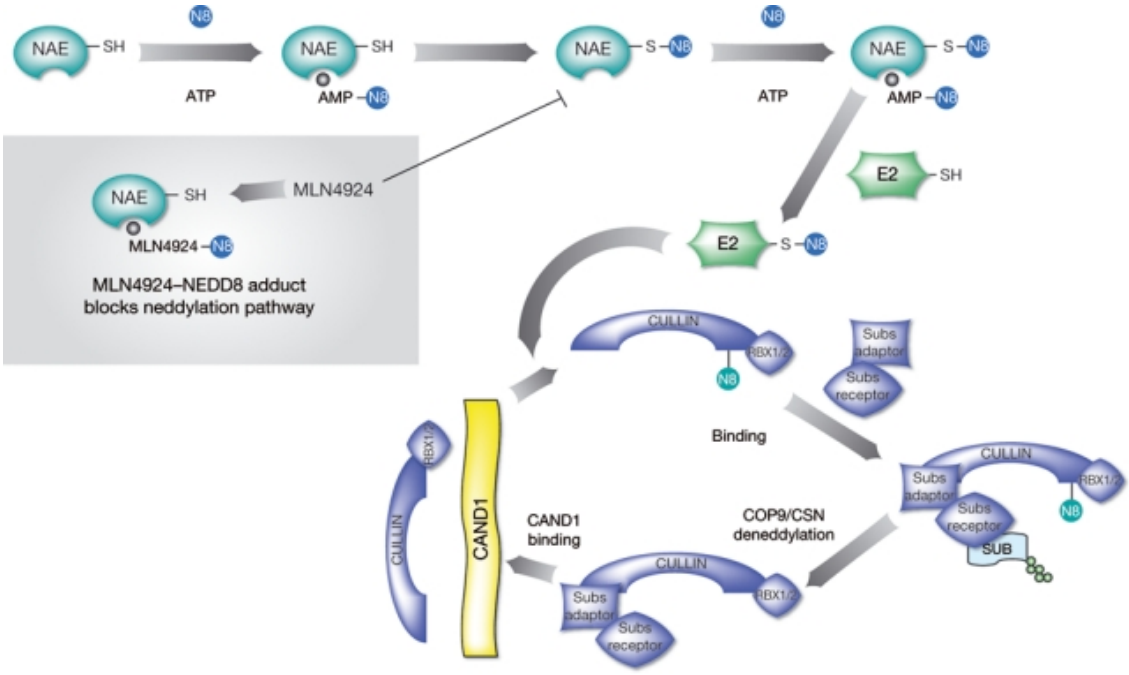

Figure 7. Neddylation cascade and CRL activation. CRL are complexes containing a cullin protein as the scaffold of the complex, a RING finger domain-containing protein which interacts with the E2 ligase and substrate recognizing adaptors that bind the target proteins that will be ubiquitinated. Unneddylated cullin-Ring complexes can be found interacting with CAND1 protein until the substrate recognizing adaptors bind the cullin-RING complexes. Nae1 enzyme starts the neddylation cascade by activating NEDD8 with ATP. NEDD8-adenylate is transferred to UBA3 allowing it to be transferred by transthiolation to the active site cysteine in UBC12 or UBEF2 (Nedd8s E2 ligases). The Nae1 inhibitor MLN4924 forms a covalent interaction with Nedd8 catalyzed by Nae1, inactivating the enzyme. Figure adapted from Soucy et al. (2009)[192]

One of the best known enzymes that removes NEDD8 from substrates is zinc metalloprotease constitutive photomorphogenesis 9 (COP9) signalosome (CSN)[193]. The signalosome is a complex of 8 subunits, with CSN5 the subunit responsible of the catalytic activity. The other best studied de-neddylase is NEDD8-specific protease 1 (Nedp1)[194], although it has a 3 fold lower activity in cleaving neddylated Cul1 compared to COP9. It has been proposed that Nedp1 could be involved in neddylation of non-Cullin substrates[195].

2.5.3. Specificity of the NEDD8 cascade

During last decades, different studies have identified the enzymes involved in the neddylation pathway. Some of these proteins are shared between ubiquitin and NEDD8 pathways, and some of them are specific for the neddylation cascade. One of main differences is the first step of neddylation pathway, where Uba1 and Uba3 (Nae1) interact specifically with the alanine residue 72 in NEDD8 (while in ubiquitin is Arginine) allowing Uba3 to bind NEDD8 and repel ubiquitin[163]. However, it has been shown that under stress conditions and low levels of ubiquitin, NEDD8 can be charged by Uba1 and be incorporated in ubiquitination cascade. This is one of the main obstacles for identifying novel NEDD8 targets (most of the detected targets could be false positives because they are ubiquitination targets that have been modified with NEDD8 instead of ubiquitin). Another main difference between the two post translational modifications is that NEDD8 E2 like Ubc12 recognizes specifically a motif in Uba3, preventing the interaction between E1s and E2s from ubiquitination and neddylation.

2.5.4. NEDD8 substrates and biological roles of NEDD8

Cullins are the proteins that function as scaffolds for the CRLs [196]. The family of Cullins is composed in humans of 9 proteins: CUL1, 2, 3, 4A, 4B, 5, and 7, Apc2 (it is one of the proteins that form the anaphase promoting complex/cyclosome), and PARC (parkin E3 ubiquitin ligase). Cullins are the best known target of neddylation, and they have to be neddylated to be able to mediate the ubiquitin transfer in the CRLs[197]. Cullin neddylation changes the conformation of the Cullin C-terminus and the Ring-domain of Rbx1 allowing the correct interaction with the ubiquitin E2 ligase. The neddylation of Cullins increase the ubiquitylation activity of CRLs because it reduces the distance between the substrate recognition subunit (function normally developed by adaptor proteins) and the E2[198], improving both the transfer of the first ubiquitin and the polyubiquitination[197]. Cullin neddylation also allows dissociation of the CRL with CAND1, which inhibits the activity of non-neddylated CRLs not allowing the interaction with the adaptors and substrate recognition components[191]. However, CSN-mediated deneddylation has the reverse effect on the activity of CRL-based E3s, and the CSN also recruits the deubiquitinating

enzyme Ubp12/USP15 to prevent ubiquitin chain assembly by CRLs[199]. The dynamic cycle of Nedd8 conjugation and deconjugation was shown to be essential to maintain CRL fully active. The removal of any CSN subunit or the interaction with CAND1 leads to a reduced CRL activity[197]. Neddylation and the binding of CAND1 do not determine the activation of the Cullins. Instead, it is the abundance and binding of the adaptor proteins which determine the activation of the CRLs[200]. In this model, neddylation allows the conformational change in the CRL but it is the binding of the adaptor protein, which allows the CRL to be fully active.

2.5.5 Main neddylation targets

The number of described NEDD8 targets has increased notably over the last few years. Since its discovery in 1992, many different groups have tried to identify the range of neddylated proteins in cells[201]. Unfortunately, the main limitation has been the high number of false positive targets detected in the lysates analyzed. In these assays, NEDD8 overexpression, which is required for the detection of neddylated proteins in cellular cultures, produces a disequilibrium in NEDD8 ubiquitin homeostasis[201,202]. This disequilibrium causes E3 ligases that can bind both ubiquitin and NEDD8 to transfer NEDD8 from E2 enzymes to targets that were supposed to be ubiquitinated and, as a consequence, producing a high amount of putative neddylated proteins that are ubiquitination targets instead. Nowadays the range and specificity of detection of the modern mass spectrometry devices has increased and has bypassed this issue with the false positives.

Although NEDD8 and ubiquitin are similar in structure and sequence, they have their own functions and enzymatic machinery. Some E3 ligases are shared between both pathways but NEDD8 has its own E2 ligases, UBE2M,UBE2F[203] and UBC12[204]. NEDD8 can regulate the activity of its targets by producing conformational changes or allowing the exposure of Nuclear import/export signals[205]. It has also been reported that neddylation could prevent ubiquitination[206] and promote nuclear aggregation protecting nuclear UPS from proteotoxic stress upon proteotoxic stress[207].

As previously discussed, one of the main roles of NEDD8 in cells is the activation of the Cullins by inducing a change in their conformation to allow the ubiquitin transfer between the E2 and the target protein[197]. Neddylation is essential for the ubiquitination and degradation of the required targets. Neddylation inhibition can lead to DNA damage responses, autophagy, apoptosis, and abnormal cellular responses[208]. CRLs are responsible for the ubiquitin-mediated degradation of more than 20% of cellular proteins.

2.5.5.1 Cell Cycle and Cancer.

BCA3 breast cancer-associated gene (BCA3) levels are elevated in breast cancer tissue compared to healthy breast tissue[209].When neddylated, BCA3 is able to recruit SIRT1, a class III histone deacetylase, to modify gene expression. BCA3 neddylation allows it to bind p65. Only when BCA3 is neddylated, it can bind p65 and regulate cyclinD1 expression[210].

EGF induces EGFR neddylation , which allows its ubiquitination, internalization and degradation[211].

TGF-β is a cytokine which regulates gene expression during development and participate in proliferation and differentiation[212]. The Casitas B-lineage lymphoma (c-Cbl) regulates TGF-β signaling by neddylation of its receptor Type II Receptor (TßRII)[213]. This neddylation stabilizes the protein and stimulates the endocytosis to EEA1-positive early endosomes. This alternative endocytosis prevents its internalization to caveolin positive compartments where it is ubiquitinated and degraded. By removing the TßRII receptor from the membrane, c-Cbl desensitizes cells to TGF-β , which is very common characteristic observed in the development of many cancers[214].

2.5.5.2 Transcription Factors

P53 is a tumor suppressor protein which activates the transcription of hundreds of genes related with DNA damage repair, cell cycle arrest, apoptosis and senescence[215]. Neddylation by Mdm2 or FBXO11 inhibits its transcriptional activity[216]. Neddylation leads p53 to poly-ubiquitination and degradation. On the other hand, ubiquitination of p53 can also modify its cellular localization, blocking its transcriptional regulation activity[217].

P73 is important for the regulation of neural stem cell maintenance, and it is regulated by different PTMs. Neddylation reduces its stability after activation of the DNA damage response. Neddylation of p73 by Mdm2 changes its location to the cytoplasm, preventing its transcriptional activity. Only Tap73 isoform can be neddylated[218].

APP and its nuclear amyloid precursor protein intracellular domain (AICD) play a critical role in Alzheimer's disease pathogenesis. APP protein is inhibited by neddylation by BP1 protein. The consequences of APP inactivation during development is a deficient nervous system development[219].

E2F1 neddylation can affect E2F1 function and the capacity of binding to its targets. De-neddylation by SENP8 reduces p73 expression and apoptosis induced by E2F1 or DNA damage[220].

Mdm2 neddylates HuR (Human antigen R) in the cytoplasm, which stabilizes HuR, ensuring its nuclear location and thus avoiding its ubiquitination and degradation. HuR regulates mRNA expression of mdm2, establishing a cooperative influence for tumor cell growth[221].

2.5.5.4 Mitochondria

Neddylation inhibition using the Nae1 inhibitor MLN4924 can induce mitochondrial fission-to-fusion conversion in breast cancer cells. This conversion is caused by the inhibition of ubiquitination and degradation of fusion-promoting protein mitofusin 1 (MFN1) by SCFβ-TrCP E3 ligase and the translocation blockade of fusion-inhibiting protein DRP1 in the mitochondria[221]. Strikingly, the induction of mitochondrial fusion was independent of the cell cycle phase, conferring cellular survival. The neddylation inhibition blocks TCA cycle and increases mitochondrial OXPHOS[223].

Parkin is a mitochondrial E3 protein which recognizes proteins from the outer membrane of the mitochondria. It mediates clearance of damaged mitochondria via mitophagy and the proteasome. Moreover, Parkin increases cell survival inhibiting both mitochondrial dependent and independent apoptosis pathways[224].

2.5.5.5 Hypoxia

Hif1α is a dimeric transcriptional complex which participates in the maintenance of oxygen and energy homoeostasis. In normoxic cells, it is ubiquitinated and degraded by the UPS but in response to an hypoxic stress, it is upregulated, increasing blood flow and inflammation, activating vascular endothelial growth factor (VEGF), heme oxygenase-1, nitric oxide synthase (NOS) and cyclooxygenase-2 (COX-2)[225]. Neddylation inhibition activates Hif1α, which triggers the response to oxidative reactive species, stimulating angiogenesis, migration and survival in tumoral cells. Neddylation inhibition activates Hif1α through PI3k-Akt pathway, which activates zinc finger E-box binding homeobox 1 (ZEB1) stimulating the epithelial to mesenchymal transition (EMT)[226].

2.5.6 Role of neddylation in the nervous system

NEDD8 is the most abundantly expressed UBL in neurons[227]. Since its discovery in 1992, NEDD8 has been related with different targets in the nervous system, including APP, PSD-95, APPBP-1, AChR and ß catenin. Moreover, it has been linked with different neurodegenerative diseases, such as Parkinson and Alzheimer's disease. The main functions of neddylation in the nervous system have been related with the Cullin RING ligases activity and the degradation of proteins by ubiquitin proteasome system[201].

Neddylation is vital during the differentiation of neural progenitor cells (NPCs) because of its role downregulating the EGFR signaling cascade. When neddylated, APPBP-1 is responsible

for EGFR and APP signaling downregulation. Moreover, APPBP-1 knockdown causes an impairment in neurons differentiation[228].

PSD-95, a scaffold protein present in the axons, was found to be neddylated at lysine residue 202 [227], and its inhibition led to a destabilization of the neural spines and a reduction in their amount. Subsequently, they performed a serial NEDD8-ubiquitin substrates profiling (sNUSP) and found 607 neddylation sites regulated by NEDP1 and MLN492[229]. They reported cytoskeleton defects caused by neddylation inhibition, which were related with the activity of cofilin. Cofilin activity was impaired when it was non-neddylated, affecting neuronal growth.

Scudder et al inhibited neddylation in dissociated rat hippocampal neurons using MLN4924, which caused a reduction in surface glutamate receptor levels, dendritic spine width, and spine density and synaptic strength[230]. Those results suggest that neddylation is involved in the maintenance of synapses. Similarly, it has also observed that neddylation inhibition affects long-term potentiation (LTP) and long-term depression (LTD), which are the main manifestations of synaptic plasticity [231].

APP protein is the precursor of amyloid β (Aβ) protein and its misfolding is the main cause of Alzheimer's disease. In fact, APP-BP1, a protein that was identified because its interaction with APP is one of the subunits that conforms Nae1. Overexpression of APP-BP1 in primary neurons causes apoptosis through ß catenin pathway and this over activation leads to a reduction of cell to cell adhesion and ß-catenin degradation[232] . When neddylation is blocked, the apoptosis mediated by APP-BP1 is inhibited and neurons enter in cell cycle despite being non-mitotic cells[232].

The degradation of APP starts in the lysosome after its internalization. When a familiar AD mutant APP protein is exogenously expressed in neurons, it increases APP mediated endocytosis that depends on APPBP1[233]. Neddylation is inhibited by APPBP1 downregulation, which causes the accumulation of APP and ß-secretase cleaved C-terminal fragment of APP and Aß[234]. Those results suggest that neddylation of APP signals could stimulate APP degradation reducing its signaling pathway.

A recent study revealed that ß-catenin is neddylated and this post translational modification is vital for correct cortical development. Neddylation inhibits Wnt/ß-catenin, allowing migration and differentiation of the neurons. Upon neddylation inhibition, ß-catenin accumulates in the nucleus[235].

The GDNF/Ret/Akt signaling pathway is key for the correct development of the enteric nervous system (ENS) and kidney[236]. The group of L. Zhang demonstrated that NEDL2-mediated upregulation of GDNF-stimulated Akt activity was dependent of its NEDD8 ligase activity but not its ubiquitin ligase activity. This results suggest that NEDL2 NEDD8 ligase activity is essential for

ENS and kidney development[237]. Furthermore, they demonstrated the role of NEDL2 as a scaffold protein for recruiting SHC, Grb2, PI3K (p110 and p85), PDK1 and Akt promoting their signaling transduction cascade.

Fragile X associated tremor/ataxia syndrome (FXTAS) is a neurodegenerative disorder caused by an increase in CGG repeats in the 5' untranslated region (UTR) of the fragile X mental retardation 1 gene (FMR1)[238]. When neddylation levels are reduced, there is an increase of neurodegeneration symptoms, while an upregulation of neddylation could rescue these phenotypes[239]. The study showed that Sima protein, a target of Cul3 and Vhl, could regulate rCGG repeat-mediated toxicity found in FXTAS[239]

Autophagy plays a crucial role in nervous system homeostasis, regulating the degradation of malfunctioning mitochondria and preventing the aggregation of proteins that can cause neurodegenerative diseases like PD or AD[240]. It also acts in the maintenance and pruning of neuronal synapses during development and the degradation of neurotransmitter receptors[241]. A study showed that treatment of mice with MLN4924 led to a reduction of p62 levels in brain tissue. P62 is a protein which participates in the regulation of mitophagy and autophagy, implicating neddylation in the regulation of autophagy and in the pathogenesis of these disorders.

In summary, Neddylation is associated with neurodegenerative diseases, such as Parkinson disease or Alzheimer disease, the stability of the neural spines, neuronal growth , Wnt/ß-catenin regulation during neuronal differentiation, autophagy and mitophagy regulation.

3 MATERIALS AND METHODS

3 MATERIALS AND METHODS

3.1 ANIMALS

All the experiments performed in this project were done in accordance with the International Animal care and Use committee standards and the Spanish Guide for the Care and use of laboratory animals. The procedures developed in this thesis follow the ethical guidelines establish by the Biosafety and Welfare Committee at CIC bioGUNE. The animal facility at CIC bioGUNE is accredited with the Assessment and Accreditation of Laboratory Animal Care (AAALAC).

Animals used in the experiments mentioned were handled in accordance with the European Communities Council Directive at CIC bioGUNE, under standard housing conditions (22± 2 ºC, 55 ±10 humidity, 12 hours day/night cycle) and with *ad libitum* access to food and water. They were fed with a standard diet (Harlan Teckad).

All experiments and procedures were planned to reduce as much as possible the number of animals and minimize their suffering.

3.1.1 Animal strains

For the experiments in this thesis, the following strains were used C57/BL6J animals and Wistar rats. To generate the constitutive Nae1 knockout mice (*Nae1* cKO), NAE1 floxed mice were crossed with an *MPZ*-cre line[242], which expresses Cre recombinase specifically in Schwann cells from embryonic day E14.5 (Strain #017927; The Jackson Laboratory). We generated NAE1 floxed by crossing a transgenic mouse line bearing an NAE1 "knockout-first" allele ($Nae1^{tm1a(EUCOMM)Wtsi}$) (obtained from the group of Maria Luz Martinez Chantar at CIC bioGUNE) with an ACTB-FLP (Strain #005703; The Jackson Laboratory) to remove Frt-flanked neo cassette. We also generated an inducible Nae1 knockout mice (*Nae1 i*cKO) by crossing NAE1 floxed mice were crossed with an $Mbp^{tm2(EGFP/cre/ERT2)Wtsi}$ line, which expresses Cre recombinase specifically in myelinating glial cells (Schwann cells and oligodendrocytes) after treatment with tamoxifen.

3.2 GENOTYPING

Genotyping was performed on genomic DNA from mice tails or toe samples. 100 µl of lysis reagent (DirectPCR lysis reagent tail, Viagen Biotech) mixed with 4 µl of proteinase K (22 mg/ml, Proteinase K, Roche) was used to extract DNA from each tail or 50 µl lysis reagent + 2 µl Proteinase K in case of extracting from toes. The samples were incubated at 55 ºC while shaking for 3-16 hours and then at 85 ºC to inactivate the protease. A 10 µl PCR reaction adapted to

each of the primers was performed with 5µl of DreamTaq Green PCR Master Mix (Thermo Scientific), 0.5 µl of primer mix (10um) and 4µl of Nuclease free water H_2O (VWR).

The amplified samples were then loaded on a 2% agarose gel (Agarose D1 Low EEO, Pronadisa) prepared with TAE 1X buffer [40 mM Tris (pH 7.6), 20 mM acetic acid, 1 mM EDTA] and Red Save^{Tm} Nucleic Acid Stain (1:20000, Intron). We loaded 5ul of 1kb DNA marker (Invitrogen) in one of the wells. The gel was run at 135 V for 30 min in TAE 1X buffer in horizontal electrophoresis (Gel XL-Ultra V2, Labnet). Once the 30 min are over, a picture of the gel was taken in a transilluminator with UV light. Primers for genotyping by PCR are available in Table 1.

Gene	Primers	Annealing Tª	Bands size
MPZ-Cre	MPZ-Cre Fw: TAAGCAATCCCCAGAAATGC MPZ-Cre RV: ATGTTTAGCTGGCCCAAATG	55ºC	MPZ-Cre+= 500bp
MBP-Cre ^{ERT2}	MBP-Cre Fw: CATTTGGGCCAGCTAAACAT MBP-Cre RV: TAAGCAATCCCCAGAAATGC	58ºC	WT= 636bp MUT= 336bp
ER/EF (Nae1)	Nae1- Fw: ATGTGTGGGAGGAAGTCTGAATGAA Nae1- RV: TGAGAGAAAAGAGTCCCAAGAACGA	62ºC	Flox ≈ 450bp WT ≈ 300bp
Recombination PCR	L3F: TGGGTTTAGCTCACTTTCTAATCTGG L3R: TGTGTGCATGTGCGTGTGTAGTTTA	61ºC	Flox ≈ 600bp MUT ≈ 300bp

Table 1. Genotyping primers. Table showing Annealing temperatures and expected band sizes of the different primers used in genotyping PCRs.

3.3 CELL LINES

3.3.1 HEK293T

HEK93T cells were used for lentiviral production. They were maintained in a complete growth medium prepared with: DMEM, 10% FBS (Gibco), 0.1mM, 1mM sodium pyruvate (Gibco), 2mM L-glutamine (Gibco) and 1% A/A antibiotic/antimitotic (Gibco). Cells were incubated at 37 ºC and 5% CO_2.

3.3.2 Immortalized Schwann cells

Immortalized normal human Schwann cell line (iHSCλ2) was obtained from Nancy Ratner (Cincinnati children's hospital medical center). The cells were maintained in DMEM supplemented medium with 10% FBS and 1% A/A under standard culture conditions at 37ºC

degrees and 5% CO_2. These cells were used to check the effects of the inhibition of neddylation by MLN4924.

3.3.3 IMCD3 cells

Inner medullary collecting duct (IMCD3) were maintained in F12 supplemented medium with 10% FBS and 1% A/A under standard culture conditions at 37ºC degrees and 5% CO2. They were used to test the inhibition of cullins by lentiviral infection.

3.3.4 Primary rat Schwann cells

Primary rat Schwann cells were used for in vitro culture assays. Schwann cells were isolated from Wistar rat sciatic nerves and brachial plexus at postnatal day 3-5 (P3-5). The sciatic nerves were dissected, placed in ice cold Leibovitz's medium (Gibco) supplemented with A/A. The epineural sheath was removed with sharp forceps and the help of a dissection lens. To dissociate the nerves, an enzymatic cocktail consisting of 100µl of 0.25% trypsin (Gibco) and 100µl of 0.4% collagenase mix per rat at 37 ºC 5% CO_2 and 95% humidity was used. The nerves were incubated in the enzymatic cocktail for 35 minutes and then the tissue was triturated to further dissociate the tissue. An equal volume of DMEM with 10% FBS was then added, and this mix was centrifuged for 10 min at 1000 rpm and 4 ºC. The supernatant was discarded, and the cell pellet was suspended in DMEM supplemented with 10% FBS and 10^{-3}M AraC. The cells were then cultured onto PDL (Sigma-Aldrich) and laminin-coated 3 5mm tissue culture dishes for 3 days. The serum on the medium stimulates fibroblast proliferation in the cultures while the presence of anti-mitotic compound AraC blocks the replication and kills them, leaving relatively pure Schwann cell cultures.

Reverse immunopanning was carried out to remove the few remaining fibroblasts. For this, petri dishes were coated with Thy1.1 antibody and Schwann cells added to them. Fibroblasts attach to the surface of the dish, while Schwann cells remain floating in the culture medium, and can be easily recovered for further expansion.

The antibody coating was performed by adding first rabbit anti-mouse IgG (DAKO) (7 ml 590 mM Tris pH 9.5 and 50 µl IgG per dish) to 90 mm petri dishes (Falcon) and then treating the dishes with Thy 1.1 antibody [4ml OX-7 supernatant, 2ml L15 medium and 400 µl 35% BSA (Sigma-Aldrich) per dish]. Schwann cells, after 3 days of treatment with AraC (see above) were treated with 0.25% trypsin-EDTA (2,2,' 2'', 2'''-Ethane-1,2-diyldinitrilo-tretracetic acid; Gibco) to detach the cells from the dishes, and then centrifuged and resuspended in 10ml DMEM containing 10% FBS. Finally, the cell suspension was added to the Thy 1.1-coated dishes and

cultured at 37 ºC, 5% CO_2 and 95% humidity for 20 min. While fibroblast become attached to the dishes, Schwann cells remain in cell suspension and can be recovered, pelleted by centrifugation and resuspended in expansion medium (see below) to be then cultured onto PDL and laminin-coated dishes. The medium was replaced every 3 days until the cells were confluent.

Schwann cell specific mediums used:

1. **Defined Medium** : DMEM/F12 (Gibco) supplemented with SATO [(100 µg/ml bovine serum albumin (BSA; Sigma-Aldrich), 100 µg/ml transferrin powder (Sigma-Aldrich), 16µg/ml putrescine; 60ng/ml progesterone (Sigma-Aldrich) and 40ng/ml sodium selenite (Sigma-Aldrich) in Neurobasal medium (Gibco)], 1X B27 supplement, 0.101 mg/ml of 3,3',5-Triiodo-L-thyronine sodium salt (T3, Sigma-Aldrich), 10mM Insulin, 1% L-glutamine and 1% A/A.
2. **Expansion medium**: Defined medium supplemented with 0.5% FBS, 10 ng/ml of neuregulin (NRG1, R&D Systems) and 2µM of forskolin (Calbiochem).

3.4. CELL CULTURE

3.4.1 EdU proliferation kit

To quantify cell proliferation, we analyzed DNA synthesis using Click-it EdU proliferation assay kit for imaging (Thermo scientific). This kit performs a copper catalyzed covalent reaction between an azide (alexa fluor dye) and an alkyne (EdU). Because of the small size of the dye azide, the detection of the incorporated EdU is efficient. Thus, 10µM EdU was added to cultures for 4h at 37 and 5% CO2. The cells were fixed by incubation with 3.7% formaldehyde for 30 min at RT and then they were permeabilized with 0.5% Triton X-100 for 20 min. For the staining, 0.45ml of click-iT reaction cocktail was added per coverslip, prepared following manufacturer's instructions. 50ng/ml of DAPI (Merck) dye was used for 30 min at RT to stain DNA.
An AxioImager.D1 fluorescent microscope 20X objective (Zeiss) was used to take 4 pictures from different fields of each coverslip.

To visualize proliferation in vivo, an intraperitoneal injection of EdU of 100mg/kg was administered in the animals. 5h later, animals were sacrificed and both sciatic nerves were extracted and fixed in 3.7% formaldehyde (Santa Cruz Biotechnology) in individualized small plastic cassettes overnight. The next day, the nerves were washed 3 times in PBS 1X and then cryoprotected in 30% sucrose solution overnight. The samples were then introduced in plastic molds with OCT and frozen over dry ice. Samples were stored at -80 ºC. 10µm sections were taken with a cryotome and placed onto superfrost slides.

For EdU staining, the slides were warmed at room temperature, washed with PBS, permeabilized with 0.5% Triton X-100 for 10 min, washed with PBS, blocked with 1% BSA, 0.1% triton in PBS for 30 min, washed with PBS and then click-iT protocol was followed using 0.1ml of Click-iT reaction cocktail per sample. This cocktail was prepared following manufacturer's instructions. 50ng/ml of DAPI (Merck) dye was used for 30 min at RT to stain DNA.

3.4.2 In vitro Schwann cell myelination assay

An increase in intracellular cAMP levels in Schwann cells produces an activation of myelin related genes such P0 (MPZ), Krox20 in rat and human Schwann cell cultures[83]. This is accompanied by a downregulation in the expression of negative regulators of myelination (c-Jun, Notch and Sox2) and genes expressed in immature SCs (as $p75^{NTR}$, GFAP), making the supplementation of cAMP analogues in Schwann cell cultures a useful *in vitro* model of myelination.

Purified and expanded Schwann cells were dissociated and counted and seeded onto PDL and laminin-treated dishes or coverslips and cultured overnight in starvation medium (defined medium (see section 2.4) supplemented with 0.5% FBS). Then they were treated with 4mM N^6, 2'-O-Dibutyryladenoside 3'-5'-cyclic monophosphate sodium salt (db cAMP), which is a cell permeable and non-hydrolysable cAMP analogue, for 48h to induce upregulation of myelin differentiation markers.

3.4.3 Plasmid amplification

The medium for the bacterial growth was prepared by dissolving 8 g of LB BROTH1 (Pronadisa) in 400 ml H_2O. To prepare LB agar plates, 7.2 g of Miller LB agar was dissolved in 200 ml H_2O, and both medium were autoclaved right after preparing them. Once autoclaved, the bottles were opened close to a flame (in a clean work area) and the antibiotic of interest was added in a 1:1000 dilution. For the LB plates ,15-20 ml of the medium per petri was distributed, avoiding the formation of bubbles. Petri dishes were allowed to cool until they they solidified, and the plates were sealed with parafilm (Bemis) and kept inverted at 4ºC in a for 1 month.

An aliquot of bacterial stab or a glycerol was opened near the flame and a small amount of it was spread with a sterile tip on an LB agar plate prepared with the selected antibiotic. The plates were incubated overnight at 37 ºC. The next day, a pre-culture was established by picking a single colony and placing it in 1ml of LB broth medium (with the appropriate antibiotic) in a 15ml sterile tube. The tubes were placed 4-8h in a shaker set at 37°C, 200 rpm to establish a pre culture.

To amplify the plasmids, the bacterial precultures were inoculated with 25 ml, 100 ml or 250 ml of LB broth containing the appropriate antibiotic for mini-, midi- or maxi- preparations respectively, and incubated overnight for no more than 16h in a shaker at 200 rpm and at 37 ºC

3.4.4 Silencing of gene expression by lentiviral infection.

shRNAs were used for silencing gene expression in Schwann cells and were purchased from Merck.

3.4.5 Production and concentration of lentivirus in HEK293FT cells

3 x 10^6 HEK293T cells (for a P100 plate) were plated with DMEM supplemented with 10% FBS during the morning and then transfected during the evening with Turbofect (Thermofisher). All the plasmids used were mixed in serum free DMEM with A/A (See table).

Plasmid	Amount of plasmid per dish
MDL	2.55 µg
VSV-G	1.37 µg
REV	0.98 µg
Plasmid of interest	10 µg

Table 2. Primer concentrations for the lentivirus production.

To this mix of plasmids, 18 µl of turbofect reagent was added, and mixed by pipetting following vortexing for 10 sec. The mix was incubated at RT during 20 min. At the end of the 20 min, HEK293T cells was medium changed to fresh DMEM/10% FBS (9ml), and plasmid mix added to the plates dropwise. The medium was removed again 6h later and substituted with 4ml of DMEM 10 % FBS**.** 48h later the supernatant of HEK293T cells was filtered with a 0.22 µm filter and replaced with fresh medium (DMEM, 10%FBS). The filtered supernatant was mixed with 1/3 of the volume with Lenti X concentrator (Takara Cat. Nos. 631231) and incubated at 4 ºC overnight or during at least 12h. The mixture was centrifuged at 1500g for 45 min at 4 ºC. The pellet obtained was resuspended in 100µL PBS (for a p100 plate) and frozen at -80 ºC. The next day, the HEK293T supernatant was filtered and concentrated again as the day before (Figure 6).

3.4.6 Infection of cells with lentiviral particles

For lentiviral of Schwann cells, 250,000 rats Schwann cells were plated per well of a PDL-laminin coated 6-multiwell plate. The next day, the culture medium was removed and substituted with 1ml expansion medium (see 2.4 primary Schwann cells) and 15 µl of

concentrated lentivirus. This medium was removed 6h later and substituted by 1.5ml of expansion medium per well. We kept one well as non-infected control (Figure 8). The Schwann cells were re-infected again the next day following the same instructions.

To select the transfected cells, 2 days after the last infection the selection antibiotic was added to the petri dishes at the established selection concentration for Schwann cells. This was done by performing a death curve with different concentrations in normal Schwann cells, and the minimum concentration inducing full death was selected. To check the efficiency of silencing, expression of relevant genes was analyzed by qPCR or WB.

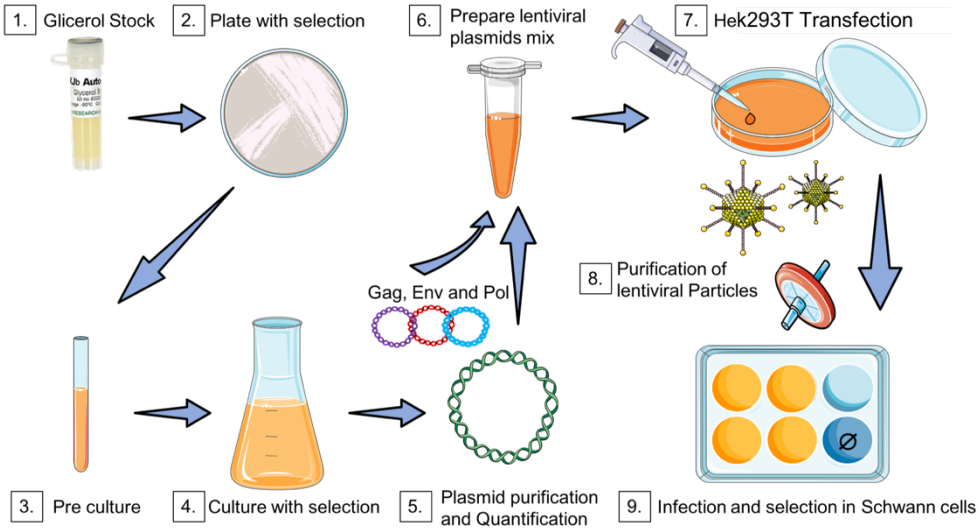

Figure 8. Plasmid amplification protocol and lentivirus production in Heck293T cells.

3.4.7 Protein Extraction

To extract proteins from cultured cells, an established concentration of cells were seeded per well in duplicates and incubated for 48h. Cells were washed twice with cold PBS (Gibco) and scraped in 200µl RIPA lysis buffer [1.6 mM NaH_2PO_4 (Merck), 8.4 mM Na_2HPO_4 (Merck), 0.1% triton X-100 (VWR), 0.1M NaCl (Ambicon), 0.1% SDS (fisher Scientific) in ddH_2O] supplemented with sodium deoxycholate (Merck), 1mM sodium fluoride and 1X protease and phosphatase inhibitor cocktails (Roche), IAA 1.84 mg/ml (Merck) and NEM 1.25mg/ml (Thermo Fisher Scientific). Immediately after, lysates were snap frozen, defrosted, vortexed and incubated on ice in order to improve the lysis process. After that, lysates were centrifuged for 30 min at 13,000 rpm and 4ºC and the supernatants were collected. To determine the total protein content, cell lysates were quantified using BCA protein assay (Bio-Rad) in a Synergy HT spectrophotometrer (Biotek). A protein standard curve was obtained using different concentrations of bovine serum albumin (BSA).

For sciatic nerve samples, a piece of nerve was excised and homogenized in supplemented RIPA buffer using the Precellys homogenizer (Bertin technologies). The protocol used was 5 cycles of: 6000rpm of 60s of of homogenization followed by an incubation of 5 min in ice, and a centrifugation of 5000 rpm 4 ºC for 5 min.

3.5 MOLECULAR BIOLOGY TECHNIQUES

3.5.1 Western Blot

Protein aliquots (8-10 µg each prepared with RIPA buffer to have the same volume) were denaturalized in 5X loading buffer [0.25 M Tris, pH 6.8 (VWR), 5% SDS (Fisher Scientific), 2-mercaptoethanol (Merck), 50% glycerol and bromophenol blue powder (Merck)] for 5 min at 95ºC. Samples were loaded on 8%, 11% or 15% tris-glycine SDS-polyacrylamide gels with Tris-glicine-SDS 1X buffer (BioRad) and transferred to a 0.2µm nitrocellulose membrane (Amersham) with transfer buffer 1X [Glycine (VWR), Tris (Trizma base, VWR), 20% Methanol (Panreac AppliChem) and ddH_2O] at 4ºC and 100V for 1h or 20V overnight. Membranes were blocked for 1h with 5% non-fat dry milk in TBS-T 1X [50 mM Tris, q50 MM NaCl (Sigma-Aldrich), pH 8.0) containing 0.1% Tween20 (TBS-T, Sigma-Aldrich)] and then incubated with specific primary antibodies at 1/1000 concentration in TBS-T (or 5% non-fat dry milk in TBS-T) overnight at 4 ºC. Next day, membranes were washed three times with TBS-T 1X for 15 minutes at RT, incubated with HRP (Horse Peroxidase)-linked rabbit or mouse secondary antibodies at 1/5000 concentration in blocking solution (5% non-fat dry milk) for 1h at RT and samples were developed with Clarity Western ECL substrate (BioRad). Membranes were exposed to X-ray films (Fujifilm) in a Curix Developer (Agfa) or in an Ibright (Invitrogen) machine with a multi exposition protocol adapted to the signal intensity detected in the membrane. Representative immunoblot pictures from a minimum of 3 experiments/biological replicates are shown in Results.

3.5.2 Ribonucleic acid RNA extraction and processing

3.5.2.1 RNA isolation

Total RNA was isolated from Schwann cells, after washing in PBS with Trizol® reagent (Thermo Fisher Scientific) according to the manufacturer's instructions. Total RNA was treated with DNAse I (Invitrogen) for 30 min at 37 ºC and cleaned with Genejet RNA cleanup and Concentration kit (thermos scientific) (the columns were eluted with 20-30µl). RNA concentration was determined using RNA BR Qubit® assay kit (life technologies) in a Qubit® 2.0

fluorometer (Life technologies) according to the manufacturer's instructions. RNA integrity was assessed by electrophoresis in a 1% agarose gel.

Antibody	Dilution	Host	Company
C-Jun	1/1000	Rabbit	Cell Signaling
Cullin 1	1/1000	Mouse	Santa Cruz Biotechnology
Cullin 2	1/1000	Mouse	Santa Cruz Biotechnology
Cullin 3	1/1000	Mouse	Santa Cruz Biotechnology
Cullin 5	1/1000	Mouse	Santa Cruz Biotechnology
mTOR	1/1000	Rabbit	Santa Cruz Biotechnology
MBP	1/1000	Mouse	Cell Signaling
MPZ	1/1000	Rabbit	Abcam
Nae-1	1/1000	Rabbit	Millipore
NEDD8	1/1000	Rabbit	Cell Signaling
Notch	1/1000	Rabbit	
SOX2	1/1000	Rabbit	Santa Cruz Biotechnology
ß-Actin	1/5000	Mouse	Sigma-Aldrich
TAZ	1/1000	Mouse	Santa Cruz Biotechnology
TAZ	1/1000	Rabbit	Cell Signaling
YAP1	1/1000	Mouse	Santa Cruz Biotechnology
YAP1	1/1000	Rabbit	Cell Signaling
Mouse IgG HRP linked	1/5000	-	Cell Signaling
Rabbit IgG HRP linked	1/5000	-	Cell Signaling
Fbxw7	1/1000		

Table 3. Antibodies used in WB experiments.

3.5.2.2 Reverse transcription RT followed by quantitative Polymerase Chain Reaction qPCR analysis.

A minimum of 200 ng of total RNA and up to 1µg was reversed transcribed in a 20µl reaction containing dNTPs (Invitrogen), random hexamers (Invitrogen), 0,1M DTT (Invitrogen), RNase OUT (Thermo Fisher Scientific), 5X Buffer (Invitrogen) and M-MLV Reverse Trascriptase (Thermo Fisher Scientific) according to manufacturer's instruction. Reactions were carried out in a thermocycler (Biometra). The resulting cDNA was diluted 1/5 with 80µl RNase free H_2O (Sigma-

Aldrich). QPCR was performed in a 5µl reaction mix containing 2.5µl PerfeCTa® SYBR® Green SuperMix® FastMix™ with low ROX reference dye (Quanta Biosciences), 0.5 µl of 10 µM primers and 2µl cDNA. All reactions were performed in triplicates in a QS6 Real – Time PCR System (Applied Biosystems). 40 cycles with a melting temperature of 60ºC, and 30 seconds of each step were used. Specific primers were designed with Primer Blast database (https://www.ncbi.nlm.nih.gov/tools/primer-blast/)(Table5) and synthesized by Sigma-Aldrich. Quantification was performed using the ΔΔCT method and data was normalized using *GADPH* mRNA as a Standard.

3.6 PROTEOMICS

Sciatic nerves were dissected from 15 days old mice and homogenized with a Fastprep machine in RIPA buffer supplemented with deoxycholate, IAA, NEM, phosphatase and protease inhibitors. The proteomic analyses were carried out at the CIC bioGUNE Proteomics Service. FASP protocol[243] was used for sample processing and digestion. Trypsin was added to a trypsin:protein ratio of 1:50, and the mixture was incubated overnight at 37oC, dried out in a RVC2 25 speedvac concentrator (Christ), and resuspended in 0.1% FA. Peptides were desalted and resuspended in 0.1% FA using C18 stage tips (Millipore). Peptides were analyzed in an LTQ Orbitrap XL mass spectrometer (Thermo Electron) coupled online to a nanoACQUITY UPLC System (Waters), and also in a novel hybrid trapped ion mobility spectrometry – quadrupole time of flight mass spectrometer (timsTOF Pro with PASEF, Bruker Daltonics) coupled online to a nanoElute liquid chromatograph (Bruker). Protein identification and quantification of the Orbitrap and TIMS data was carried out using Progenesis (Waters) or PEAKS software (Bioinformatics solutions), respectively.

3.7 RNA SEQ

RNA was isolated from 7 days old mice sciatic nerves. Total RNA was isolated following the Trizol reagent (Thermo Fisher Scientific) protocol. Total RNA was treated with DNAse I (Invitrogen) for 30 min at 37 ºC. Then the samples were cleaned with Genejet RNA cleanup and Concentration kit (Thermo Scientific) (the columns were eluted with 20-30µl ultra-pure water).

The samples were then processed by the Genomic platform at CIC bioGUNE to check their concentration and integrity and then, generate the sequencing libraries and further sequencing them. Thus, first, the RNA samples were analyzed with a Qubit RNA HS Assay kit (Thermo Fisher Scientific) to measure the quantity and Agilent RNA 6000 pico Chips (Agilent Technologies) to determine the quality of the samples.

The “Truseq Stranded Total RNA with Ribo-Zero Globin” kit (Illumina Inc) and “TruSeq RNA CD Index Plate” (Illumina) were used to prepare the sequencing libraries. The protocol followed was “TruSeq Stranded Total RNA Sample Prep-guide”. In brief, an amount of 250ng of total RNA was used for the cDNA preparation. SuperScript-II Reverse Transcriptase kit (Thermo Fisher Scientific) was used for the first cDNA strand synthesis and Illumina specific reagents were used for the second cDNA strand synthesis. The next step was the ligation of adaptors and A-tails followed by an enrichment PCR (30 sec at 98°C; 15 cycles of 10 sec at 98°C, 30 sec at 60°C, 30 sec at 72°C; 5min at 72°C and it was paused at 4°C). Libraries were quantified using Qubit dsDNA HS DNA Kit (Thermo Fisher Scientific, Cat. # Q32854) and visualized on an Agilent 2100 Bioanalyzer using Agilent High Sensitivity DNA kit (Agilent Technologies, Cat. # 5067-4626) and sequenced in an Illumina Inc. instrument.

3.7 IMMUNOHISTOCHEMISTRY

Sciatic nerves were dissected out, fixed in 3.7% paraformaldehyde overnight, washed 3 times with PBS 1X and then cryoprotected by incubating in 30% sucrose solution (in PBS). The nerves were removed, and excess sucrose solution removed by placing them on a filter paper and rapidly placed in a small plastic mold with OCT Q Path® medium (VWR), which was then frozen over dry ice, and kept at –80 ºC. The samples were cut in a cryotome (Leica) at 5µm thickness, and the sections placed onto Superfrost slides (thermos Scientific) and kept at -80 ºC. To stain the samples, they were defrosted, washed 3 times with 1X PBS, permeabilized with 0.5% triton in PBS for 10 min, blocked with 1X PBS with 1% BSA and 0.1% triton and incubated with the primary antibody at 1/100 concentration overnight at 4 ºC in a dark chamber. After washing 3 times with PBS, secondary antibodies at 1/500 concentration were added to the samples and incubated for 1h at RT (secondary antibodies are linked with an Alexa 488 or Alexa 545 fluorophore). After washing 3 times with PBS 1X, samples were incubated with DAPI 50ng/ml (Merck) for 30 min. Finally, slides were washed with PBS and mounted with Dako mounting medium (Agilent technologies).

Antibody	Dilution	Host	Company
MPZ	1/200	Rabbit	Abcam
Nae-1	1/100	Rabbit	Millipore
Mouse IgG Alexa488 linked	1/5000	Rabbit	Thermo Fisher Scientific
Rabbit IgG Alexa 533 linked	1/5000	Rabbit	Thermo Fisher Scientific

Table 4. Antibodies used in inmunohistochemistry experiments.

Digital images were acquired with an Axio imager A1 microscope (Carl Zeiss AG). The sections were analyzed in a blinded manner. Antibodies used for IHC are highlighted below.

3.8 MICROSCOPY

3.8.1 Confocal microscopy

Images were taken at 63X in a Leica TSC SP8 confocal microscope. At least 5 images were taken of each slide, counting 200 cells minimum per sample. DAPI 50ng/ml (Merck) was used to stain cellular DNA and to quantify the total number of cells in the samples.

3.8.2 Electron microscopy

3.8.2.1 Sample Preparation

Freshly extracted nerves were fixed with 2% glutaraldehyde (prepared in 0.1M sodium phosphate buffer) at 4 ºC overnight. The next day, the nerves were washed 3 times with 0.1M sodium phosphate buffer and stained with 1% osmium tetroxide (prepared in 0.2M sodium phosphate buffer) at 4 ºC overnight. The samples were then washed during 15 min with ddH_2O in rotation, stained with 4% Uranyl Acetate solution during 45 min at 4 ºC, followed by further washes with ddH_2O in rotation for 15 min. The nerves were then dehydrated with increasing concentrations of ethanol, starting with 25% for 5 minutes, 50% for 5 min, 70% for 5 min, 90 % for 5 min and 100% for 10 min. The 100% ethanol dehydration step was repeated a total of 4 times. After ethanol dehydration, they are treated 3 times for 10 min with 1,2-Epoxypropane (VWR), followed by incubation with a 1:1 mixture of epoxypropane and resin for 45-60 min. Samples were then incubated in a 1:1 mixture of propylene oxide and resin for 1hr and subsequently in resin alone overnight at RT. Samples were then transferred to fresh resin and incubated for a further 24hrs. Samples were placed in rubber coffin molds containing fresh resin and thermo-cured at 65 C for 16 hrs.

Resin preparation: 12g Epoxi 100 resin, 8g DDSA, 5g MNA and 16 drops of BDMA. Agar Scientific.

3.8.2.2 Semithin Section

Handmade glass knives or ultra-cut Diatome diamond knife (Leica) were used on an Ultracut E ultramicrotome (Leica, Germany) to cut 1µm semithin resin sections. Sections were collected in water and transferred to glass microscope slides, dried and stained with 0.1% toluidine blue in ethanol for 15 seconds before washing with ultrapure water and drying.

Semithin sections were visualized using a Nikon Optiphot-2 microscope and pictures taken at 20x or 60x magnification. Samples were sent for ultrathin processing at an Electron microscopy platform.

3.8.2.3 Electron microscopy

Ultrathin (50nm) sections were viewed in a Jeol 1010 transmission electron microscope (TEM), and photos acquired at various magnification.

3.9 ANIMAL PROCEDURES.

3.9.1 Nerve cut and nerve crush surgery protocol

Animals were weighed and injected 15 min before the surgery with carprofen/Rimadyl (4mg/kg)(Pfizer). Then they were anesthetized with 4% isofluorane (Zoetis). The right leg was trimmed to remove as much hair as possible. Betadine solution (*Iodopovidone*) was applied to the zone and then a small incision in the skin was performed with sharp scissors followed by a small cut in the muscle. Once the sciatic nerve was exposed, the nerve was cut with sharp scissors. Alternatively, for the nerve crush surgery, sciatic nerves were crushed by applying pressure with forceps on the nerves for 30 seconds. The muscle was sutured with a sterile monofilament surgical suture, and the skin sutured with 2-3 “reflex clips” (World precision Instruments).

3.9.2 Nerve extraction

To extract sciatic nerves, the animals were sacrificed by cervical dislocation. The legs of the animal were sprayed with 70% ethanol and the skin surrounding the legs was removed cutting with sharped scissors (FST). The muscle from the legs was cut and then the junctions of the sciatic nerves and muscles and surrounding tissue were removed. The nerves were cut close to the spinal cord and the end of the leg to maximize the amount of tissue extracted. In a clean culture dish, the epineurium was removed by using two sharp forceps (FST) carefully, trying to not damage the nerve. The nerve was snap frozen immediately.

3.9.3 Tamoxifen Induction

To induce the expression of the Cre recombinase in the inducible Nae1 conditional knockout mice (*Nae 1 i*cKO), 30- or 60-days old mice were injected with Tamoxifen (Sigma-Aldrich) at a concentration of 50mg/kg during 5 consecutive days. Tamoxifen was prepared by adding 10mg of tamoxifen in 100µl of ethanol and then adding 900µl of corn oil to the solution.

The mix was sonicated 3 times for 15 minutes at maximum potency and then incubated 2h at 55º protected from sunlight. The mix was vortexed every 30 min during incubation.

3.9.4 Sciatic functional index (SFI) Analysis

The sciatic functional index (SFI) is a widely used method to evaluate peripheral nerve function post injury, and in peripheral neuropathy models. Here, we used SFO analysis to examine nerve function after nerve crush surgery in *Nae 1 i*cKO mice. Nerve crush surgery was performed on 6 weeks old mice and during the next 8 weeks the animals paw prints were taken to calculate the SFI. For this, the mice were allowed to walk over a transparent methacrylate corridor of 50x15x12cm with a camera placed under the central part of the corridor for 1 min. Pictures of the prints were taken from the videos and analyzed in ImageJ to calculate the different distances below:

- **ETS** = Experimental Toe Spread (the distance between the first and fifth toes in injured paw of mice)
- **NTS** = Normal Toe Spread (the distance between the first and fifth toes in uninjured paw of mice)
- **EPL** = Experimental paw length (the distance between the first and third toe and the heel in injured paw of mice)
- **NPL**= Normal paw length (the distance between the first and third toe and the heel in uninjured paw of mice mice)
-

The formula used to measure SFI was:

$$\textbf{SFI} = 118{,}9\,\frac{(ETS-NTS)}{\mathrm{NTS}} - 51{,}2\frac{(EPL-NPL)}{NPL} - 7{,}5$$

Gene name	Commercial Code	Sequence 5'-3'
Cullin 1	TRCN0000279915	CCGGCCAATGTTGATGAGGTGGAATCTCGAGATTCCACCTCATCAACATTGGTTTTTG
	TRCN0000012771	CCGGCCAATGTTGATGAGGTGGAATCTCGAGATTCCACCTCATCAACATTGGTTTTT
	TRCN0000012768	CCGGCCGCACTTAAATCAATACATTCTCGAGAATGTATTGATTTAAGTGCGGTTTTT
Cullin-2	TRCN0000280155	CCGGGCATCCAAGTTCATATACTAACTCGAGTTAGTATATGAACTTGGATGCTTTTTG
	TRCN0000012774	CCGGGCCGACTATATGGACTGCTTACTCGAGTAAGCAGTCCATATAGTCGGCTTTTT
	TRCN0000012777	CCGGGCATCCAAGTTCATATACTAACTCGAGTTAGTATATGAACTTGGATGCTTTTT
Cullin 3	TRCN0000218332	GTACCGGGATAGAAAGTGGCCACATATTCTCGAGAATATGTGGCCACTTTCTATCTTTTTTG
	TRCN0000012781	CCGGCGAGATCAAGTTGTACGGTATCTCGAGATACCGTACAACTTGATCTCGTTTTT
	TRCN0000226117	CCGGGTGCGAGAAGATGTACTAAATCTCGAGATTTAGTACATCTTCTCGCACTTTTTG
Cullin 4A	TRCN0000353106	CCGGCCAGGATAGACAGTACCAGATCTCGAGATCTGGTACTGTCTATCCTGGTTTTTG
	TRCN0000012786	CCGGCCAGGATAGACAGTACCAGATCTCGAGATCTGGTACTGTCTATCCTGGTTTTT
	TRCN0000012784	CCGGCGAGACAAAGACAGTCCAAATCTCGAGATTTGGACTGTCTTTGTCTCGTTTTT
Cullin 4B	TRCN0000281899	CCGGGGTGATTCTTATACATCATTACTCGAGTAATGATGTATAAGAATCACCTTTTTG
	TRCN0000012792	CCGGCCATATAATTGATACCTGCTTCTCGAGAAGCAGGTATCAATTATATGGTTTTT
	TRCN0000012789	CCGGGCTGAATTTAAAGAGGGCAAACTCGAGTTTGCCCTCTTTAAATTCAGCTTTTT
Cullin 5	TRCN0000012793	CCGGCCCTTCATGTTGCACACTCTTCTCGAGAAGAGTGTGCAACATGAAGGGTTTTT
	TRCN0000012796	CCGGCGAGAGTCCTATGTTAATCTTCTCGAGAAGATTAACATAGGACTCTCGTTTTT
	TRCN0000012795	CCGGCCATCTCATGTCAAATGGAATCTCGAGATTCCATTTGACATGAGATGGTTTTT
Cullin 7	TRCN0000012719	CCGGCTCGTCTATCTGGTGCTAGAACTCGAGTTCTAGCACCAGATAGACGAGTTTTT
	TRCN0000012721	CCGGCCTCAGACATACCTACAAGCTCTCGAGAGCTTGTAGGTATGTCTGAGGTTTTT
c-Jun	TRCN0000042697	CCGGGAAGCGCATGAGGAACCGCATCTCGAGATGCGGTTCCTCATGCGCTTCTTTTTG
	TRCN0000229526	CCGGGAACAGGTGGCACAGCTTAAGCTCGAGCTTAAGCTGTGCCACCTGTTCTTTTTG
	TRCN0000229527	CCGGGCTAACGCAGCAGTTGCAAACCTCGAGGTTTGCAACTGCTGCGTTAGCTTTTTG
Nae 1	TRCN0000412912	CCGGATAGAATCTCATCCAGATAATCTCGAGATTATCTGGATGAGATTCTATTTTTTG
	TRCN0000112479	CCGGCCTGATATGATTGCAGATTCACTCGAGTGAATCTGCAATCATATCAGGTTTTTG
	TRCN0000112476	CCGGCCATACTCCATGGATTGTGATCTCGAGATCACAATCCATGGAGTATGGTTTTTG
NEDD8	TRCN0000273011	CCGGCAAGCAAATGAATGATGAGAACTCGAGTTCTCATCATTCATTTGCTTGTTTTTG
	TRCN0000012740	CCGGGCGGCTCATCTACAGTGGCAACTCGAGTTGCCACTGTAGATGAGCCGCTTTTT
	TRCN0000012741	CCGGCAAGCAAATGAATGATGAGAACTCGAGTTCTCATCATTCATTTGCTTGTTTTT
Sox2	TRCN0000424718	CCGGAGGAGCACCCGGATTATAAATCTCGAGATTTATAATCCGGGTGCTCCTTTTTTTG
	TRCN0000416106	CCGGCAAAGAGATACAAGGGAATTGCTCGAGCAATTCCCTTGTATCTCTTTGTTTTTTG
	TRCN0000420955	CCGGACCAATCCCATCCAAATTAACCTCGAGGTTAATTTGGATGGGATTGGTTTTTTTG

Table 5. shRNA sequences used in the silencing experiments.

Gene name	sense	Sequence 5'-3'
Cul 1 Rat	F	CCTAGTTCGGCGTTTGGGAA
	R	CACAGCAGCTCAGAAAGAATGT
Cul 2 Rat	F	GGGGGCTTCGTCCTTCAC
	R	AGCAGCTTGTTCCACGTCTC
Cul 3 Rat	F	CGGAAGCACATACTGCAAGTC
	R	GGGACTGGAGGGCTCTAACA
Cul 3 Rat F	F	CAGGCAACATCTACAGGCAAC
	R	AGGCCAATATCCCGTTGTGAG
Cul 4a Rat	F	GCTTCACGAAGCGGTCAAGG
	R	GGGGAGACTTTGTGAGAGCAC
Cul 4a Rat	F	AGAGCAGCACATCCATCAGGTA
	R	TTCTCTGAAGGGGAGGATCTGG
Cul 4b Rat	F	TCCAGTGACTCCGGCAAAAA
	R	GGCGCTCTTGATTGGAGGTT
Cul 5 Rat	F	AGAGCACTCCGATACTTAGAAACA
	R	AATGAGGTCACCAGTGCGTT
Cul 7 Rat	F	GTCCTGGTAGGGAAGCGAAAC
	R	CTCTGAGATGGGGGATCTTGG
NEDD8 Rat	F	CACTCTAGCCGCCTGTAACC
	R	ACGCTCCTTGATTCGTTCCA
Sox2 Rat	F	CAAAAACCGTGATGCCGACT
	R	GAAGCGCCTAACGTACCACT

Table 6. Primers used in the qPCR.

4 HYPOTHESIS AND OBJECTIVES

4 HYPOTHESIS AND OBJECTIVES

Over the last years, many studies have identified the signals and molecules regulating Schwann cell function during development and in disease situations. Schwann cell myelination, for instance, is regulated by several extrinsic and intrinsic signals, from transcription factors such as Egr2, Sox10, c-Jun to signaling pathways like PI3K, MAPK and Akt/mTOR.

Posttranslational modifications like ubiquitin and Ubiquitin like proteins (UBLs) have emerged as critical regulators of cell functions such as cell cycle, protein degradation and autophagy. Their role in the peripheral nervous system still remains obscure. Neddylation has been shown to regulate various pathways, several of which are key for Schwann cell myelination, in other cellular systems.

Based on this, we **hypothesize** that neddylation could be essential in the regulation of Schwann cell differentiation, directly controlling the relative levels of mayor regulators of Schwann cell myelination.

The objective of this study is to examine the role of neddylation in Schwann cell myelination. For this purpose, we will generate various models to inactivate Nae1, the main enzyme responsible for neddylation, specifically in Schwann cells using a conditional cre-lox technology and examine the importance of this pathway in Schwann cell myelination. We will also examine how neddylation affects the key pathways related to this process.

In addition, using inducible knockout models, we aim to examine whether neddylation is important for maintenance of mature myelinating sheaths, and whether it is involved in the nerve regeneration process after nerve injury.

Overall, these objectives could improve our understanding of the role of neddylation in the function and myelination of the Schwann cells during development and in response to injuries in the peripheral nerves.

5 RESULTS

5 RESULTS

5.1 Neddylation is highly active in myelinating Schwann cells

In contrast to the central nervous system, we know very little about the role of neddylation in the peripheral nervous system, except that neddylated proteins were detected in Schwann cell bodies and paranodal loops[244]. To examine a potential role of neddylation in Schwann cell myelination, we analyzed by quantitative real-time polymerase chain reaction (qRT-PCR), the levels of the mRNAs encoding both E1-NAE subunits (*Uba3* and *Nae1*), the E2 *Ubc12* and *Nedd8*, as well as deneddylases *Cops5* and *SenpP8 in* sciatic nerves from mice at different ages that broadly correspond to the main stages of the myelination process[9]. Thus, nerves were obtained from newborn mice (NB), which are highly enriched for immature Schwann cells, postnatal day 7 and 15 (P7 and P15) nerves, which contain mostly actively myelinating Schwann cells, and P30 and P90 nerves, which contain terminally differentiated myelinating Schwann cells.

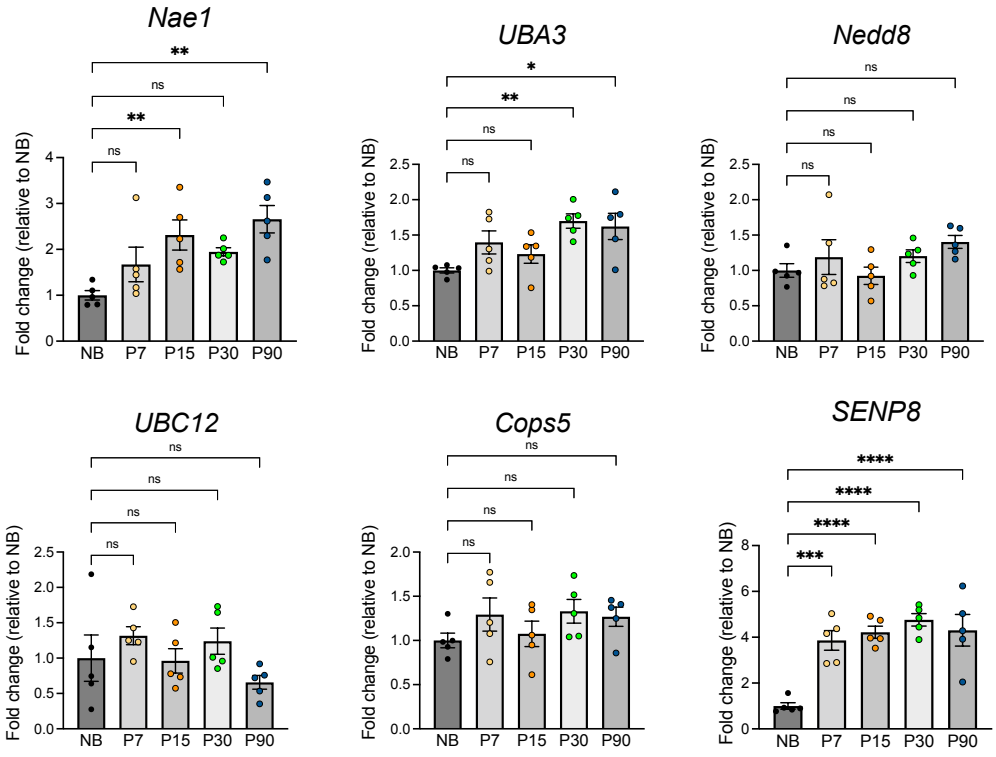

Figure 9. Neddylation pathway components are expressed in postnatal Schwann cells. qRT-PCR analyses show that the neddylation genes are expressed and regulated in sciatic nerves from mice at different ages that broadly correspond to the main stages of the myelination process. Data are presented as mean ± SEM. N=5 per condition. One-way ANOVA with Tukey's multiple-comparisons test. n.s. not significant; *P < 0.05; **P < 0.01; ***P < 0.001; ****P < 0.0001.

We found that these genes were highly expressed in Schwann cells with minimal changes across development, with the notable exception of *Senp8*, which increased dramatically in postnatal nerves (**Figure 9**).

To confirm these data, we performed Western blot analyses and found that Nae1 was highly expressed during the differentiation of Schwann cells, and notably, we found high levels of neddylated proteins at ages, corresponding to the onset of myelination (NB to P7), and a sharp downregulation as the actively myelinating Schwann cells complete their maturation to terminally differentiated Schwann cells (P15 onwards). Western blot analyses also show progressive upregulation of myelin proteins MPZ and MBP, and sharp downregulation of negative regulators c-Jun and Sox2, as immature Schwann cells undergo the myelination process (**Figure 10**).

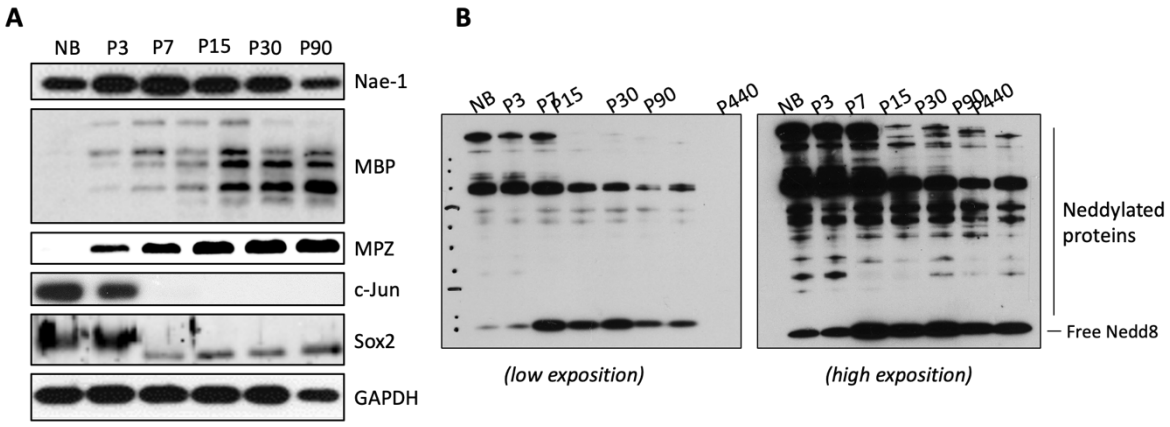

Figure 10. Neddylation pathway components are expressed in postnatal Schwann cells. WB analyses of sciatic nerves from mice at different ages that broadly correspond to the main stages of the myelination process. (**A**) Myelin proteins MBP and MPZ are upregulated as the Schwann cells differentiate and conversely, the negative regulators c-Jun and Sox2 are downregulated. Nae1 is highly expressed during this process, although there is a significant downregulation in mature nerves at P90. (**B**) Neddylated proteins are highly expressed during the initial stages of the myelination process (NB to P7), followed by a sharp decrease later on. This coincided with an increase in free Nedd8 levels, suggesting that neddylation was decreased at later time-points. GAPDH is used as a loading control.

These results show that neddylation is highly active in Schwann cells at the onset and active phases of the myelination process.

5.2 Pharmacological inhibition of neddylation in vitro blocks Schwann cell myelination

Our results above suggested that neddylation could be important for Schwann cell myelination. To test this, we examined the effects of pharmacological inhibition of neddylation on Schwann cell myelination *in vitro*. Treatment of purified Schwann cell cultures using cAMP induces upregulation of the myelin protein MPZ, and concomitant downregulation of the negative regulator c-Jun [245]. We found that treatment with the NAE1 inihibitor MLN4924 [246], abrogated these effects. We also found that cAMP induced neddylation of Cullin-2, an effect prevented by MLN4924 (**Figure 11**).

These results suggest that neddylation could be regulating Schwann cell myelination.

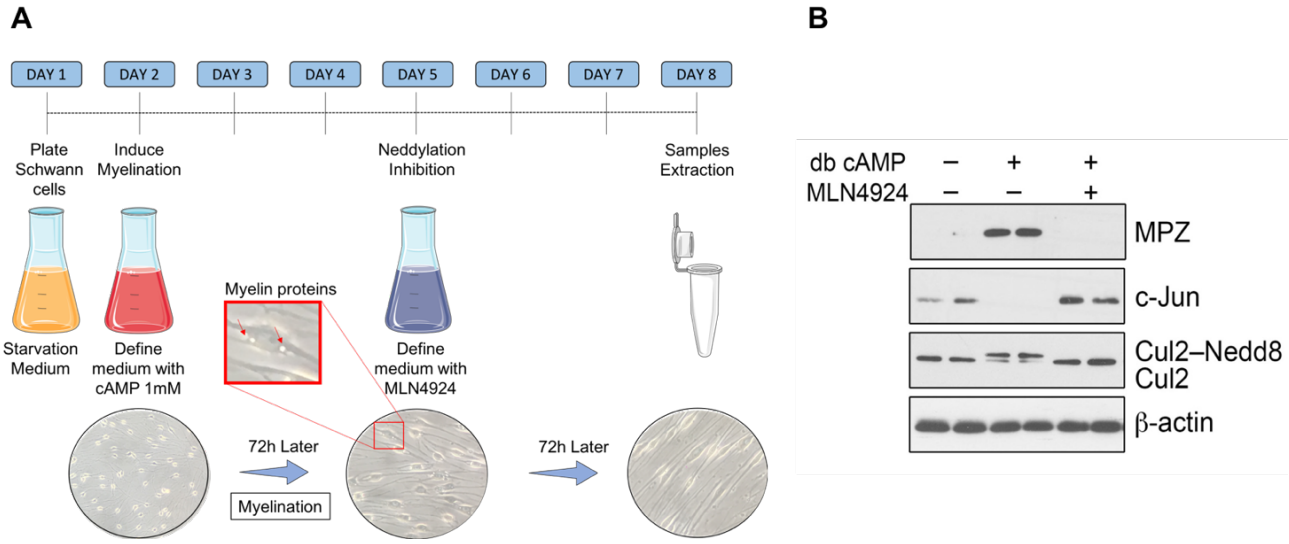

Figure 11. Neddylation inhibition blocks Schwann cell myelination in vitro. A) Protocol used to inhibit Nae1 activity with MLN4924 in myelinated rat Schwann cells. B**)** WB analysis shows upregulation of myelin protein MPZ and downregulation of negative regulator c-Jun by db cAMP treatment (48h) in primary rat Schwann cell cultures, an effect that is abrogated by supplementation with neddylation inhibitor MLN4924 (10 uM). Db cAMP treatment also induces neddylation of Cullin-2, which is blocked by MLN4924. β-actin is used as a loading control.

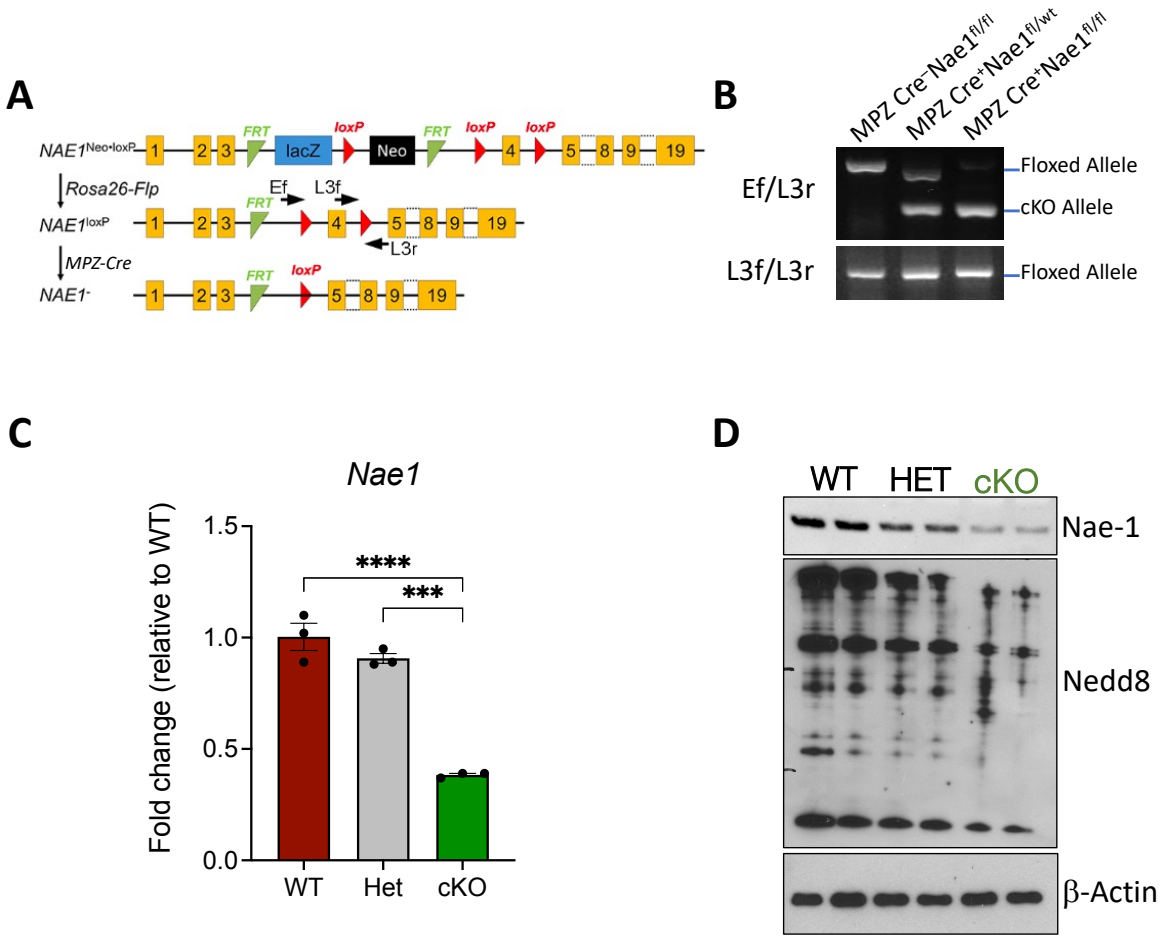

Figure 12. Schwann cell specific knockout of NAE1 (NAE1 cKO) inhibits neddylation

(**A**) Schematic diagram depicting the strategy of NAE1 cKO in mice. NAE1$^{Neo.loxP}$ mice were first crossed with Rosa26-Flp transgenic mice to remove the LacZ-Neo cassette. The resultant NAE1^{fl} mice were then crossed with MPZ-Cre+ transgenic mice to remove the exon 4 of *NAE1*, resulting in a null allele. (**B**) Genomic DNA was extracted from sciatic nerves and analyzed by PCR to detect NAE1 floxed allele (L3f and L3r) and Cre-mediated recombination (Ef and L3r). Efficient recombination (presence of cKO allele band) was observed in P15 sciatic nerves of NAE1 cKO mice (MPZ Cre^{+} NAE1$^{fl/fl}$), intermediate levels in heterozygote mice (MPZ Cre^{+} NAE1$^{fl/wt)}$, whereas no recombination was seen in control mice (mice not expressing MPZ Cre). (**C**) qRT-PCR analysis of P15 sciatic nerves shows strong decrease in *Nae1* mRNA in cKO mice, compared to controls and heterozygotes. (**D**) Western blot of NAE1 expression in the sciatic nerves of control, heterozygote and NAE1 cKO mice at P15. There is an incremental decrease in NAE1 and neddylated protein levels in het and cKO mice compared to control mice.

β-actin is used as a loading control. Data are presented as mean ± SEM. One-way ANOVA with Tukey's multiple-comparisons test. ***P < 0.001; ****P < 0.0001 n=3.

5.3 A mouse model of Schwann cell-specific neddylation inhibition

To further investigate the role of neddylation in Schwann cell development, we generated a conditional mouse model lacking Nae1, specifically in Schwann cells. For this, we generated Nae1floxed mice, and crossed them with the MPZ-Cre mice, a line where Cre recombinase is expressed under the control of the endogenous MPZ promoter that Schwann cells since E13.5 [242] (**Figure 12A**). The offspring of MPZ-Cre;Nae1$^{f/f}$ mice are referred to as Nae1 cKO mice, and their littermates Nae1$^{f/+}$ or Nae1$^{f/f}$ mice were used as controls. PCR (Figure 10B)

and qRT-PCR analyses (**Figure 12C**) confirmed the deletion of NAE1 in the NAE1 cKO P15 nerves, compared with their littermate control hearts. Western blot analyses of nerve lysates revealed a strong reduction of NAE1 levels, which was accompanied by a decrease in total neddylated proteins in P7 sciatic nerves (**Figure 12D**).

5.4 Nae1 mutant mice display severe motor deficits

NAE1 cKO mice were born at the expected Mendelian ratio and were essentially indistinguishable from littermate controls initially. However, starting from the second week, the mice began to develop severe tremor and unsteady gait and performed poorly in accelerated rotarod rest (**Figure 13A**). Upon tail suspension showed abnormal hind limb clasping (**Figure 13B**) and the NAE1 cKO mice died prematurely before P30 (**Figure 13C**).

Electrophysiological recordings of compound muscle action potentials (CMAPs) during electrical stimulation of the sciatic nerve in vivo showed a marked reduction in conduction velocity in mutant mice (**Figure 14**). The mean peak amplitudes and duration of CMAPs were also severely affected in Nae1 cKO mice (**Figure 14**), clearly showing marked conduction blocks, accounting for the defect in motor function in these mice. Interestingly, no differences were seen between control mice and heterozygous mice (MPZ-Cre; $Nae1^{f/+}$), even though heterozygous mice expressed lower levels of NAE1 (**Figure 12C, 12D**).

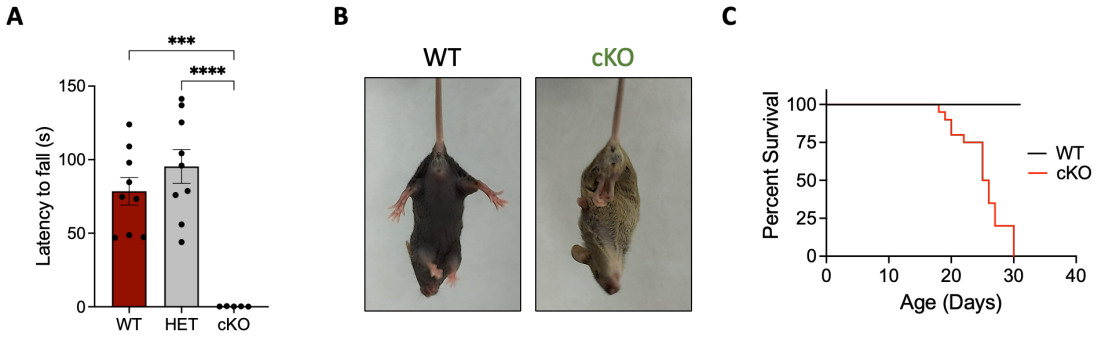

Figure 13. Nae1 mutant mice display severe motor deficits

(**A**) Latency (s) to fall off the accelerating rotarod shows poor performance in NAE1 cKO mice compared to control and heterozygous mice at P25. Data are presented as mean ± SEM. One-way ANOVA with Tukey's multiple-comparisons test. ***P < 0.001; ****P < 0.0001. (**B**) Tail suspension test showing abnormal hindlimb reflex in NAE1 cKO mice but not in a control littermate at P24. (C) Kaplan-Meier survival curves showing poor survival rates of NAE1 cKO (red) mice compared to control (black) mice (n = 15 animals/genotype).

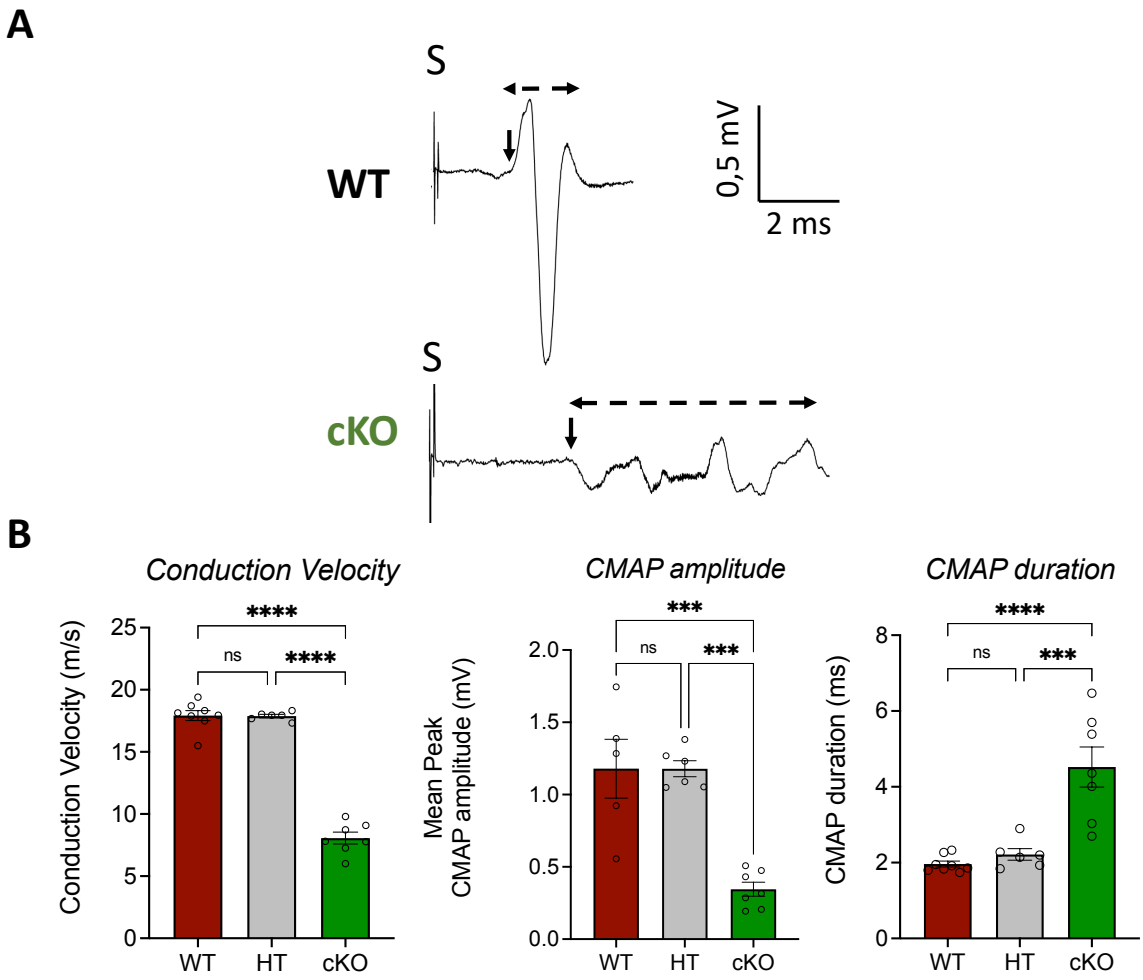

Figure 14. Nae1 mutant mice display a marked reduction in conduction velocity

(**A**) Electrophysiological recording of CMAPs from sciatic nerves of NAE1 cKO and control mice at P25. Representative traces are shown. S, stimulus; Initiation of CMAP response (black arrows). (**B**) Graphs show nerve conduction velocities, mean peak amplitudes of CMAPs, average durations of CMAPs in sciatic nerves of control, heterozygotes and NAE1 cKO mice at P25. There are no significant differences between control and heterozygotes, whereas cKO performed worse than both control and heterozygotes. Data are presented as mean ± SEM. One-way ANOVA with Tukey's multiple-comparisons test. ***P < 0.001; ****P < 0.0001. WT (n=8), HT (n=6), cKO (n=7).

5.5 NAE1 is essential for Schwann cell myelination

Our results on motor function and nerve conduction velocity in NAE1 cKO suggested major defects in myelination in these mice. To confirm these results, we performed ultrastructural examination of P28 sciatic nerves in NAE1 cKO mice by electron microscopy (EM). We found that the *Nae1*-deficient mice failed to myelinate with a striking reduction in number of myelinated axons. Notably, we found that most of the large diameter axons were in a 1:1 relationship with Schwann cells but these failed to elaborate myelin sheaths. Moreover, we found several examples of actively demyelinating Schwann cells in mutant nerves (**Figure 15A**).

This absence of myelinating Schwann cells in the NAE1 cKO mice was accompanied by a robust downregulation of myelin structural proteins CNP, MPZ and MBP, whereas expression of the master myelination transcription factor Egr2 (krox-20) was strongly reduced (**Figure 15B**).

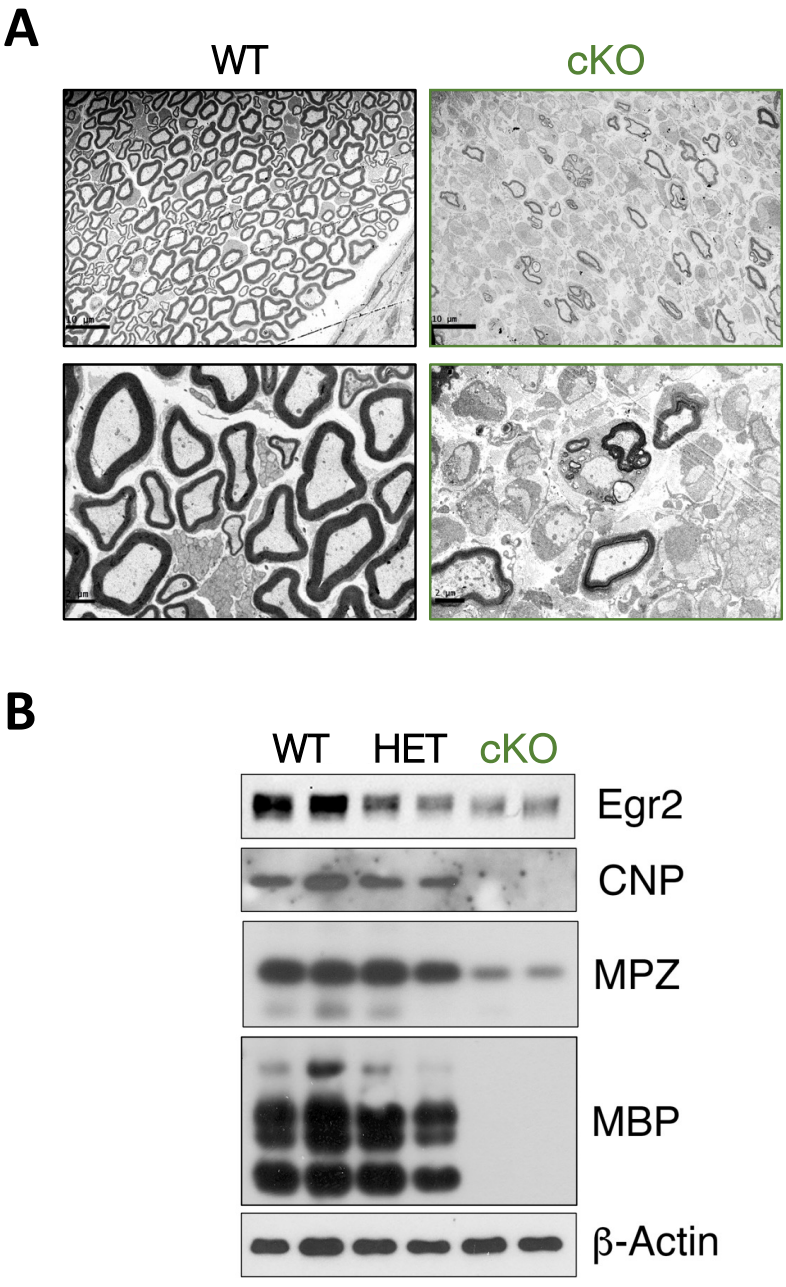

Figure 15. Neddylation is required for myelination

(**A**) Representative EM pictures showing ultrastructure of control and NAE1 cKO sciatic nerves at P28, at low (top panels) and high (bottom panels) magnification. Scale bar (top panel), 10 µm; Scale bar (bottom panel), 2 µm Electrophysiological recording of CMAPs from sciatic nerves of NAE1 cKO and control mice at P25. Representative traces are shown. S, stimulus; Initiation of CMAP response (black arrows). (**B**) WB analsyis of sciatic nerve lysates from control, heterozygote and NAE1 cKO mice at P28, showing that myelin proteins CNP, MBP and MPZ were barely detected in cKO nerves, whereas EGR2 was strongly reduced.

Defects in myelination in the NAE1 cKO mice can be caused by defects in radial sorting, in which the Schwann cells would fail to complete their differentiation to promyelin Schwann cells, not iniciating the myelination process.

Our EM analyses (**Figure 15**) did not suggest an impaired radial sorting in NAE1 cKO mice, since we found that there were several large diameter axons in a 1:1 relationship with Schwann cells. To confirm these data, we performed EM analyses of NB, P7, P14 and P28 nerves to examine the successive stages of the Schwann cell myelination process as they differentiate from the immature Schwann cells to mature myelinated Schwann cells. We found no defects in radial sorting since various pro-myelin Schwann cells could be observed in NAE1 cKO mice during all differentiation stages, with some of them already initiating the synthesis of myelin sheaths (**Figure 16**).

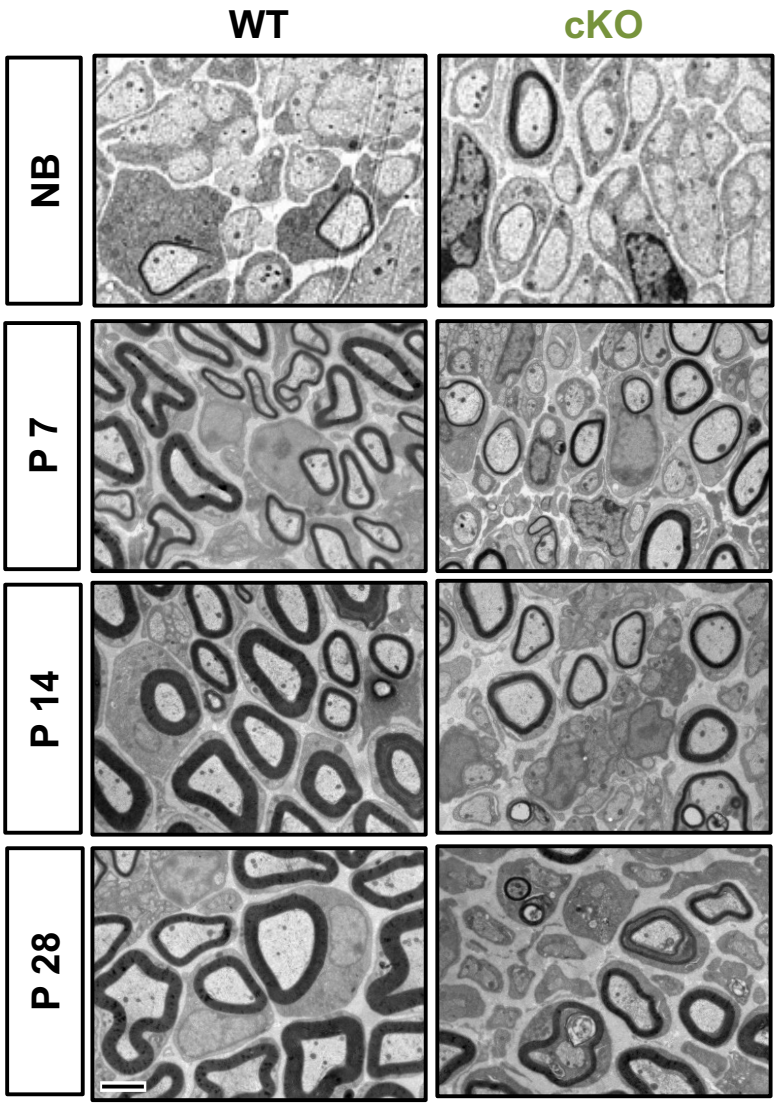

Figure 16. Neddylation is not required for radial sorting
Representative EM pictures showing ultrastructure of control and NAE1 cKO sciatic nerves at NB, P7, P14 and P28. Scale bar, 4 μm.

To confirm these observations, we performed quantifications of the number of myelinated axons, pro-myelin axons, Schwann cell nuclei and axons in sciatic nerves from control and NAE1 cKO mice at P7 and P28. We found a clear reduction in number of myelinated axons and a concomitant increase in promyelin Schwann cells in mutant nerves at P7, an effect that was exacerbated at P28. There seemed to be no differences in numbers of Schwann cell nuclei at both ages, and we found a striking decrease in number of axons at P28 (**Figure 17**).

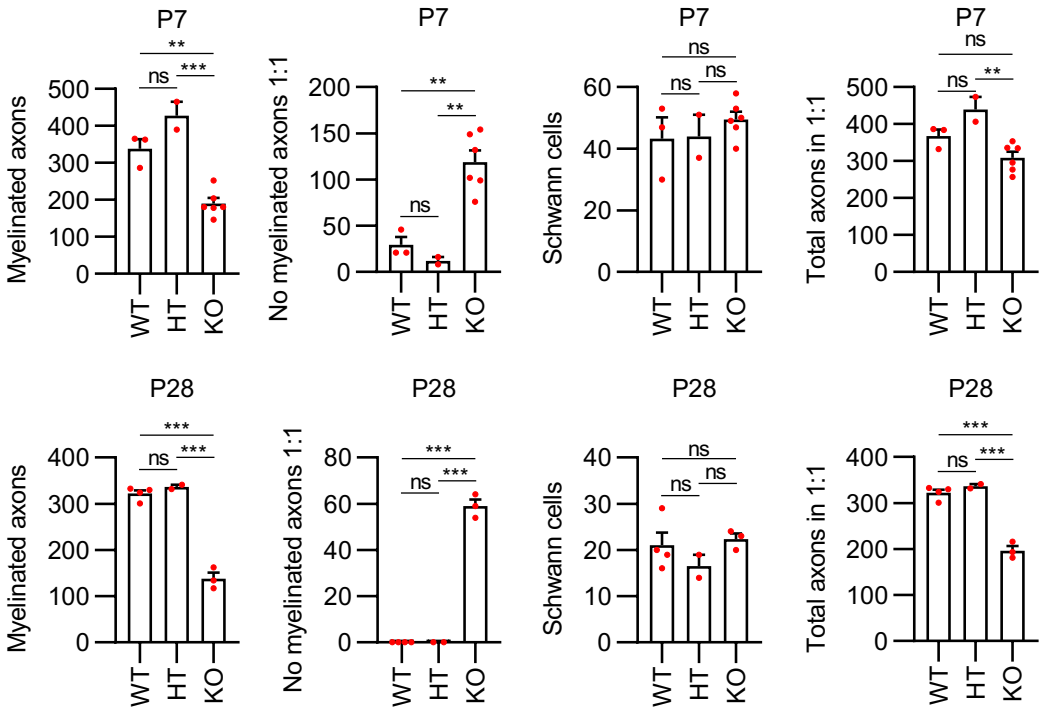

Figure 17. Neddylation inhibition induces an arrest of Schwann cells at the promyelin stage.
Graphs showing the number of myelinated axons, pro-myelin axons, Schwann cell nuclei and axons in sciatic nerves from control and NAE1 cKO mice at P7 and P28. Data are presented as mean ± SEM. One-way ANOVA with Tukey's multiple-comparisons test. n.s. not significant; **P < 0.01; ***P < 0.001.

There seem to be no defects in radial sorting since pro-myelin Schwann cells were observed in comparable number between control and mutant mice as from P1 onwards, but ultimately, these seem to fail to initiate the myelination process.

In summary, neddylation does not seem to be required for radial sorting, but instead is essential for the formation of myelin sheaths in promyelin Schwann cells. Thus, neddylation inhibition blocks the formation of myelin sheaths leading to severe motor deficits.

5.6 Neddylation inhibits Schwann cell proliferation

As the immature Schwann cells undergo radial sorting and form the promyelin Schwann cells in a 1:1 relationship, they exit the cell cycle and start their differentiation to myelinating Schwann cells [79]. Here, we examined Schwann cell proliferation using 5-ethynyl-2'-deoxyuridine (EdU) incorporation across Schwann cell development in control and mutant mice. As described previously, control nerves showed high proliferation rates at the immature Schwann cell stage (P1), and there were no differences compared to mutant mice. However, at P7, these proliferation rates remained high in mutant mice whereas they decreased substantially in control mice, as expected (**Figure 18**). At later time-points, there were no significant differences and the mutant nerves had reached the low proliferation levels observed in control mice. These results show that there is transient block in the cell cycle exit in the differentiating Schwann cells and indicate that NAE1 ablation arrests Schwann cells at the promyelin stage, blocking their transition to EGR2+ myelinating Schwann cells.

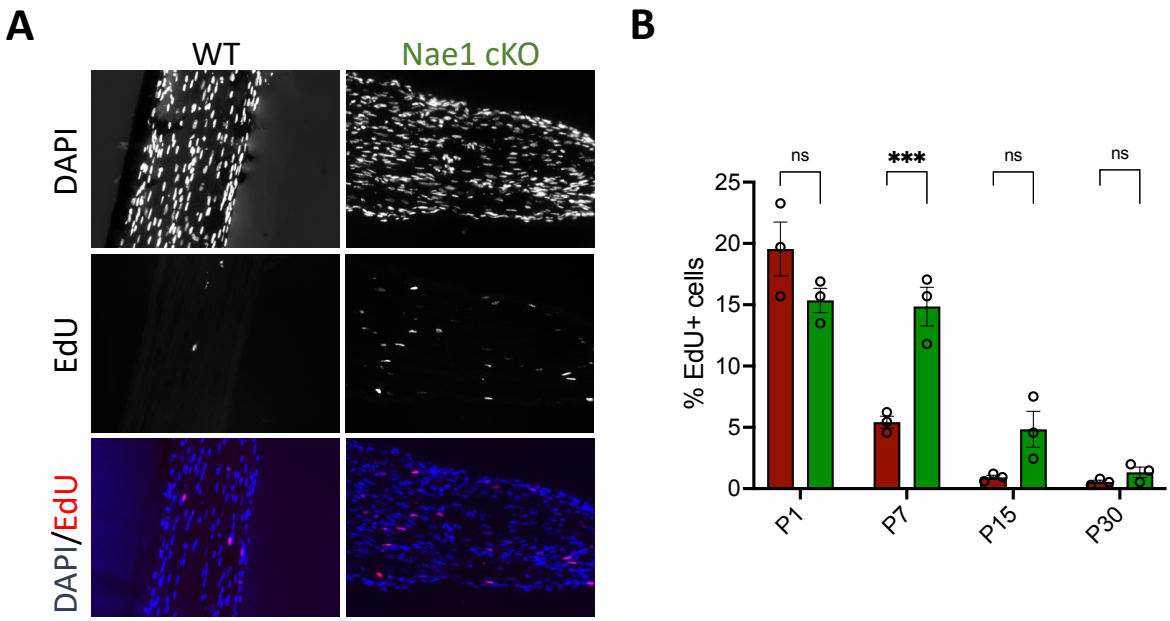

Figure 18. Neddylation inhibition induces Schwann cell proliferation.
(**A**) Immunofluorescence labelling for EdU (red) in sciatic neves from control and NAE1 cKO mice at P7. Higher number of proliferative EdU+ Schwann cells are seen in mutant nerves compared to control nerves. DAPI labels the nuclei blue. (**B**) Graphs shows quantification of EdU+ cells at P1, P7, P15 and P30 nerves. Data are presented as mean ± SEM. Student´s *t*-test. n.s. not significant; ***P < 0.001, n=3 genotype/age.

5.7 NAE1 ablation leads to profound transcriptomic and proteomic changes

To examine the effects Nae1 ablation in Schwann cells at the genome-wide level, we performed an RNA-Seq transcriptome analysis of control and NAE1 cKO sciatic nerves at P7. We identified distinct transcriptomic profiles between the control and mutant nerves, and differential expression analysis revealed that a notable proportion of the transcriptome changed significantly. We identified 1,402 misregulated transcripts in mutant nerves, 834 of which were increased and 568 of which were decreased at a 5% false discovery rate and fold-change of 2 (**Figure 19** and **Supplementary Table 1**).

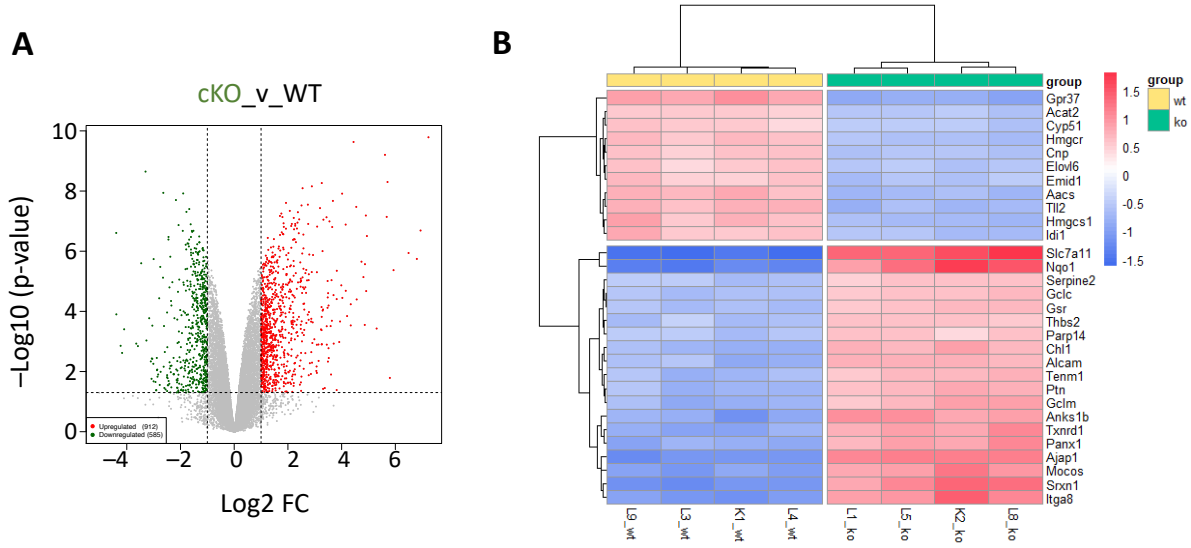

Figure 19. Neddylation inhibition induces large sale changes in transcriptomic profiles
(**A**) Volcano plot of transcriptome profiles from P7 sciatic nerves in control (n = 4) and NAE1 cKO (n = 4) mice. Red and green dots represent genes significantly upregulated and downregulated, respectively, in cKO nerves (fold change >2; adjusted P value < 0.05). (B) Heatmap representation of top differentially expressed genes control (n = 4) and NAE1 cKO (n = 4) mice (fold change >2; adjusted P value < 0.05).

Gene ontology analysis of differentially regulated genes indicated that the functions of downregulated genes were particularly pertinent to lipid biosynthesis (**Figure 20A**), whereas those of upregulated genes could be classified into categories involving cell proliferation control and adhesion (**Figure 20B**).

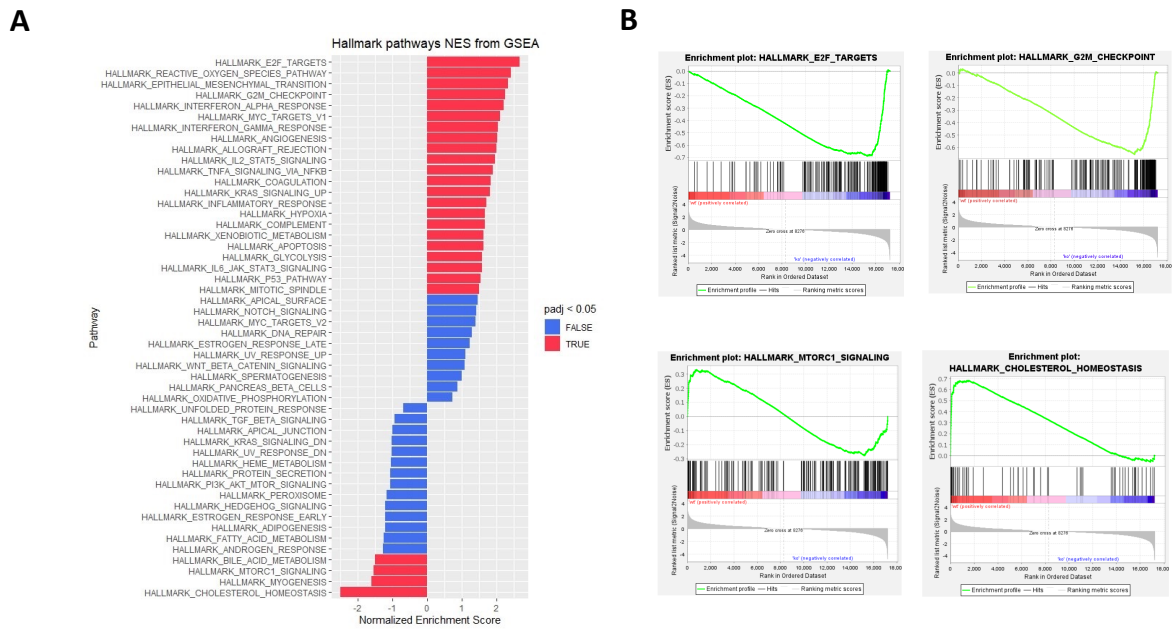

Figure 20. Neddylation controls key processes in Schwann cells

(**A**) GSEA analysis of control and NAE1 cKO transcriptomic profiles for MSigDB Hallmark pathways signatures. (**B**) GSEA plots showing enrichment of proliferation-related signature in NAE1 cKO mice compared to control mice (top panels), and conversely, enrichment of myelination-related signatures in control mice compared to mutant mice (bottom panels).

As mentioned above, CRLs mediate the proteolysis of about 20% of cellular proteins. This prompted us to examine the proteomic profile of control and NAE1 cKO sciatic nerves at P15 to examine whether neddylation-mediated CRL activation could be involved in shaping the Schwann cell proteome during myelination. We found widespread changes in proteomic profile between control and NAE1 cKO sciatic nerves. Notably, pathway analysis showed an enrichment of cholesterol biosynthesis as one of the most enriched categories in the dysregulated proteins, similar to transcriptomic profile previously mentioned (**Figure 20**). Furthermore, several proteins related to proteosome and U3 ligases were dysregulated (**Figure 21**), a clear indication of the potential role of neddylation in regulating proteasomal degradation by CRLs during myelin differentiation.

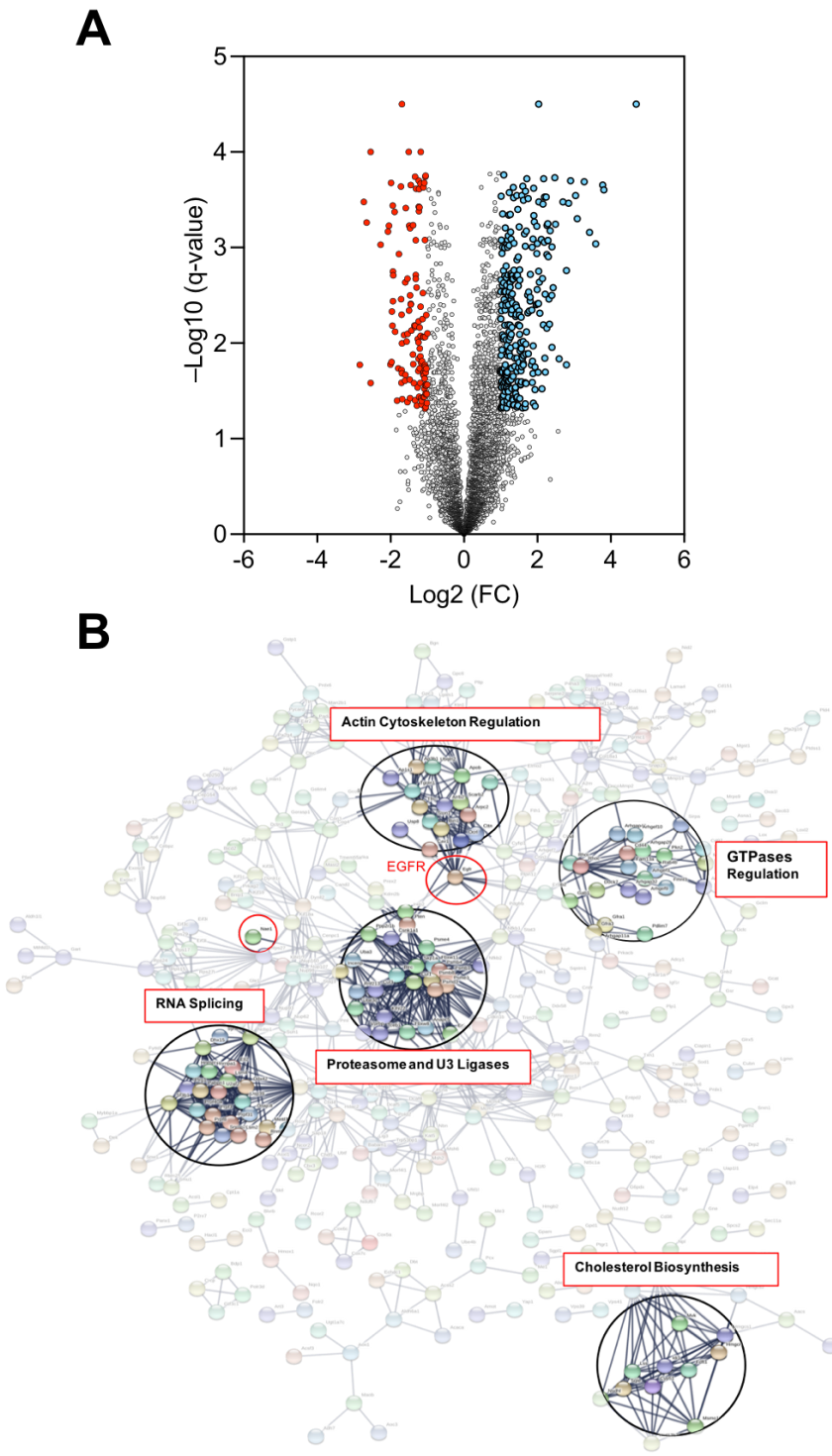

Figure 21. Neddylation inhibition induces large sale changes in proteomic profiles

(**A**) Volcano plot of proteomic profiles from P15 sciatic nerves in control (n = 5) and NAE1 cKO (n = 4) mice. Red and blue dots represent genes significantly downregulated and upregulated, respectively, in cKO nerves (fold change >2; adjusted P value < 0.05).

(**B**) Representation of the upregulated and downregulated genes obtained in the RNAseq data using the STRING software. The parameters used were: Full string network, evidence network edges, all interaction sources active, required interaction 0.4 minimum. Highlighted zones of the interactome show the main affected cellular functions or pathways. In a red circle were highlighted EGFR and Nae1. Original image in supplementary p130.

5.8 Neddylation regulates expression of negative regulators of myelination

Our results show that neddylation is critical for Schwann cell myelination, and that its inhibition leads to widespread molecular changes in the cells. Next, we wanted to identify the precise molecular mechanisms regulated by neddylation in myelinating Schwann cells. First, we examined expression of the negative regulators of myelination c-Jun and Sox 2. We found that c-Jun and Sox 2 were highly elevated in Nae1 cKO mice compared to control or heterozygous mice (**Figure 22**).

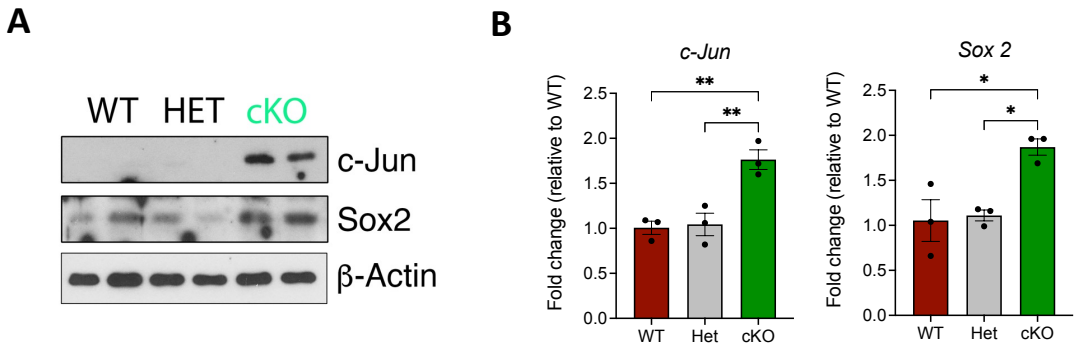

Figure 22. Neddylation inhibition leads to an increase in c-Jun and Sox2 levels
(**A**) WB analysis showing elevated c-Jun and Sox2 levels in P28 sciatic nerves of control, heterozygote and NAE1 cKO mice at P15. There is an incremental decrease in NAE1 and neddylated protein levels in het and cKO mice compared to control mice. β-actin is used as a loading control. Data are presented as mean ± SEM. One-way ANOVA with Tukey's multiple-comparisons test. ***P < 0.001; ****P < 0.0001.

Furthermore, in the case of c-Jun, we found that there is the expected downregulation of c-Jun levels as the Schwann cells differentiate in control nerves, whereas the high c-Jun levels are maintained in Nae1 cKO (**Figure 23**). These elevated c-Jun levels were accompanied by an increase in levels of c-Jun targets *Olig1*, *Gdnf* and Shh (data not shown).

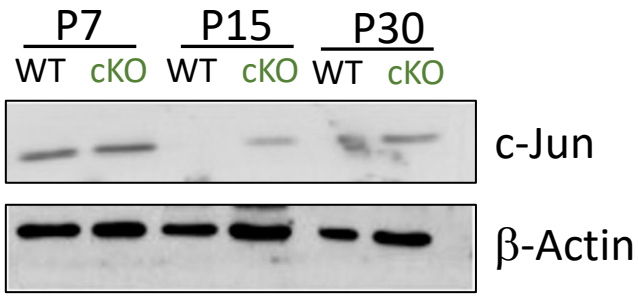

Figure 23. Neddylation inhibition leads to an increase in c-Jun and Sox2 levels
(**A**) WB analysis showing the downregulation of c-Jun in progressively more mature sciatic nerves of control mice, an effect which is not seen in NAE1 cKO mice at P15. β-actin is used as a loading control.

Next, to further investigate how neddylation regulated the expression of c-Jun and Sox2, we turned to our in vitro model of myelination (Figure 22). As described, pharmacological inhibition of neddylation using MLN4924 can prevent cAMP-induced degradation of c-Jun and Sox2 at 48h. We first examined the effects of cAMP treatment in primary Schwann cell cultures on c-Jun and Sox2 mRNA and protein levels with time. In control conditions, we found that c-Jun mRNA levels were dramatically decreased after only 1 hr after cAMP treatment while protein levels decreased more gradually, requiring up to 8 hrs of treatment to decrease significantly (**Figure 24**). Notably, we found that MLN4924 treatment blocked the decrease in c-Jun protein levels but did not have any effect on c-Jun mRNA levels. Furthermore, we found similar effects on Sox2 levels, although in this case the effects were retarded (**Figure 24**). Sox2 mRNA levels required about 12 hrs to decrease to low levels whereas protein levels required about 24 hrs. Similar to c-Jun, MLN4924 treatment blocked the decrease in Sox2 protein levels, whilst having no effect on Sox2 mRNA levels.

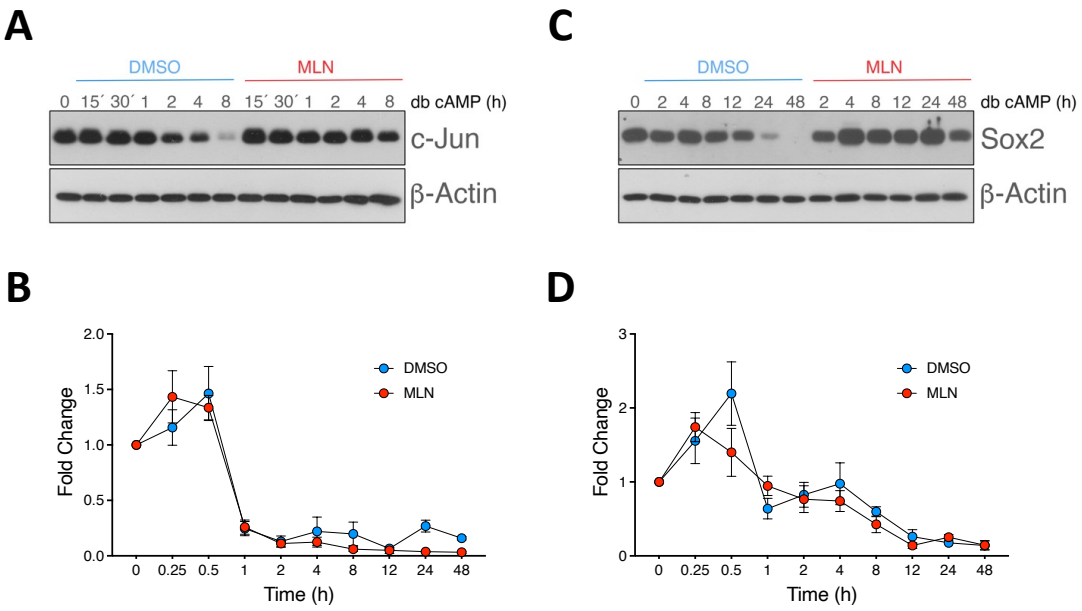

Figure 24. MLN4924 blocks cAMP-induced c-Jun and Sox2 protein but not mRNA levels in cultured Schwann cells

(**A, C**) WB analysis showing progressive downregulation of c-Jun (**A**) and Sox2 (**B**) levels with time after addition of cAMP in cultured Schwann cells, an effect that was blocked by co-supplementation with neddylation inhibitor MLN4924. β-actin is used as a loading control.

(**B**, **D**) qRT-PCR analysis shows a rapid downregulation of *c-Jun* (**A**) and *Sox2* (**B**) mRNA levels after addition of cAMP in cultured Schwann cells, an effect that is independent of neddylation (n=4 independent experiments). Data are presented as mean ± SEM. Two-way ANOVA with Sidak's multiple-comparisons test.

Next, we started the DMSO or MLN4924 treatments of the cells 1 hr after cAMP supplementation. At this time for example, c-Jun mRNA levels would have decreased considerably. Here, similar to above, we observed that MLN4924 prevented the decrease of c-Jun or Sox2 protein levels. However, MLN4924 had no effect on their mRNA levels (**Figure 25**).

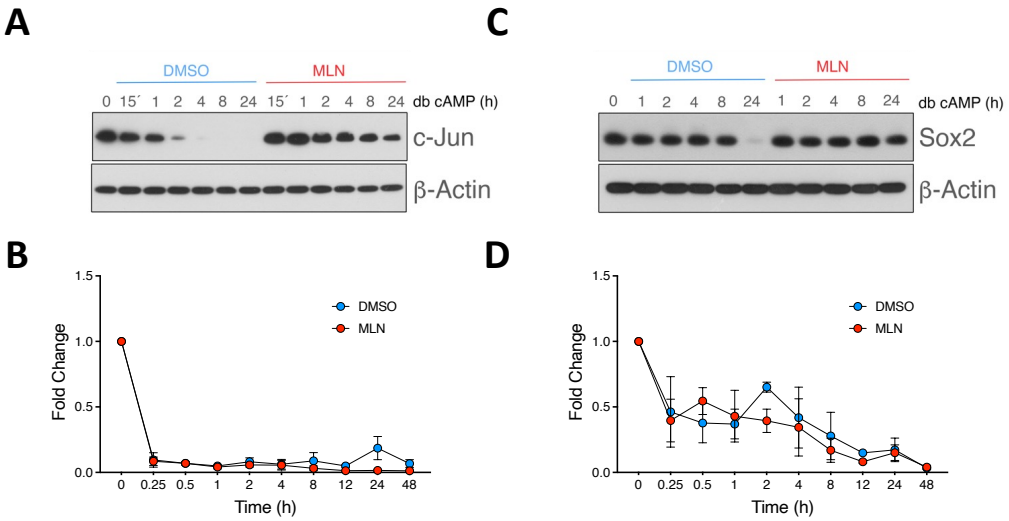

Figure 25. MLN4924 blocks cAMP-induced c-Jun and Sox2 protein but not mRNA levels in cultured Schwann cells

(**A, C**) WB analysis showing progressive downregulation of c-Jun (**A**) and Sox2 (**B**) levels with time after addition of cAMP in cultured Schwann cells, an effect that was blocked by co-supplementation with neddylation inhibitor MLN4924, 1 hr after addition of cAMP. β-actin is used as a loading control.

(**B**, **D**) qRT-PCR analysis shows a rapid downregulation of *c-Jun* (**A**) and *Sox2* (**B**) mRNA levels after addition of cAMP in cultured Schwann cells, an effect that was not blocked by co-supplementation with neddylation inhibitor MLN4924, 1 hr after addition of cAMP(n=4 independent experiments). Data are presented as mean ± SEM. Two-way ANOVA with Sidak's multiple-comparisons test.

Finally, we challenged even further this system by starting MLN4924 treatments of the Schwann cells 24 hr after cAMP supplementation. At this time point, both mRNA and protein levels of c-Jun and Sox2 are at minimum levels. We found that DMSO treatment did not alter the protein or mRNA levels of either TF, and neither did MLN4924 treatment on their mRNA levels. In contrast, and quite strikingly, we found that MLN4924 treatment was able to progressively increase c-Jun and Sox2 protein levels with time (**Figure 26**).

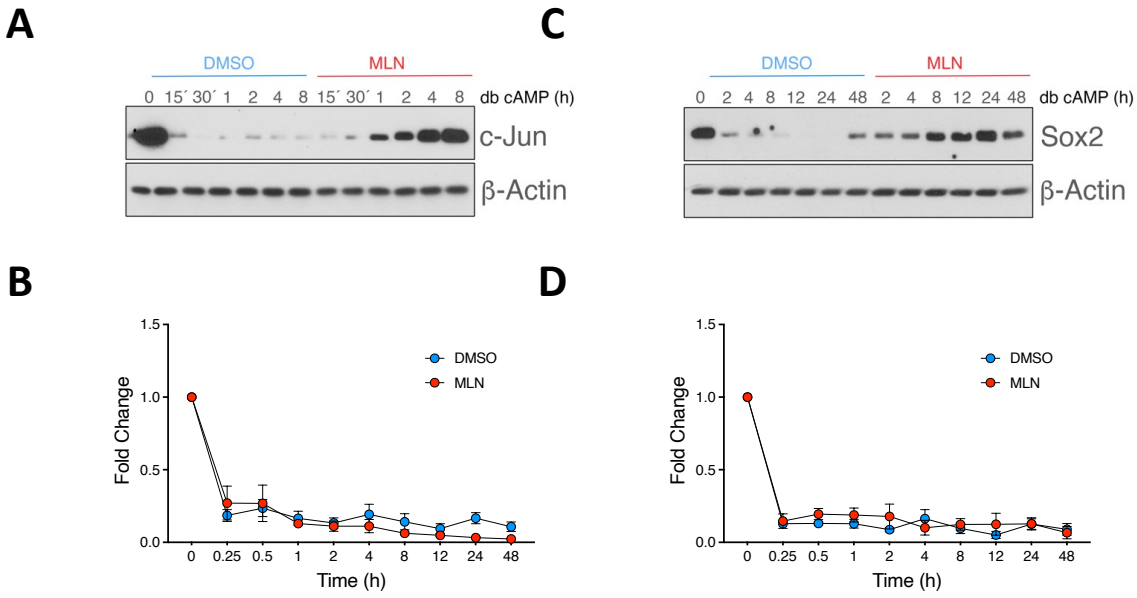

Figure 26. MLN4924 can induce recovery of cAMP-induced c-Jun and Sox2 protein downregulation in cultured Schwann cells

(**A, C**) WB analysis shows robust downregulation of c-Jun (**A**) and Sox2 (**C**) levels 24hs after addition of cAMP in cultured Schwann cells, compared to untreated cultures (0 h), an effect that is maintained with time in culture. Neddylation inhibitor with MLN4924, however, can induce a recovery of their levels with time. β-actin is used as a loading control.

(**B**, **D**) qRT-PCR analysis shows robust downregulation of *c-Jun* (**B** and *Sox2* (**D**) mRNA levels 24hs after addition of cAMP in cultured Schwann cells, compared to untreated cultures (0 h), an effect that is maintained with time in culture. Neddylation inhibitor with MLN4924, in this case, cannot lead to a recovery of their mRNA levels unlike their protein levels (n=4 independent experiments). Data are presented as mean ± SEM. Two-way ANOVA with Sidak's multiple-comparisons test.

These results above show that neddylation can regulate c-Jun and Sox2 protein expression, either at the level of translation or degradation without affecting their transcription. Next, to distinguish between these two possibilities, we performed a cycloheximide (CHX)-based pulse-chase assay, which permits visualization of the degradation kinetics of the steady state population of a variety of cellular proteins. We added CHX with a final concentration of 100 ug/mL to Schwann cells and collected cells over a period of time and performed western blotting for c-Jun and Sox2, which was then normalized to b-actin. The band intensities were quantified and normalized, while protein half-life was determined by using Graph Pad Prism. Here, we found that after blocking protein translation using CHX, c-Jun and Sox2 levels rapidly decreased over the next few hours as they get degraded (**Figure 27**). MLN4924 treatment however was able to block this degradation, and consequently c-Jun half-life was considerably higher in MLN4924 conditions than in control conditions. Sox2 levels, on the other hand, were barely affected by MLN4924 treatment and its half-life in both conditions was similar. These results

suggest that neddylation downregulates c-Jun and Sox2 protein levels under mielinogenic conditions by regulating their degradation.

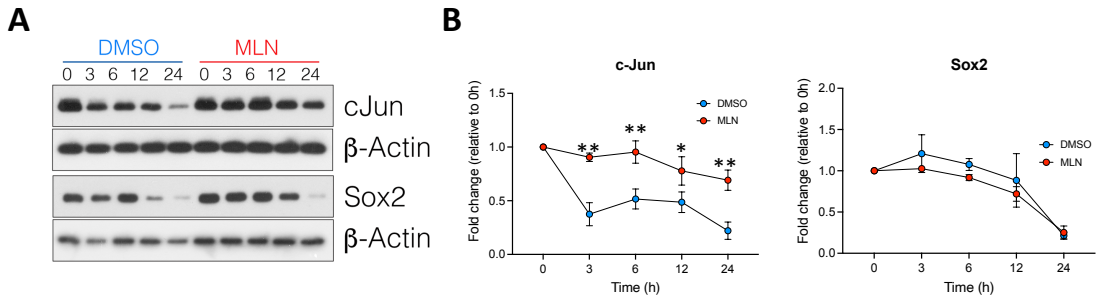

Figure 27. MLN4924 can block cycloheximide-induced downregulation of c-Jun but not of Sox2 levels in cultured Schwann cells

(**A**) WB analysis shows robust downregulation of c-Jun (**A**) and Sox2 (**C**) levels after addition of CHX in cultured Schwann cells, compared to untreated cultures (0 h). Neddylation inhibitor with MLN4924 can induce block this downregulation of c-Jun and Sox2 levels. β-actin is used as a loading control. (**B**) Densitometry analyses of c-Jun and Sox2 expression in CHX-treated cultures after DMSO (control) or MNL4924 supplementation (n=4 independent experiments). Data are presented as mean ± SEM. Two-way ANOVA with Sidak's multiple-comparisons test. *P<0.01; **P < 0.001

5.9 Neddylation regulates proteasomal degradation of c-Jun and Sox2 during myelination by CRLs

Next, we wanted to investigate how neddylation regulates degradation of these negative regulators of myelination. As mentioned, cullins are amonst the best characterized targets of neddylation[201], and this is required for the activation of CRLs, which are the largest family of E3 ubiquitin ligases that promote the ubiquitination and degradation of about 20% of cellular proteins.

To investigate a potential role of CRLs in the degradation of c-Jun and Sox2 during Schwann cell myelination, we first examined the expression of the main components of CRLs: Cullins 1-7, and specific examples of substrate recognizing adaptors that bind the target proteins, including Fbxw7, b-TRCP and Skp2. As shown by qRT-PCR analyses, all *Cullin* genes were expressed in sciatic nerves and there were no overt changes in their expression as the Schwann cells undergo their differentiation from immature Schwann cells to myelinating Schwann cells (**Figure 28**). Similar to this, *Fbxw7* and *b-TRCP* were expressed during the myelination process whereas Skp2 was downregulated as the Schwann cells differentiated.

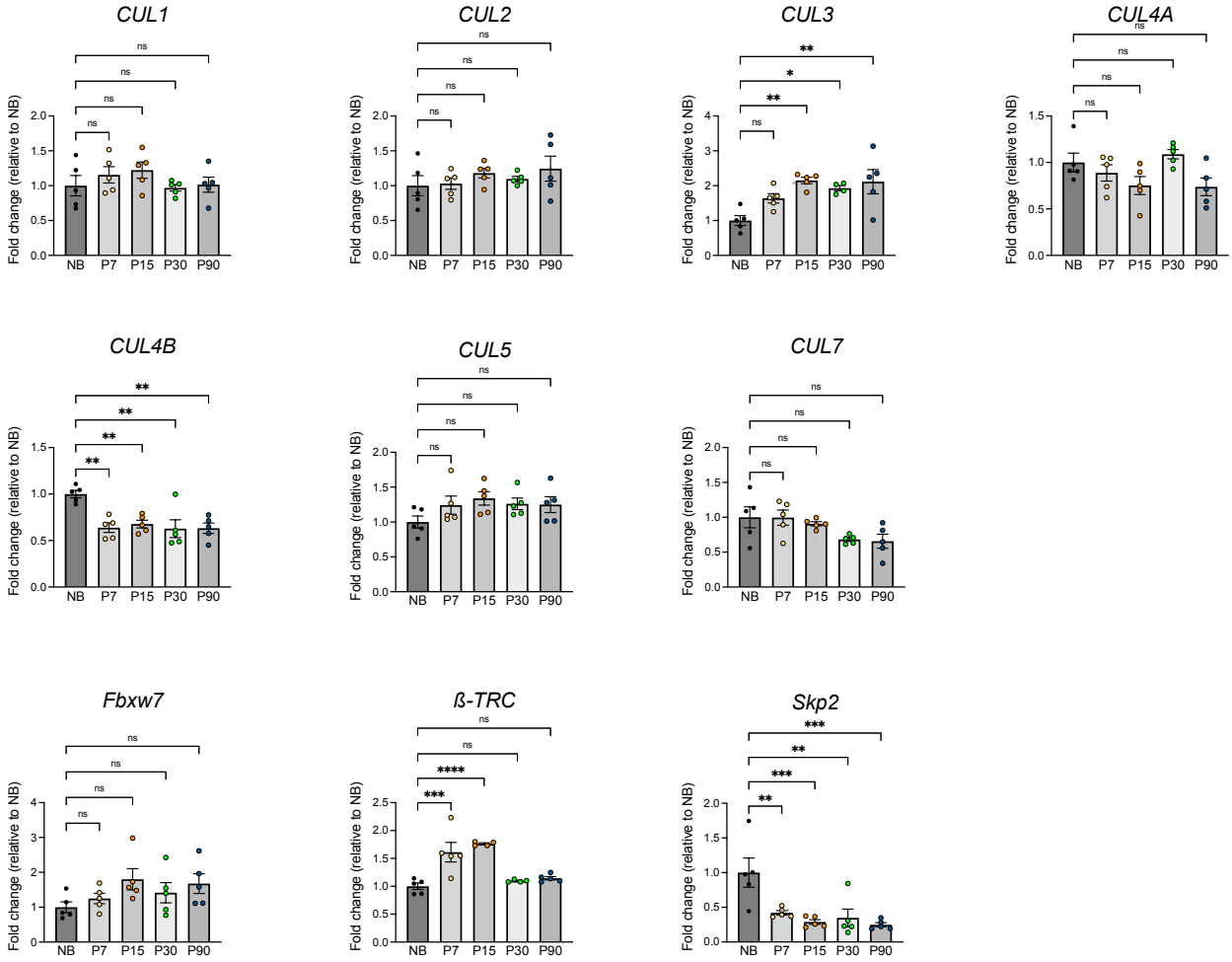

Figure 28. CRL pathway components are expressed in postnatal sciatic nerves. qRT-PCR analyses show that Cullins and substrate receptors are expressed and regulated in sciatic nerves from mice at different ages that broadly correspond to the main stages of the myelination process. Data are presented as mean ± SEM. One-way ANOVA with Tukey's multiple-comparisons test. n.s. not significant; *P < 0.05; **P < 0.01; ***P < 0.001; ****P < 0.0001, n=5 .

We next confirmed these data by Western blotting. Here, we found that Cullins were highly expressed at initial stages of the myelination process with a peak of expression in P7 nerves, a stage at which the pro-myelin Schwann cells start the elaboration of their myelin sheaths, followed by a progressive decline in expression in mature Schwann cells. Fbxw7 and b-TRCP followed a similar pattern of expression as the Cullins.

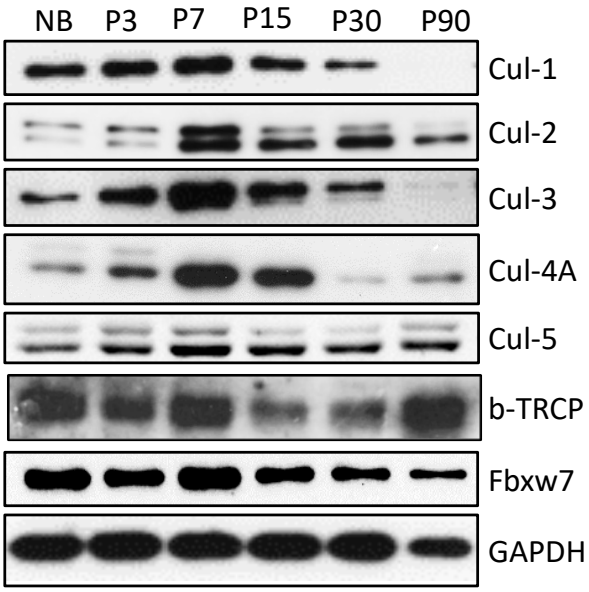

Figure 29. CRL pathway components are expressed in postnatal sciatic nerves. WB analyses of Cullins and substrate receptors of sciatic nerves from mice at different ages that broadly correspond to the main stages of the myelination process. GAPDH is used as a loading control.

These data show that the major components of the CRLs are expressed in Schwann cells during the myelination process and their expression coincide with the downregulation of the negative regulators of myelination, suggesting that they could be involved in their ubiquitination and proteasomal degradation (**Figure 29**). To demonstrate this, we silenced the different Cullins using lentiviral shRNA vectors and examined their effect on c-Jun and Sox2 expression after cAMP treatment. We used 3 different vectors to silence each Cullin but we could not obtain data from all of them since we had low infectivity rates for several of them despite several trials, and puromycin selection resulted in the cell death of these cells. Despite this, we found that silencing cullin1 led to a slight recovery of c-Jun levels after cAMP treatment, whereas silencing cullin3 led to a slight recovery of Sox2 levels, suggesting that CRLs comprising Cul1 and Cul3 could be involved in degradation of c-Jun and Sox2 respectively (**Figure 30**)

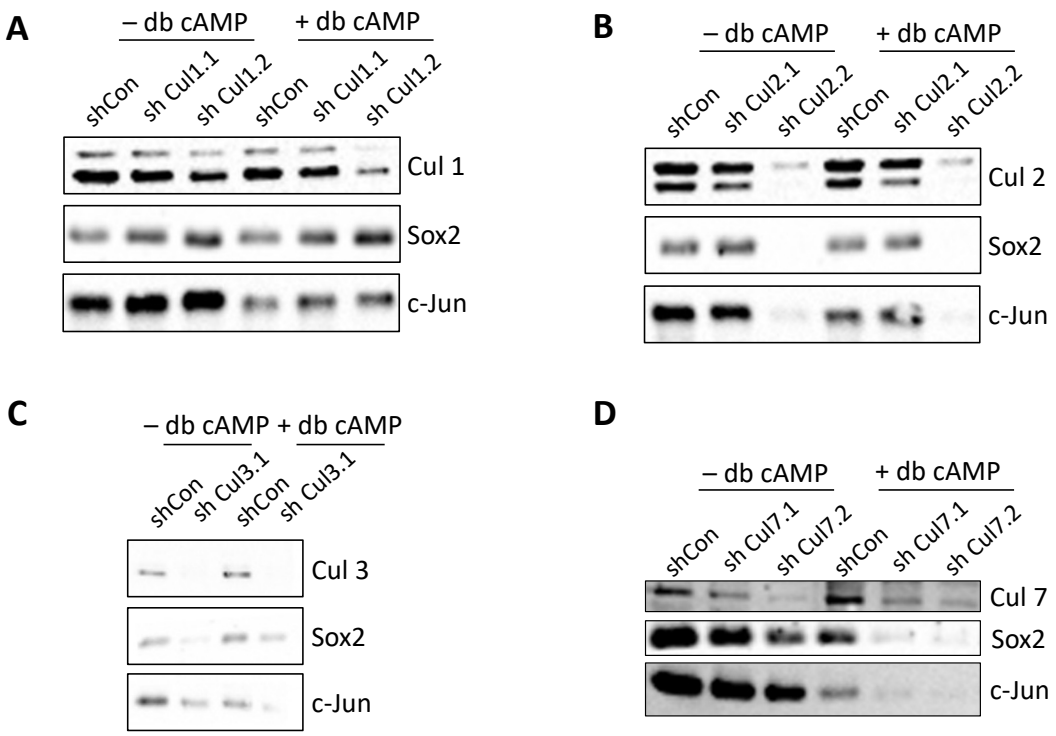

Figure 30. CRL pathway regulate cAMP-mediated c-Jun and Sox2 degradation in cultured Schwann cells. WB analyses of c-Jun and Sox2 levels after (A) Cul1, (B) Cul2, (C) Cul3 and (D) Cul7 silencing.

c-Jun is known to be degraded by Fbxw7 via the proteasomal pathway [247]. Fbwx7 (F box and WD repeat domain-containing 7) is the substrate recognition component of the evolutionary conserved CRL SCF^{Fbw7} complex. To determine whether Fbxw7 interacts with c-Jun, Fbxw7 was immunoprecipitated with anti-Fbxw7 antibody from Schwan cell culture homogenates, and then probed with c-Jun antibody (**Figure 31**). We found that Fbxw7 and c-Jun interacted together under basal control conditions, and interestingly there was an increased interaction when cells were treated with cAMP. Importantly, we found that MNL4924 treatment completely abolished this interaction between Fbxw7 and c-Jun. This suggests that neddylation is required for the activation of the Cullins in the CRL complexes that could bring together Fbxw7 and c-Jun to induce its ubiquitination and subsequent degradation.

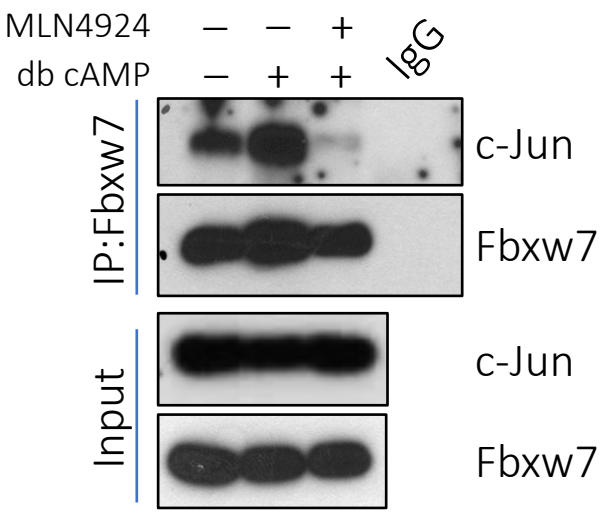

Figure 31. c-Jun interacts with Fbw7 in a neddylation dependent manner.
WB analyses showing that cAMP enhances the complex formation between Fbxw7 and c-Jun in vitro, an effect blocked by MLN4924 supplementation. IP was performed with Fbwx7 antibodies, followed by WB for c-Jun and Fbxw7.

5.10 Neddylation regulates the YAP/TAZ pathway in Schwann cells.

Recent studies have shown the essential role of the YAP/TAZ pathway during Schwann cell myelination [248,249]. Using conditional mice knockout models, several groups demonstrated that YAP or YAP/TAZ promote differentiation of immature Schwann cells, thereby forming and maintaining the myelin sheath around peripheral axons, by upregulating myelin-associated genes, thereby mediating developmental myelination[249–253]. Neddylation was shown to be important in cardiac development through repression of Hippo signaling and consequently enabling YAP signaling. They found that neddylation regulates Mst1 and LATS2 degradation and that Cullin 7, a NEDD8 substrate, acts as the ubiquitin ligase of Mst1 to enable YAP signalling and cardiomyocyte proliferation.

In this Hippo signaling pathway, the sequential activation of Hippo kinases Mst1/2 and LATS1/2 mediates phosphorylation of YAP, which inhibits its nuclear translocation and transcriptional activity (**Figure 32A**). Western blot analysis of sciatic nerve lysates from NAE1 cKO mice demonstrated an increase in the Hippo kinase (LATS1) and a decrease in MST1 and MST2 their associating partner SAV1 compared with control mice (**Figure 32B**). We also observed increased phosphorylation of MOB1 and elevated phosphorylation of YAP at serine 397, suggesting the activation of Hippo signaling, and repression of YAP signalling in Schwann cells.

It would be important to determine in future studies how neddylation regulates expression of the Hippo kinases, in particular Lats1, which could explain the anticipated repression of YAP signaling in the NAE1 cKO mice, but also the functional outcome of this repression of YAP signaling on myelination. It would be interesting to examine whether a recovery of YAP signalling after neddylation inhibition in Schwann cells could rescue the myelination defects.

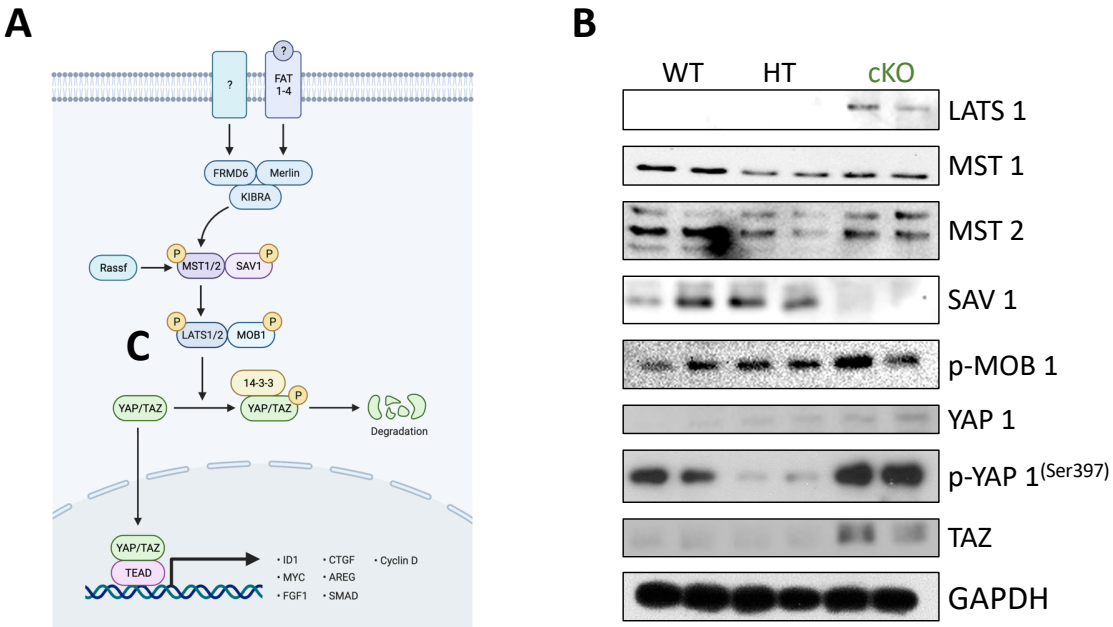

Figure 32. Neddylation inhibition in vivo blocks YAP/TAZ pathway

(**A**) Schematic diagram describing the HIPPO/YAP-TAZ pathway. When the Hippo signaling pathway is active/on, multiple upstream signals regulate the phosphorylation of MST1/MST2, LATS1/LATS2 kinases, leading to phosphorylation of YAP/TAZ protein, which recruits 14-3-3 proteins that stimulate cytoplasmic retention or proteolytic degradation. When Hippo signaling pathway is inactive/off, YAP/TAZ are not phosphorylated, and thus can localize to the nucleus to form a complex with transcription factor TEADs to regulate gene expression.

(**B**) WB analyses of sciatic nerve lysates from control, heterozygote and NAE1 cKO mice at P28, showing that LATS1, p-MOB1 and p-YAP1 are upregulated in cKO nerves, showing a block in activation of YAP/TAZ pathway. GAPDH is used as a loading control.

5.11 Neddylation regulates the mTOR pathway in Schwann cells.

The mechanistic Target Of Rapamycin (mTOR), a central signaling hub coordinating cell metabolism, plays a complex role in myelinating Schwann cells. On the one hand, before the onset of myelination, mTOR suppresses the transition from promyelinating to myelinating Schwann cells by transiently blocking expression of Krox-20[254]. As the cells differentiate, a decline in mTORC1 activity releases this block and allows myelination to proceed. On the other hand, after the onset of myelination, mTORC1 positively regulates myelin production. Western blot analysis of sciatic nerve lysates from NAE1 cKO mice demonstrated an increase in phosphorylation of S6K and 4EBP1, indicating hyperactivation of mTOR signaling in Schwann cells (**Figure 33A**).

Next, we examined whether suppressing this hyperactivation of mTOR in Schwann cells could rescue the defects in myelination. For this, we used our in vitro culture system. Primary Schwann cells were treated with cAMP in the presence/absence of MLN4924 and/or Rapamycin, and mTOR inhibition. As shown above, MNL4924 is able to suppress cAMP-induced upregulation of MPZ and conversely cAMP-induced downregulation of c-Jun. Co-treatment with rapamycin, however, which blocks the hyperactivation of mTOR, was not sufficient to restore the levels of MPZ or downregulate c-Jun levels (**Figure 33B**). These data suggest that, while neddylation inhibition results in mTOR hyperactivation, this alone does not seem sufficient to block myelination, and is likely to be one of several regulators that are responsible for this effect.

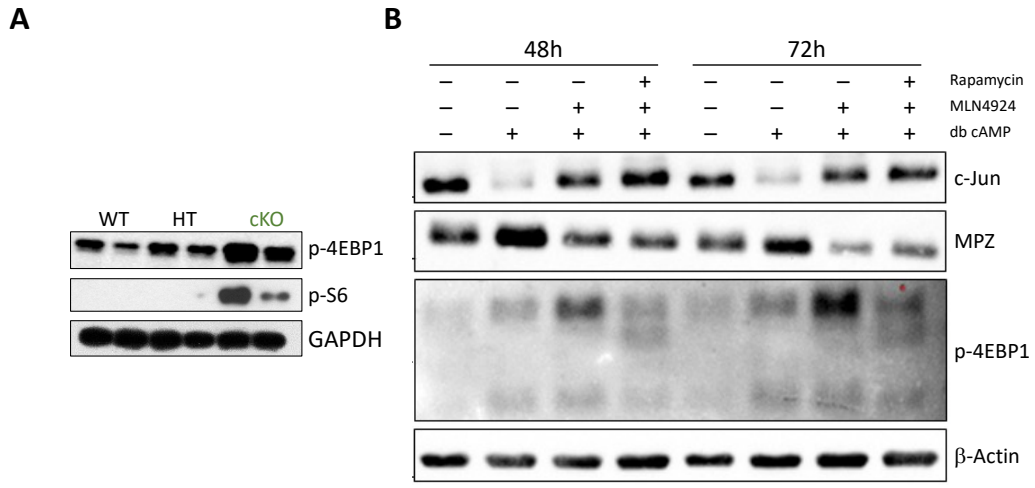

Figure 33. Neddylation inhibition in vivo leads to hyperactivation of mTOR pathway
(A) WB analyses of sciatic nerve lysates from control, heterozygote and NAE1 cKO mice at P28, showing that a hyperactivation of the mTOR pathway in cKO nerves. GAPDH is used as a loading control.
(B) WB analyses showing that blocking the mTOR pathway using rapamycin in cultured Schwann cells cannot rescue the MLN4924-induced block in MPZ upregulation and c-Jun downregulation after cAMP treatment. β-actin is used as a loading control.

5.12 Inducible inactivation of neddylation in vivo

Our constitutive conditional Nae1 cKO model has been vital to understand the process of Schwann cell myelination. However, because of the profound phenotype and the early lethality of these mice, we could not address the role of neddylation in later stages of the myelination process nor in Wallerian degeneration and nerve regeneration after injury. To address this, we generated an inducible conditional knockout model that allow us to circumvent the problems associated with lethality in our constitutive model. For this, we used a tamoxifen-inducible $Mbp^{tm2(EGFP/cre/ERT2)Wtsi}$ driver line that expresses Cre recombinase under the control of Mbp promoter following tamoxifen induction. This mouse line was crossed with Nae1 floxed mice, to generate the inducible Nae1 cKO mice (Nae1 *ic*KO). Using PCR analyses, we found that tamoxifen was able to induce highly efficient recombination of the Nae1 allele in sciatic nerves (**Figure 34**). In these experiments, mice of about 2 months of age were injected with tamoxifen at a concentration of 100mg/kg for 5 consecutive days, and then the nerves or brain dissected out 1 month later.

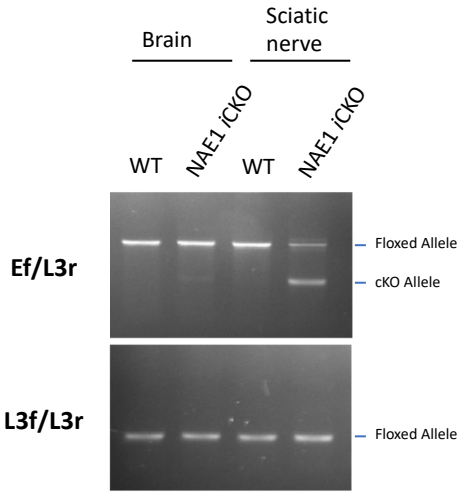

Figure 34. Tamoxifen-inducible Schwann cell specific knockout of NAE1 (NAE1 *ic*KO)
(**B**) Genomic DNA was extracted from sciatic nerves and brain and analyzed by PCR to detect NAE1 floxed allele (L3f and L3r) and Cre-mediated recombination (Ef and L3r) in P90 NAE1 icKO mice, 1 month after tamoxifen treatment. Efficient recombination (presence of cKO allele band) was observed in sciatic nerves of NAE1 icKO mice whereas no recombination was seen in control mice, or in brain tissue.

Las secciones 5.13, 5.14, 5.15 y 5.16 están sujetas a confidencialidad por el autor

6 DISCUSSION

6 DISCUSSION

Post translational modifications play an essential role in regulating the activity and viability of thousands of proteins in cells. They drive significant changes in the cellular proteome in a short period of time, helping the cells to respond to different stimuli and environmental changes. In this thesis, we have found that the PTM neddylation is a critical regulator of Schwann cell myelination. We found that genetic ablation of Nae 1 (Nae1 cKO), a key enzyme in the neddylation pathway, in Schwann cells, led to striking defects in peripheral nerves that had all the hallmarks of a severe neuropathy, which was characterised by a severe reduction in nerve conduction velocity, near complete absence of peripheral myelination and active myelin breakdown. This was accompanied by widespread changes in the transcriptomic and proteomic profiles, and on a mechanistic level, our data suggests that the myelination defects could be due to a block in activity of Cullin Ring Ligases (CRL) that could be responsible for degradation of negative regulators of myelination, including c-Jun and Sox2. On the other hand, we did not find any robust role of neddylation for the maintenance of mature myelin sheaths, and in pilot studies, on the regeneration of nerves after nerve injury.

Neddylation is essential for Schwann cell myelination

We found that the key genes that form part of the neddylation pathway were highly expressed during the early stages of Schwann cell development that was accompanied by an accumulation of neddylated protein and elevated expression of NAE1, suggesting a key role of neddylation in Schwann cell myelination. Notably, when we ablated NAE1 specifically in Schwann cells, we found a striking phenotype in Schwann cell myelination. We found that the Schwann cells were arrested at the pro-myelin stage that were not able to proceed with the myelination process. These defects were unlikely to be related with impaired radial sorting since there were no overt differences in the generation of pro-myelin Schwann cells from immature Schwann cells. In addition, we found that a large proportion of the Schwann cells that had managed to form the myelin sheaths in the *NAE1* cKO mice, underwent active myelin degeneration, suggesting that the few myelinated cells were unstable.

These profound defects in myelination led to severe gait abnormalities, muscle weakness, and hindlimb clasping, a typical presentation of neuromuscular dysfunction very early after birth. Consistent with the defective myelination in the NAE1 cKO mutants, the motor unit function of mutant mice was severely impaired, as reflected by a marked reduction in conduction velocity. Furthermore, the mean peak amplitudes and duration of CMAPs were also severely affected, accounting for the defect in motor function in NAE1 mutants. Notably, most

mice did not survive past three weeks of age. This was likely due to respiratory failure caused by demyelination in the phrenic nerves that innervate the diaphragm leading to its paralysis, as well as other contributory factors including weakness of the intercostal and other accessory muscles of respiration, a typical complication of the demyelinating disease Guillain–Barré Syndrome[255]. It would be interesting to examine whether the neddylation pathway is dysregulated in nerves from the various myelin disorders, such as CMT, GBS, etc. This could lead to the identification of a novel pathway involved in the pathogenesis of these debilitating nerve disorders.

These defects in myelination in NAE1 cKO mice was accompanied by a dramatic decrease in expression of the major peripheral myelin proteins, including MPZ, MBP and CNP. There was also a major decrease in expression of the key myelination transcriptional regulator EGR2 (Figure 15). We did not find any overt differences between wild-type and heterozygous mice, either at the ultrastructural or biochemical levels suggesting that the NAE1 gene was haplosuficient and any overt phenotype in myelination requires the inactivation of both alleles to alter the neddylation profiles of key targets.

As expected, transcriptomic and proteomic profiles of the NAE1 mutant nerves showed widespread changes that were consistent with the demyelination phenotype. Several genes/proteins related to lipid metabolism were found to be downregulated, likely resulting in the lack of formation of the highly lipid-rich myelin sheaths. On the other hand, we found that one of the most significant categories associated with the upregulated genes in the NAE1 cKO mice was related to cell cycle. Importantly, we found that this was associated with an increase in proliferation rates in Schwann cells in the mutant mice. At birth, immature Schwann cells exit the cell cycle and begin their differentiation into myelinating Schwann cells [256] as shown by a sharp decrease in proliferation rates in control mice. In NAE1 cKO mice, on the other hand, we found that these high proliferation rates were maintained at early stages. This is in sharp contrast to cancer cells, in which neddylation inhibition can instead potently suppress cellular proliferation [257–259]. These results suggest that the Schwann cells in the mutant mice remain arrested in an undifferentiated proliferative state and cannot further proceed with the myelin differentiation program.

Neddylation regulates CRL-mediated degradation of negative regulators of myelination

Several studies in the past decades have shown that the myelination program involves a balance between positive and negative regulators[260]. Several negative regulators, including c-Jun, Sox2[261] and Notch[9] have been identified that oppose this myelination program during development. These regulators are highly expressed in immature Schwann cells and their levels

gradually decrease as the cells undergo differentiation. Importantly, artificially preventing the decrease in level of these negative regulators in vivo can induce a block myelination[91] , suggesting that their downregulation is an essential prerequisite of the myelination program. Here, we found that levels of c-Jun and Sox2 were highly upregulated in the mutant nerves, suggesting that this could be partly responsible for the defects in myelination in the NAE1 cKO mice.

We found that these elevated c-Jun and Sox2 levels in the NAE1 cKO mice was caused by an impairment in their proteasomal degradation via CRLs during development. We found that major components of the CRL family were highly expressed in Schwann cells during development, and that they were likely responsible for the protein degradation of the negative regulators, uncovering a novel layer of control in Schwann cell myelination. Treatment of primary Schwann cell cultures with cAMP analogues, which can potently induce expression of myelin proteins[83], led to a progressive downregulation of the protein expression of the negative regulators c-Jun and Sox-2. Strikingly though, neddylation inhibition with the pharmacological inhibitor MLN4924 was able to prevent this decrease in protein expression. Importantly, this was not due to an effect on c-Jun and Sox2 mRNA levels, since there were no differences in expression when control cultures were compared to MLN4924-treated cultures, suggesting that neddylation was required for their turnover. A cycloheximide-based pulse-chase assay demonstrated that MLN significantly increased the stability of these proteins. Using shRNA silencing experiments, we found that a CRL complex consisting of Cullin-1 and Fbxw7 were likely to be responsible for the ubiquitination and degradation of c-Jun and Sox2.

Neddylation drives expression of key pathways in Schwann cell myelination

We also found that neddylation inhibition led to an inactivation of the YAP pathway in vivo, by inducing an accumulation of the Hippo kinases LATS1 and MOB, likely due to an impairment in their proteasomal degradation via CRLs. This would be in line with previous studies showing that neddylation was essential for ventricular chamber maturation through repression of Hippo signalling by CRL-mediated degradation of the Hippo kinases Mst1 and LATS1/2 [262]. The YAP/TAZ pathway has been previously shown to be critically important for Schwann cell myelination by several laboratories [251,253], and our studies show that neddylation could be important for regulating activation of the YAP/TAZ pathway during this process. Similarly, the mTOR pathway plays complex roles in the metabolic control of Schwann cell myelination. Whilst mTOR promotes the production and expansion of myelin sheaths [120,254], it can, on the other hand, negatively regulate the onset of the differentiation process itself. mTOR blocks the transition from promyelinating to myelinating SCs by suppressing transiently Krox20

expression, and a decline in mTORC1 activity releases this block and allows myelination to proceed. mTOR hyperactivation in immature Schwann cells in various mouse models, can either arrest or delay the onset of myelination [120,263,264]. Here, we show that nerves from NAE1 cKO mice show a strong hyperactivation of the mTOR pathway, which coincided with a suppression of Krox20 levels. These results suggest that neddylation is required for suppression of mTOR activity at the onset of myelination, although the exact mechanisms still need to be uncovered. In summary, in this thesis, we have shown that neddylation is crucial for the initiation of Schwann cell myelination, by controlling, likely via its main direct targets, CRLs, the expression/activation of several critical regulators, placing neddylation as a central hub in this process.

Neddylation is not involved in maintenance of myelin nor in Schwann cell responses to injury

In contrast, we found that the maintenance of already formed myelin was unlikely to be dependent on neddylation. In vivo ablation of NAE1 in mature myelinating Schwann cells using our inducible mouse models, had no overt effect and the myelin sheaths appeared normal. This is in contrast to ablation of other key regulators such as Krox-20[265] or Sox10 [266], which result in severe demyelination in adult nerves. These results are in line with a sharp decrease in NAE1 levels and neddylated proteins, when adult nerves were compared to developing nerves.

As established in previous studies, nerve injury leads to a gradual increase in c-Jun levels, which is key for driving the reprogramming of mature Schwann cells to cells specialized for promoting regeneration and repair[107]. In pilot studies, we found that neddylation inhibition in our inducible mouse model led to a striking decrease in c-Jun levels in injured nerves compared to control mice after the initial stages of nerve injury. This was quite an unexpected result since we had found that neddylation inhibition during development instead induces a dramatic increase in c-Jun levels. These results clearly suggest that different mechanisms operate in peripheral nerves during development and injury to regulate c-Jun levels. On the one hand, during development, c-Jun protein levels are high and for myelination to proceed, their levels have to be strongly downregulated. In this case, neddylation activates a CRL complex that would likely include Cullin-1 and Fbxw7 to induce this degradation of c-Jun, and when neddylation inhibition would lead to an accumulation of c-Jun. On the other hand, after nerve injury, there is a strong activation of c-Jun transcription and an increase in its protein levels. In this case, we postulate that neddylation, via a different CRL complex, could be important for degradation of a negative regulator of c-Jun transcription, and/or proteins that promote its translation or stability, and neddylation inhibition would lead to a decrease in c-Jun levels. It would be

imperative in future studies to identify these regulators, and the CRL complexes that regulate their expression.

In conclusion, in this thesis, we have found that neddylation plays a critical role for Schwann cell myelination and acts a central hub of control of this process by regulating some of the key molecules involved. On the hand, neddylation participates in suppressing the expression of several negative regulators, thus releasing their block exerted on this process, and on the other hand, participates in promoting expression of positive regulators, thus potentiating their role in the activation of this process. Importantly, we found that neddylation could have context-dependent functions in Schwann cells. Thus, we found, for example, that neddylation inhibition can both increase or decrease c-Jun levels in Schwann cells, depending on the physiological status of the cells.

7 CONCLUSIONS

7 CONCLUSIONS

- Neddylation pathway components are expressed at ages that correspond to Schwann cell myelination.
- Inactivation of neddylation in Schwann cells, by tissue-specific ablation of *Nae1* leads to profound defects in peripheral nerve development.
- Nae1 cKO mice are characterized by an almost complete lack of myelinated pheripheral axons, causing profound gait and locomotory defects and sever reductions in nerve conduction velocity.
- The defects in Schwann cell myelination are likely related to a block in the inactivation of the myelination after the immature Schwann cells establish a 1:1 relationship with axons (pro-myelin Schwann cells).
- Sustained expression of negative regulators of myelination c-Jun and Sox2 may be associated with the myelination defects observed in Nae1 cKO mice.
- Neddylation is important for CRL-mediated degradation of c-Jun and Sox2.
- YAP/TAZ and mTOR pathway activation is regulated by neddylation in Schwann cells.
- Even though neddylation appears to be important during developmental myelination it may be not important for maintenance of mature myelin sheaths.
- Neddylation does not appear to have a fundamental role in nerve regeneration after injury.

8 BIBLIOGRAPHY

1. Catala M, Kubis N. *Gross Anatomy and Development of the Peripheral Nervous System*. Vol 115. 1st ed. Elsevier B.V.; 2013. doi:10.1016/B978-0-444-52902-2.00003-5

2. Jessen KR, Mirsky R. The repair Schwann cell and its function in regenerating nerves. *J Physiol*. 2016;594(13):3521-3531. doi:10.1113/JP270874

3. Reed CB, Feltri ML, Wilson ER. Peripheral glia diversity. *J Anat*. 2021;(May):1-16. doi:10.1111/joa.13484

4. Verkhratsky A, Butt A. Peripheral Glial Cells. *Glial Physiol Pathophysiol*. 2013;(i):381-430. doi:10.1002/9781118402061.ch8

5. Zujovic V, Thibaud J, Bachelin C, et al. Boundary cap cells are peripheral nervous system stem cells that can be redirected into central nervous system lineages. *Proc Natl Acad Sci*. 2011;108(26):10714-10719. doi:10.1073/pnas.1018687108

6. Jessen KR, Mirsky R. Schwann Cell Precursors; Multipotent Glial Cells in Embryonic Nerves. *Front Mol Neurosci*. 2019;12:69. doi:10.3389/fnmol.2019.00069

7. Newbern J, Birchmeier C. Nrg1/ErbB signaling networks in Schwann cell development and myelination. *Semin Cell Dev Biol*. 2010;21(9):922-928. doi:10.1016/j.semcdb.2010.08.008

8. Quintes S, Brinkmann BG, Ebert M, et al. Zeb2 is essential for Schwann cell differentiation, myelination and nerve repair. *Nat Neurosci*. 2016;19(8):1050-1059. doi:10.1038/nn.4321

9. Woodhoo A, Alonso MBD, Droggiti A, et al. Notch controls embryonic Schwann cell differentiation, postnatal myelination and adult plasticity. *Nat Neurosci*. 2009;12(7):839-847. doi:10.1038/nn.2323

10. Parkinson DB, Bhaskaran A, Droggiti A, et al. Krox-20 inhibits Jun-NH2-terminal kinase/c-Jun to control Schwann cell proliferation and death. *J Cell Biol*. 2004;164(3):385-394. doi:10.1083/jcb.200307132

11. Khalilian S, Hojati Z, Dehghanian F, et al. Gene expression profiles of YAP1, TAZ, CRB3, and VDR in familial and sporadic multiple sclerosis among an Iranian population. *Sci Rep*. 2021;11(1). doi:10.1038/s41598-021-87131-z

12. Hirata H, Hibasami H, Yoshida T, et al. Nerve growth factor signaling of p75 induces differentiation and ceramide-mediated apoptosis in Schwann cells cultured from degenerating nerves. *Glia*. 2001;36(3):245-258. doi:10.1002/GLIA.1113

13. Jessen KR, Mirsky R. The success and failure of the schwann cell response to nerve injury. *Front Cell Neurosci*. 2019;13(February):1-14. doi:10.3389/fncel.2019.00033

14. Jessen KR, Mirsky R. Negative regulation of myelination: Relevance for development, injury, and demyelinating disease. *Glia*. 2008;56(14):1552-1565. doi:10.1002/glia.20761

15. Nocera G, Jacob C. Mechanisms of Schwann cell plasticity involved in peripheral nerve repair after injury. *Cell Mol Life Sci*. 2020;77(20):3977-3989. doi:10.1007/s00018-020-03516-9

16. Stoll G, Jander S, Myers RR. *Degeneration and Regeneration of the Peripheral Nervous System: From Augustus Waller's Observations to Neuroinflammation*. Vol 7.; 2002.

17. Clements MP, Byrne E, Camarillo Guerrero LF, et al. The Wound Microenvironment Reprograms Schwann Cells to Invasive Mesenchymal-like Cells to Drive Peripheral Nerve Regeneration. *Neuron*. 2017;96(1):98-114.e7. doi:10.1016/j.neuron.2017.09.008

18. Widenfalk J, Wu W, Hao J, Person JKE, Wiesenfeldt-Hallin Z, Risling M. Treatment of transected peripheral nerves with artemin improved motor neuron regeneration, but did not reduce nerve injury-induced pain behaviour. *Scand J Plast Reconstr Surg Hand Surg*. 2009;43(5):245-250. doi:10.3109/02844310903259082

19. Brushart TM, Aspalter M, Griffin JW, et al. Schwann cell phenotype is regulated by axon modality and central–peripheral location, and persists in vitro. *Exp Neurol*. 2013;247:272-281. doi:10.1016/j.expneurol.2013.05.007

20. Gomez-Sanchez JA, Carty L, Iruarrizaga-Lejarreta M, et al. Schwann cell autophagy, myelinophagy, initiates myelin clearance from injured nerves. *J Cell Biol*. 2015;210(1):153-168. doi:10.1083/jcb.201503019

21. Ydens E, Amann L, Asselbergh B, et al. Profiling peripheral nerve macrophages reveals two macrophage subsets with distinct localization, transcriptome and response to injury. *Nat Neurosci*. 2020;23(5):676-689. doi:10.1038/s41593-020-0618-6

22. Dubový P, Jančálek R, Kubek T. Role of Inflammation and Cytokines in Peripheral Nerve Regeneration. In: ; 2013:173-206. doi:10.1016/B978-0-12-410499-0.00007-1

23. Thornton MR, Mantovani C, Birchall MA, Terenghi G. Quantification of N-CAM and N-cadherin expression in axotomized and crushed rat sciatic nerve. *J Anat*. 2005;206(1):69-78. doi:10.1111/j.0021-8782.2005.00369.x

24. Gordon T. The role of neurotrophic factors in nerve regeneration. *Neurosurg Focus*. 2009;26(2):1-10. doi:10.3171/FOC.2009.26.2.E3

25. English AW, Liu K, Nicolini JM, Mulligan AM, Ye K. Small-molecule trkB agonists promote axon regeneration in cut peripheral nerves. *Proc Natl Acad Sci U S A*. 2013;110(40):16217-16222. doi:10.1073/pnas.1303646110

26. Koenig H. Role of progesterone in peripheral nerve repair. *Rev Reprod*. 2000;5(3):189-199. doi:10.1530/ror.0.0050189

27. Sohn EJ, Park HT. MicroRNA Mediated Regulation of Schwann Cell Migration and Proliferation in Peripheral Nerve Injury. *Biomed Res Int*. 2018;2018. doi:10.1155/2018/8198365

28. Fazal S V, Gomez-Sanchez JA, Wagstaff LJ, et al. Development/Plasticity/Repair Graded Elevation of c-Jun in Schwann Cells In Vivo: Gene Dosage Determines Effects on Development, Remyelination, Tumorigenesis, and Hypomyelination. Published online 2017. doi:10.1523/JNEUROSCI.0986-17.2017

29. Gomez-Sanchez JA, Pilch KS, Van Der Lans M, et al. After nerve injury, lineage tracing shows that myelin and Remak Schwann cells elongate extensively and branch to form repair Schwann cells, which shorten radically on remyelination. *J Neurosci*. 2017;37(37):9086-9099. doi:10.1523/JNEUROSCI.1453-17.2017

30. Yang DP, Zhang DP, Mak KS, Bonder DE, Pomeroy SL, Kim HA. Schwann cell proliferation during Wallerian degeneration is not necessary for regeneration and remyelination of the peripheral nerves: Axon-dependent removal of newly generated Schwann cells by apoptosis. *Mol Cell Neurosci*. 2008;38(1):80-88. doi:10.1016/j.mcn.2008.01.017

31. Nave KA. Myelination and the trophic support of long axons. *Nat Rev Neurosci*. 2010;11(4):275-283. doi:10.1038/nrn2797

32. Tasaki I. THE ELECTRO-SALTATORY TRANSMISSION OF THE NERVE IMPULSE AND THE EFFECT OF NARCOSIS UPON THE NERVE FIBER. *Am J Physiol Content*. 1939;127(2):211-227. doi:10.1152/ajplegacy.1939.127.2.211

33. Ronchi G, Haastert-Talini K, Fornasari BE, Perroteau I, Geuna S, Gambarotta G. The Neuregulin1/ErbB system is selectively regulated during peripheral nerve degeneration and regeneration. *Eur J Neurosci*. 2016;43(3):351-364. doi:10.1111/ejn.12974

34. Salzer JL. Schwann Cell Myelination. *Cold Spring Harb Perspect Biol*. 2015;7(8):a020529. doi:10.1101/cshperspect.a020529

35. Kou Y, Yu F, Yuan Y, et al. *Original Article Effects of NP-1 on Proliferation,*

Migration, and Apoptosis of Schwann Cell Line RSC96 through the NF-KB Signaling Pathway. Vol 12.; 2020. www.ajtr.org

36. He X, Zhang L, Queme LF, et al. A histone deacetylase 3-dependent pathway delimits peripheral myelin growth and functional regeneration. *Nat Med*. 2018;24(3):338-351. doi:10.1038/nm.4483

37. Monk KR, Feltri ML, Taveggia C. New insights on schwann cell development. *Glia*. 2015;63(8):1376-1393. doi:10.1002/glia.22852

38. Norrmén C, Figlia G, Lebrun-Julien F, et al. mTORC1 Controls PNS Myelination along the mTORC1-RXRγ-SREBP-Lipid Biosynthesis Axis in Schwann Cells. *Cell Rep*. 2014;9(2):646-660. doi:10.1016/j.celrep.2014.09.001

39. Wüst HM, Wegener A, Fröb F, et al. Egr2-guided histone H2B monoubiquitination is required for peripheral nervous system myelination. *Nucleic Acids Res*. 2020;48(16):8959-8976. doi:10.1093/nar/gkaa606

40. Ha N, Choi Y Il, Jung N, et al. *A Novel Histone Deacetylase 6 Inhibitor Improves Myelination of Schwann Cells in a Model of Charcot–Marie–Tooth Disease Type 1A*. Vol 177.; 2020. doi:10.1111/bph.15231

41. Stassart RM, Möbius W, Nave KA, Edgar JM. The Axon-Myelin Unit in Development and Degenerative Disease. *Front Neurosci*. 2018;12. doi:10.3389/fnins.2018.00467

42. Terada N, Saitoh Y, Kamijo A, Yamauchi J, Ohno N, Sakamoto T. Structures and Molecular Composition of Schmidt–Lanterman Incisures. In: ; 2019:181-198. doi:10.1007/978-981-32-9636-7_12

43. Miyamoto T, Morita K, Takemoto D, et al. Tight junctions in Schwann cells of peripheral myelinated axons. *J Cell Biol*. 2005;169(3):527-538. doi:10.1083/jcb.200501154

44. Nualart-Marti A, Solsona C, Fields RD. Gap junction communication in myelinating glia. *Biochim Biophys Acta - Biomembr*. 2013;1828(1):69-78. doi:10.1016/j.bbamem.2012.01.024

45. Marani E, Lakke EAJF. Peripheral Nervous System Topics. In: *The Human Nervous System*. Elsevier; 2012:82-140. doi:10.1016/B978-0-12-374236-0.10004-5

46. Kidd GJ, Ohno N, Trapp BD. Biology of Schwann cells. In: ; 2013:55-79. doi:10.1016/B978-0-444-52902-2.00005-9

47. Poitelon Y, Kopec AM, Belin S. Myelin Fat Facts: An Overview of Lipids and Fatty Acid Metabolism. *Cells*. 2020;9(4). doi:10.3390/cells9040812

48. Kondo Y, Wenger DA, Gallo V, Duncan ID. From The Cover:

Galactocerebrosidase-deficient oligodendrocytes maintain stable central myelin by exogenous replacement of the missing enzyme in mice. *Proc Natl Acad Sci*. 2005;102(51):18670-18675. doi:10.1073/pnas.0506473102

49. Morell P QR. Characteristic Composition of Myelin. *Basic Neurochem Mol Cell Med Asp 6th Ed*. Published online 1999. https://www.ncbi.nlm.nih.gov/books/NBK28221/

50. Zenker J, Stettner M, Ruskamo S, et al. A role of peripheral myelin protein 2 in lipid homeostasis of myelinating schwann cells. *Glia*. 2014;62(9):1502-1512. doi:10.1002/glia.22696

51. Torii T, Miyamoto Y, Yamauchi J. Cellular Signal-Regulated Schwann Cell Myelination and Remyelination. *Adv Exp Med Biol*. 2019;1190:3-22. doi:10.1007/978-981-32-9636-7_1

52. Glenn TD, Talbot WS. Signals regulating myelination in peripheral nerves and the Schwann cell response to injury. *Curr Opin Neurobiol*. 2013;23(6):1041-1048. doi:10.1016/j.conb.2013.06.010

53. Fricker FR, Bennett DL. The role of neuregulin-1 in the response to nerve injury. *Future Neurol*. 2011;6(6):809-822. doi:10.2217/fnl.11.45

54. Ronchi G, Cillino M, Gambarotta G, et al. Irreversible changes occurring in long-term denervated Schwann cells affect delayed nerve repair. *J Neurosurg*. 2017;127(4):843-856. doi:10.3171/2016.9.JNS16140

55. Li H, Terenghi G, Hall SM. Effects of delayed re-innervation on the expression of c-erbB receptors by chronically denervated rat Schwann cells in vivo. *Glia*. 1997;20(4):333-347. doi:10.1002/(SICI)1098-1136(199708)20:4<333::AID-GLIA6>3.0.CO;2-6

56. Guertin AD. Microanatomy of Axon/Glial Signaling during Wallerian Degeneration. *J Neurosci*. 2005;25(13):3478-3487. doi:10.1523/JNEUROSCI.3766-04.2005

57. Syed N, Reddy K, Yang DP, et al. Soluble Neuregulin-1 Has Bifunctional, Concentration-Dependent Effects on Schwann Cell Myelination. *J Neurosci*. 2010;30(17):6122-6131. doi:10.1523/JNEUROSCI.1681-09.2010

58. Yamauchi J, Miyamoto Y, Chan JR, Tanoue A. ErbB2 directly activates the exchange factor Dock7 to promote Schwann cell migration. *J Cell Biol*. 2008;181(2):351-365. doi:10.1083/jcb.200709033

59. Atanasoski S. ErbB2 Signaling in Schwann Cells Is Mostly Dispensable for Maintenance of Myelinated Peripheral Nerves and Proliferation of Adult Schwann Cells after Injury. *J Neurosci*. 2006;26(7):2124-2131. doi:10.1523/JNEUROSCI.4594-05.2006

60. Fricker FR, Antunes-Martins A, Galino J, et al. Axonal neuregulin 1 is a rate limiting but not essential factor for nerve remyelination. *Brain*. 2013;136(7):2279-2297. doi:10.1093/brain/awt148

61. Stassart RM, Fledrich R, Velanac V, et al. A role for Schwann cell–derived neuregulin-1 in remyelination. *Nat Neurosci*. 2013;16(1):48-54. doi:10.1038/nn.3281

62. Shin YK, Jang SY, Park JY, et al. The Neuregulin-Rac-MKK7 pathway regulates antagonistic c-jun/Krox20 expression in Schwann cell dedifferentiation. *Glia*. 2013;61(6):892-904. doi:10.1002/glia.22482

63. Fleck D, van Bebber F, Colombo A, et al. Dual Cleavage of Neuregulin 1 Type III by BACE1 and ADAM17 Liberates Its EGF-Like Domain and Allows Paracrine Signaling. *J Neurosci*. 2013;33(18):7856-7869. doi:10.1523/JNEUROSCI.3372-12.2013

64. Fleck D, N. Garratt A, Haass C, Willem M. BACE1 Dependent Neuregulin Processing: Review. *Curr Alzheimer Res*. 2012;9(2):178-183. doi:10.2174/156720512799361637

65. Hu X, Hou H, Bastian C, et al. BACE1 regulates the proliferation and cellular functions of Schwann cells. *Glia*. 2017;65(5):712-726. doi:10.1002/glia.23122

66. La Marca R, Cerri F, Horiuchi K, et al. TACE (ADAM17) inhibits Schwann cell myelination. *Nat Neurosci*. 2011;14(7):857-865. doi:10.1038/nn.2849

67. Frohnert PW, Stonecypher MS, Carroll SL. Constitutive activation of the neuregulin-1/ErbB receptor signaling pathway is essential for the proliferation of a neoplastic Schwann cell line. *Glia*. 2003;43(2):104-118. doi:10.1002/glia.10232

68. Huijbregts RPH, Roth KA, Schmidt RE, Carroll SL. Hypertrophic Neuropathies and Malignant Peripheral Nerve Sheath Tumors in Transgenic Mice Overexpressing Glial Growth Factor β3 in Myelinating Schwann Cells. *J Neurosci*. 2003;23(19):7269-7280. doi:10.1523/JNEUROSCI.23-19-07269.2003

69. Celhar T, Magalhães R, Fairhurst AM. TLR7 and TLR9 in SLE: when sensing self goes wrong. *Immunol Res*. 2012;53(1-3):58-77. doi:10.1007/s12026-012-8270-1

70. Thakur A, Mikkelsen H, Jungersen G. Intracellular Pathogens: Host Immunity and Microbial Persistence Strategies. *J Immunol Res*. 2019;2019:1-24. doi:10.1155/2019/1356540

71. Boivin A, Pineau I, Barrette B, et al. Toll-Like Receptor Signaling Is Critical for Wallerian Degeneration and Functional Recovery after Peripheral Nerve Injury. *J Neurosci*. 2007;27(46):12565-12576. doi:10.1523/JNEUROSCI.3027-07.2007

72. Lee H, Jo EK, Choi SY, et al. Necrotic neuronal cells induce inflammatory Schwann cell activation via TLR2 and TLR3: Implication in Wallerian degeneration. *Biochem Biophys Res Commun*. 2006;350(3):742-747. doi:10.1016/j.bbrc.2006.09.108

73. Thakur KK, Saini J, Mahajan K, et al. Therapeutic implications of toll-like receptors in peripheral neuropathic pain. *Pharmacol Res*. 2017;115:224-232. doi:10.1016/j.phrs.2016.11.019

74. Mogha A, Harty BL, Carlin D, et al. Gpr126/Adgrg6 has Schwann cell autonomous and nonautonomous functions in peripheral nerve injury and repair. *J Neurosci*. 2016;36(49):12351-12367. doi:10.1523/JNEUROSCI.3854-15.2016

75. Petersen SC, Luo R, Liebscher I, et al. The Adhesion GPCR GPR126 Has Distinct, Domain-Dependent Functions in Schwann Cell Development Mediated by Interaction with Laminin-211. *Neuron*. 2015;85:755-769. doi:10.1016/j.neuron.2014.12.057

76. Monk KR, Naylor SG, Glenn TD, et al. A G Protein–Coupled Receptor Is Essential for Schwann Cells to Initiate Myelination. *Science (80-)*. 2009;325(5946):1402-1405. doi:10.1126/science.1173474

77. Monk KR, Oshima K, Jörs S, Heller S, Talbot WS. Gpr126 is essential for peripheral nerve development and myelination in mammals. *Development*. 2011;138(13):2673-2680. doi:10.1242/dev.062224

78. Wen J, Tan D, Li L, Wang X, Pan M, Guo J. RhoA regulates Schwann cell differentiation through JNK pathway. *Exp Neurol*. 2018;308:26-34. doi:10.1016/j.expneurol.2018.06.013

79. Ackerman SD, Luo R, Poitelon Y, et al. GPR56/ADG RG1 regulates development and maintenance of peripheral myelin. *J Exp Med*. 2018;215(3):941-961. doi:10.1084/jem.20161714

80. Anliker B, Choi JW, Lin ME, et al. Lysophosphatidic acid (LPA) and its receptor, LPA 1 , influence embryonic schwann cell migration, myelination, and cell-to-axon segregation. *Glia*. 2013;61(12):2009-2022. doi:10.1002/glia.22572

81. Trimarco A, Forese MG, Alfieri V, et al. Prostaglandin D2 synthase/GPR44: a signaling axis in PNS myelination. *Nat Neurosci*. 2014;17(12):1682-1692. doi:10.1038/nn.3857

82. Bacallao K, Monje P V. Correction: Opposing Roles of pka and epac in the cAMP-Dependent Regulation of Schwann Cell Proliferation and Differentiation. Linden R, ed. *PLoS One*. 2014;9(1). doi:10.1371/annotation/fa651e8d-ed5a-4937-8d7e-8009b10dcbe0

83. Morgan L, Jessen KR, Mirsky R. The effects of cAMP on differentiation of

cultured Schwann cells: progression from an early phenotype (04+) to a myelin phenotype (P0+, GFAP-, N-CAM-, NGF-receptor-) depends on growth inhibition. *J Cell Biol*. 1991;112(3):457-467. doi:10.1083/jcb.112.3.457

84. Glenn TD, Talbot WS. Analysis of Gpr126 function defines distinct mechanisms controlling the initiation and maturation of myelin. *Development*. 2013;140(15):3167-3175. doi:10.1242/dev.093401

85. Schweisguth F. Regulation of Notch Signaling Activity. *Curr Biol*. 2004;14(3):R129-R138. doi:10.1016/j.cub.2004.01.023

86. Wang J, Ren KY, Wang YH, et al. Effect of active Notch signaling system on the early repair of rat sciatic nerve injury. *Artif Cells, Nanomedicine, Biotechnol*. 2015;43(6):383-389. doi:10.3109/21691401.2014.896372

87. Wu LMN, Wang J, Conidi A, et al. Zeb2 recruits HDAC–NuRD to inhibit Notch and controls Schwann cell differentiation and remyelination. *Nat Neurosci*. 2016;19(8):1060-1072. doi:10.1038/nn.4322

88. Morton PD, Dellarole A, Theus MH, Walters WM, Berge SS, Bethea JR. Activation of NF- B in Schwann Cells Is Dispensable for Myelination In Vivo. *J Neurosci*. 2013;33(24):9932-9936. doi:10.1523/JNEUROSCI.2483-12.2013

89. Boerboom A, Dion V, Chariot A, Franzen R. Molecular mechanisms involved in schwann cell plasticity. *Front Mol Neurosci*. 2017;10(February):1-18. doi:10.3389/fnmol.2017.00038

90. Parrinello S, Napoli I, Ribeiro S, et al. EphB signaling directs peripheral nerve regeneration through Sox2-dependent Schwann cell Sorting. *Cell*. 2010;143(1):145-155. doi:10.1016/j.cell.2010.08.039

91. Parkinson DB, Bhaskaran A, Arthur-Farraj P, et al. c-Jun is a negative regulator of myelination. *J Cell Biol*. 2008;181(4):625-637. doi:10.1083/jcb.200803013

92. Roskoski R. ERK1/2 MAP kinases: Structure, function, and regulation. *Pharmacol Res*. 2012;66(2):105-143. doi:10.1016/j.phrs.2012.04.005

93. Wortzel I, Seger R. The ERK Cascade: Distinct Functions within Various Subcellular Organelles. *Genes Cancer*. 2011;2(3):195-209. doi:10.1177/1947601911407328

94. Rodríguez-Molina JF, Lopez-Anido C, Ma KH, et al. Dual specificity phosphatase 15 regulates Erk activation in Schwann cells. *J Neurochem*. 2017;140(3):368-382. doi:10.1111/jnc.13911

95. Napoli I, Noon LA, Ribeiro S, et al. A Central Role for the ERK-Signaling Pathway in Controlling Schwann Cell Plasticity and Peripheral Nerve Regeneration In Vivo. *Neuron*. 2012;73(4):729-742. doi:10.1016/j.neuron.2011.11.031

96. Cervellini I, Galino J, Zhu N, Allen S, Birchmeier C, Bennett DL. Sustained MAPK/ERK Activation in Adult Schwann Cells Impairs Nerve Repair. *J Neurosci*. 2018;38(3):679-690. doi:10.1523/JNEUROSCI.2255-17.2017

97. Lee HJ, Shin YK, Park HT. Mitogen Activated Protein Kinase Family Proteins and c-jun Signaling in Injury-induced Schwann Cell Plasticity. *Exp Neurobiol*. 2014;23(2):130-137. doi:10.5607/en.2014.23.2.130

98. Tournier C, Dong C, Turner TK, Jones SN, Flavell RA, Davis RJ. MKK7 is an essential component of the JNK signal transduction pathway activated by proinflammatory cytokines. *Genes Dev*. 2001;15(11):1419-1426. doi:10.1101/gad.888501

99. Zhou Z, Liu Y, Nie X, et al. Involvement of upregulated SYF2 in Schwann cell differentiation and migration after sciatic nerve crush. *Cell Mol Neurobiol*. 2014;34(7):1023-1036. doi:10.1007/s10571-014-0078-1

100. Apra C, Richard L, Coulpier F, et al. Cthrc1 is a negative regulator of myelination in schwann cells. *Glia*. 2012;60(3):393-403. doi:10.1002/glia.22273

101. Yamauchi J, Miyamoto Y, Hamasaki H, et al. The Atypical Guanine-Nucleotide Exchange Factor, Dock7, Negatively Regulates Schwann Cell Differentiation and Myelination. *J Neurosci*. 2011;31(35):12579-12592. doi:10.1523/JNEUROSCI.2738-11.2011

102. Yang DP, Kim J, Syed N, et al. p38 MAPK Activation Promotes Denervated Schwann Cell Phenotype and Functions as a Negative Regulator of Schwann Cell Differentiation and Myelination. *J Neurosci*. 2012;32(21):7158-7168. doi:10.1523/JNEUROSCI.5812-11.2012

103. Mechta-Grigoriou F, Gerald D, Yaniv M. The mammalian Jun proteins: redundancy and specificity. *Oncogene*. 2001;20(19):2378-2389. doi:10.1038/sj.onc.1204381

104. Fazal S V., Gomez-Sanchez JA, Wagstaff LJ, et al. Graded Elevation of c-Jun in Schwann Cells In Vivo : Gene Dosage Determines Effects on Development, Remyelination, Tumorigenesis, and Hypomyelination. *J Neurosci*. 2017;37(50):12297-12313. doi:10.1523/JNEUROSCI.0986-17.2017

105. Wu C, Watts ME, Rubin LL. MAP4K4 Activation Mediates Motor Neuron Degeneration in Amyotrophic Lateral Sclerosis. *Cell Rep*. 2019;26(5):1143-1156.e5. doi:10.1016/j.celrep.2019.01.019

106. Hantke J, Carty L, Wagstaff LJ, et al. c-Jun activation in Schwann cells protects against loss of sensory axons in inherited neuropathy. *Brain*. 2014;137(11):2922-2937. doi:10.1093/brain/awu257

107. Arthur-Farraj PJ, Latouche M, Wilton DK, et al. c-Jun Reprograms Schwann

Cells of Injured Nerves to Generate a Repair Cell Essential for Regeneration. *Neuron*. 2012;75(4):633-647. doi:10.1016/j.neuron.2012.06.021

108. Heinen A, Lehmann HC, Küry P. Negative regulators of schwann cell differentiation-novel targets for peripheral nerve therapies? *J Clin Immunol*. 2013;33 Suppl 1:S18-26. doi:10.1007/s10875-012-9786-9

109. Heinen A, Kremer D, Gottle P, et al. The cyclin-dependent kinase inhibitor p57kip2 is a negative regulator of Schwann cell differentiation and in vitro myelination. *Proc Natl Acad Sci*. 2008;105(25):8748-8753. doi:10.1073/pnas.0802659105

110. Heinen A, Tzekova N, Graffmann N, et al. Histone methyltransferase enhancer of zeste homolog 2 regulates Schwann cell differentiation. *Glia*. 2012;60(11):1696-1708. doi:10.1002/glia.22388

111. Wu W, Liu Y, Wang Y. Sam68 promotes Schwann cell proliferation by enhancing the PI3K/Akt pathway and acts on regeneration after sciatic nerve crush. *Biochem Biophys Res Commun*. 2016;473(4):1045-1051. doi:10.1016/j.bbrc.2016.04.013

112. Wu W, Liu Q, Liu Y, Yu Z, Wang Y. Dixdc1 targets CyclinD1 and p21 via PI3K pathway activation to promote Schwann cell proliferation after sciatic nerve crush. *Biochem Biophys Res Commun*. 2016;478(2):956-963. doi:10.1016/j.bbrc.2016.08.058

113. Tao T, Ji Y, Cheng C, et al. Tumor necrosis factor-alpha inhibits Schwann cell proliferation by up-regulating Src-suppressed protein kinase C substrate expression. *J Neurochem*. 2009;111(3):647-655. doi:10.1111/j.1471-4159.2009.06346.x

114. Chen MS, Kim H, Jagot-Lacoussiere L, Maurel P. Cadm3 (Necl-1) interferes with the activation of the PI3 kinase/Akt signaling cascade and inhibits Schwann cell myelination in vitro. *Glia*. 2016;64(12):2247-2262. doi:10.1002/glia.23072

115. Cotter L, Özçelik M, Jacob C, et al. Dlg1-PTEN Interaction Regulates Myelin Thickness to Prevent Damaging Peripheral Nerve Overmyelination. *Science (80-)*. 2010;328(5984):1415-1418. doi:10.1126/science.1187735

116. Pinzón CE, Serrano ML, Sanabria MC. Papel de la vía fosfatidilinositol 3 kinasa (PI3K/Akt) en humanos. *Rev Ciencias la Salud*. 2009;7(2):47-66. Accessed December 16, 2021. http://www.scielo.org.co/scielo.php?script=sci_arttext&pid=S1692-72732009000200007&lng=en&nrm=iso&tlng=es

117. Laplante M, Sabatini DM. Regulation of mTORC1 and its impact on gene expression at a glance. *J Cell Sci*. Published online January 1, 2013. doi:10.1242/jcs.125773

118. Thoreen CC. The molecular basis of mTORC1-regulated translation. *Biochem Soc Trans*. 2017;45(1):213-221. doi:10.1042/BST20160072

119. Ma XM, Blenis J. Molecular mechanisms of mTOR-mediated translational control. *Nat Rev Mol Cell Biol*. 2009;10(5):307-318. doi:10.1038/nrm2672

120. Figlia G, Gerber D, Suter U. Myelination and mTOR. *Glia*. 2018;66(4):693-707. doi:10.1002/glia.23273

121. Montani L, Pereira JA, Norrmén C, et al. De novo fatty acid synthesis by Schwann cells is essential for peripheral nervous system myelination. *J Cell Biol*. 2018;217(4):1353-1368. doi:10.1083/jcb.201706010

122. Sherman DL, Krols M, Wu LMN, et al. Arrest of Myelination and Reduced Axon Growth When Schwann Cells Lack mTOR. *J Neurosci*. 2012;32(5):1817-1825. doi:10.1523/JNEUROSCI.4814-11.2012

123. Dai J, Bercury KK, Macklin WB. Interaction of mTOR and Erk1/2 signaling to regulate oligodendrocyte differentiation. *Glia*. 2014;62(12):2096-2109. doi:10.1002/glia.22729

124. Liu X, Peng S, Zhao Y, et al. AMPK Negatively Regulates Peripheral Myelination via Activation of c-Jun. *Mol Neurobiol*. 2017;54(5):3554-3564. doi:10.1007/s12035-016-9913-3

125. Grigoryan T, Stein S, Qi J, et al. Wnt/Rspondin/ -catenin signals control axonal sorting and lineage progression in Schwann cell development. *Proc Natl Acad Sci*. 2013;110(45):18174-18179. doi:10.1073/pnas.1310490110

126. Shackleford G, Makoukji J, Grenier J, Liere P, Meffre D, Massaad C. Differential regulation of Wnt/beta-catenin signaling by Liver X Receptors in Schwann cells and oligodendrocytes. *Biochem Pharmacol*. 2013;86(1):106-114. doi:10.1016/j.bcp.2013.02.036

127. Hichor M, Sampathkumar NK, Montanaro J, et al. Paraquat Induces Peripheral Myelin Disruption and Locomotor Defects: Crosstalk with LXR and Wnt Pathways. *Antioxid Redox Signal*. 2017;27(3):168-183. doi:10.1089/ars.2016.6711

128. Shi L, Huang L, He R, et al. Modeling the Pathogenesis of Charcot-Marie-Tooth Disease Type 1A Using Patient-Specific iPSCs. *Stem Cell Reports*. 2018;10(1):120-133. doi:10.1016/j.stemcr.2017.11.013

129. Ylikallio E, Johari M, Konovalova S, et al. Targeted next-generation sequencing reveals further genetic heterogeneity in axonal Charcot–Marie–Tooth neuropathy and a mutation in HSPB1. *Eur J Hum Genet*. 2014;22(4):522-527. doi:10.1038/ejhg.2013.190

130. Murphy SM, Laura M, Fawcett K, et al. Charcot–Marie–Tooth disease:

frequency of genetic subtypes and guidelines for genetic testing. *J Neurol Neurosurg Psychiatry*. 2012;83(7):706-710. doi:10.1136/jnnp-2012-302451

131. Passage E, Norreel JC, Noack-Fraissignes P, et al. Ascorbic acid treatment corrects the phenotype of a mouse model of Charcot-Marie-Tooth disease. *Nat Med*. 2004;10(4):396-401. doi:10.1038/nm1023

132. Lewis RA. High-Dosage Ascorbic Acid Treatment in Charcot-Marie-Tooth Disease Type 1A. *JAMA Neurol*. 2013;70(8):981. doi:10.1001/jamaneurol.2013.3178

133. Attarian S, Young P, Brannagan TH, et al. A double-blind, placebo-controlled, randomized trial of PXT3003 for the treatment of Charcot–Marie–Tooth type 1A. *Orphanet J Rare Dis*. 2021;16(1):433. doi:10.1186/s13023-021-02040-8

134. Caillaud M, Msheik Z, Ndong-Ntoutoume GMA, et al. Curcumin–cyclodextrin/cellulose nanocrystals improve the phenotype of Charcot-Marie-Tooth-1A transgenic rats through the reduction of oxidative stress. *Free Radic Biol Med*. 2020;161:246-262. doi:10.1016/j.freeradbiomed.2020.09.019

135. Das I, Krzyzosiak A, Schneider K, et al. Preventing proteostasis diseases by selective inhibition of a phosphatase regulatory subunit. *Science (80-)*. 2015;348(6231):239-242. doi:10.1126/science.aaa4484

136. Bai Y, Treins C, Volpi VG, et al. Treatment with IFB-088 improves neuropathy in CMT1A and CMT1B mice. *bioRxiv*. Published online January 1, 2021:2021.10.18.464779. doi:10.1101/2021.10.18.464779

137. Klein D, Groh J, Weishaupt A, Martini R. Endogenous antibodies contribute to macrophage-mediated demyelination in a mouse model for CMT1B. *J Neuroinflammation*. 2015;12(1):49. doi:10.1186/s12974-015-0267-y

138. Groh J, Weis J, Zieger H, Stanley ER, Heuer H, Martini R. Colony-stimulating factor-1 mediates macrophage-related neural damage in a model for Charcot–Marie–Tooth disease type 1X. *Brain*. 2012;135(1):88-104. doi:10.1093/brain/awr283

139. Klein D, Patzkó Á, Schreiber D, et al. Targeting the colony stimulating factor 1 receptor alleviates two forms of Charcot–Marie–Tooth disease in mice. *Brain*. 2015;138(11):3193-3205. doi:10.1093/brain/awv240

140. Fledrich R, Stassart RM, Klink A, et al. Soluble neuregulin-1 modulates disease pathogenesis in rodent models of Charcot-Marie-Tooth disease 1A. *Nat Med*. 2014;20(9):1055-1061. doi:10.1038/nm.3664

141. Steere AC, Strle F, Wormser GP, et al. Lyme borreliosis. *Nat Rev Dis Prim*. 2016;2. doi:10.1038/nrdp.2016.90

142. Ford L, Tufts DM. Lyme neuroborreliosis: Mechanisms of b. burgdorferi

infection of the nervous system. *Brain Sci*. 2021;11(6):789. doi:10.3390/brainsci11060789

143. Ding Z, Ma M, Tao L, et al. Rhesus Brain Transcriptomic Landscape in an ex vivo Model of the Interaction of Live Borrelia Burgdorferi With Frontal Cortex Tissue Explants. *Front Neurosci*. 2019;13. doi:10.3389/fnins.2019.00651

144. Donta ST, States LJ, Adams WA, et al. Report of the Pathogenesis and Pathophysiology of Lyme Disease Subcommittee of the HHS Tick Borne Disease Working Group. *Front Med*. 2021;8. doi:10.3389/fmed.2021.643235

145. Feldman EL, Callaghan BC, Pop-Busui R, et al. Diabetic neuropathy. *Nat Rev Dis Prim*. 2019;5(1). doi:10.1038/s41572-019-0092-1

146. Jankovic M, Novakovic I, Nikolic D, et al. Genetic and epigenomic modifiers of diabetic neuropathy. *Int J Mol Sci*. 2021;22(9):1-19. doi:10.3390/ijms22094887

147. Ilnytska O, Lyzogubov V V., Stevens MJ, et al. Poly(ADP-Ribose) Polymerase Inhibition Alleviates Experimental Diabetic Sensory Neuropathy. *Diabetes*. 2006;55(6):1686-1694. doi:10.2337/db06-0067

148. Kim ES, Isoda F, Kurland I, Mobbs C V. Glucose-Induced Metabolic Memory in Schwann Cells: Prevention by PPAR Agonists. *Endocrinology*. 2013;154(9):3054-3066. doi:10.1210/en.2013-1097

149. Ziegler D, Behler M, Schroers-Teuber M, Roden M. Near-normoglycaemia and development of neuropathy: a 24-year prospective study from diagnosis of type 1 diabetes. *BMJ Open*. 2015;5(6):e006559. doi:10.1136/bmjopen-2014-006559

150. Martin CL, Albers JW, Pop-Busui R. Neuropathy and Related Findings in the Diabetes Control and Complications Trial/Epidemiology of Diabetes Interventions and Complications Study. *Diabetes Care*. 2014;37(1):31-38. doi:10.2337/dc13-2114

151. Singleton JR, Marcus RL, Lessard MK, Jackson JE, Smith AG. Supervised exercise improves cutaneous reinnervation capacity in metabolic syndrome patients. *Ann Neurol*. 2015;77(1):146-153. doi:10.1002/ana.24310

152. Hardiman O, Al-Chalabi A, Chio A, et al. Amyotrophic lateral sclerosis. *Nat Rev Dis Prim*. 2017;3. doi:10.1038/nrdp.2017.71

153. Morgan S, Orrell RW. Pathogenesis of amyotrophic lateral sclerosis. *Br Med Bull*. 2016;119(1):87-97. doi:10.1093/bmb/ldw026

154. Banfi P, Ticozzi N, Lax A, Guidugli GA, Nicolini A, Silani V. A Review of Options for Treating Sialorrhea in Amyotrophic Lateral Sclerosis. *Respir Care*. 2015;60(3):446-454. doi:10.4187/respcare.02856

155. Roth B, Schiro DB, Ohlsson B. Diseases which cause generalized peripheral

neuropathy: a systematic review. *Scand J Gastroenterol*. 2021;0(0):1-11. doi:10.1080/00365521.2021.1942542

156. Leonhard SE, Mandarakas MR, Gondim FAA, et al. Diagnosis and management of Guillain–Barré syndrome in ten steps. *Nat Rev Neurol*. 2019;15(11):671-683. doi:10.1038/s41582-019-0250-9

157. Malek E, Salameh J. Guillain - Barre Syndrome Medication. *Semin Neurol*. 2019;39(05):589-595.

158. Vedeler CA, Farbu E, Mellgren SI. Chronic inflammatory demyelinating polyneuropathy (CIDP). *Acta Neurol Scand*. 2013;127(S196):48-51. doi:10.1111/ane.12049

159. Zhou L. Small Fiber Neuropathy. *Semin Neurol*. 2019;39(5):570-577. doi:10.1055/s-0039-1688977

160. Levine TD. Small Fiber Neuropathy: Disease Classification Beyond Pain and Burning. *J Cent Nerv Syst Dis*. 2018;10:117957351877170. doi:10.1177/1179573518771703

161. Kim S, Maynard JC, Sasaki Y, et al. Schwann cell O-GlcNAc glycosylation is required for myelin maintenance and axon integrity. *J Neurosci*. 2016;36(37):9633-9646. doi:10.1523/JNEUROSCI.1235-16.2016

162. Haas AL, Siepmann TJ. Pathways of ubiquitin conjugation. *FASEB J*. 1997;11(14):1257-1268. doi:10.1096/fasebj.11.14.9409544

163. Huang DT, Walden H, Duda D, Schulman BA. Ubiquitin-like protein activation. *Oncogene*. 2004;23(11):1958-1971. doi:10.1038/sj.onc.1207393

164. Cappadocia L, Lima CD. Ubiquitin-like Protein Conjugation: Structures, Chemistry, and Mechanism. *Chem Rev*. 2018;118(3):889-918. doi:10.1021/acs.chemrev.6b00737

165. Edelmann MJ, Kessler BM. Ubiquitin and ubiquitin-like specific proteases targeted by infectious pathogens: Emerging patterns and molecular principles. *Biochim Biophys Acta - Mol Basis Dis*. 2008;1782(12):809-816. doi:10.1016/j.bbadis.2008.08.010

166. Meng Y, Qiu L, Zhang S, Han J. The emerging roles of E3 ubiquitin ligases in ovarian cancer chemoresistance. *Cancer Drug Resist*. Published online 2021. doi:10.20517/cdr.2020.115

167. Stewart MD, Ritterhoff T, Klevit RE, Brzovic PS. E2 enzymes: more than just middle men. *Cell Res*. 2016;26(4):423-440. doi:10.1038/cr.2016.35

168. van Wijk SJL, de Vries SJ, Kemmeren P, et al. A comprehensive framework of E2–RING E3 interactions of the human ubiquitin–proteasome system. *Mol Syst*

Biol. 2009;5(1):295. doi:10.1038/msb.2009.55

169. Chau V, Tobias JW, Bachmair A, et al. A Multiubiquitin Chain Is Confined to Specific Lysine in a Targeted Short-Lived Protein. *Science (80-)*. 1989;243(4898):1576-1583. doi:10.1126/science.2538923

170. Welchman RL, Gordon C, Mayer RJ. Ubiquitin and ubiquitin-like proteins as multifunctional signals. *Nat Rev Mol Cell Biol*. 2005;6(8):599-609. doi:10.1038/nrm1700

171. Mukhopadhyay D, Riezman H. Proteasome-Independent Functions of Ubiquitin in Endocytosis and Signaling. *Science (80-)*. 2007;315(5809):201-205. doi:10.1126/science.1127085

172. Kirkin V, Dikic I. Role of ubiquitin- and Ubl-binding proteins in cell signaling. *Curr Opin Cell Biol*. 2007;19(2):199-205. doi:10.1016/j.ceb.2007.02.002

173. Saeki Y, Kudo T, Sone T, et al. Lysine 63-linked polyubiquitin chain may serve as a targeting signal for the 26S proteasome. *EMBO J*. 2009;28(4):359-371. doi:10.1038/emboj.2008.305

174. Bernassola F, Karin M, Ciechanover A, Melino G. The HECT Family of E3 Ubiquitin Ligases: Multiple Players in Cancer Development. *Cancer Cell*. 2008;14(1):10-21. doi:10.1016/j.ccr.2008.06.001

175. Kee Y, Huibregtse JM. Regulation of catalytic activities of HECT ubiquitin ligases. *Biochem Biophys Res Commun*. 2007;354(2):329-333. doi:10.1016/j.bbrc.2007.01.025

176. Rotin D, Kumar S. Physiological functions of the HECT family of ubiquitin ligases. *Nat Rev Mol Cell Biol*. 2009;10(6):398-409. doi:10.1038/nrm2690

177. George AJ, Hoffiz YC, Charles AJ, Zhu Y, Mabb AM. A Comprehensive Atlas of E3 Ubiquitin Ligase Mutations in Neurological Disorders. *Front Genet*. 2018;9. doi:10.3389/fgene.2018.00029

178. Li Y, Reverter D. Molecular Mechanisms of DUBs Regulation in Signaling and Disease. *Int J Mol Sci*. 2021;22(3):986. doi:10.3390/ijms22030986

179. Ronau JA, Beckmann JF, Hochstrasser M. Substrate specificity of the ubiquitin and Ubl proteases. *Cell Res*. 2016;26(4):441-456. doi:10.1038/cr.2016.38

180. Komander D, Clague MJ, Urbé S. Breaking the chains: structure and function of the deubiquitinases. *Nat Rev Mol Cell Biol*. 2009;10(8):550-563. doi:10.1038/nrm2731

181. Zeng C, Zhao C, Ge F, et al. Machado-Joseph Deubiquitinases: From Cellular Functions to Potential Therapy Targets. *Front Pharmacol*. 2020;11. doi:10.3389/fphar.2020.01311

182. Kumar S, Tomooka Y, Noda M. Identification of a set of genes with developmentally down-regulated expression in the mouse brain. *Biochem Biophys Res Commun*. 1992;185(3):1155-1161. doi:10.1016/0006-291X(92)91747-E

183. Zhou L, Jiang Y, Luo Q, Li L, Jia L. Neddylation: A novel modulator of the tumor microenvironment. *Mol Cancer*. 2019;18(1):1-11. doi:10.1186/s12943-019-0979-1

184. Gong L, Kamitani T, Millas S, Yeh ETH. Identification of a Novel Isopeptidase with Dual Specificity for Ubiquitin- and NEDD8-conjugated Proteins. *J Biol Chem*. 2000;275(19):14212-14216. doi:10.1074/jbc.275.19.14212

185. Rabut G, Peter M. Function and regulation of protein neddylation. *EMBO Rep*. 2008;9(10):969-976. doi:10.1038/embor.2008.183

186. Coleman KE, Békés M, Chapman JR, et al. SENP8 limits aberrant neddylation of nedd8 pathway components to promote cullin-RING ubiquitin ligase function. *Elife*. 2017;6:1-27. doi:10.7554/eLife.24325

187. Kurz T, Özlü N, Rudolf F, et al. The conserved protein DCN-1/Dcn1p is required for cullin neddylation in C. elegans and S. cerevisiae. *Nature*. 2005;435(7046):1257-1261. doi:10.1038/nature03662

188. Kurz T, Chou YC, Willems AR, et al. Dcn1 Functions as a Scaffold-Type E3 Ligase for Cullin Neddylation. *Mol Cell*. 2008;29(1):23-35. doi:10.1016/j.molcel.2007.12.012

189. Xirodimas DP, Saville MK, Bourdon JC, Hay RT, Lane DP. Mdm2-Mediated NEDD8 Conjugation of p53 Inhibits Its Transcriptional Activity. *Cell*. 2004;118(1):83-97. doi:10.1016/j.cell.2004.06.016

190. Monda JK, Scott DC, Miller DJ, et al. Structural Conservation of Distinctive N-terminal Acetylation-Dependent Interactions across a Family of Mammalian NEDD8 Ligation Enzymes. *Structure*. 2013;21(1):42-53. doi:10.1016/j.str.2012.10.013

191. Keuss MJ, Thomas Y, Mcarthur R, Wood NT, Knebel A, Kurz T. Characterization of the mammalian family of DCN-type NEDD8 E3 ligases. *J Cell Sci*. 2016;129(7):1441-1454. doi:10.1242/jcs.181784

192. Soucy TA, Dick LR, Smith PG, Milhollen MA, Brownell JE. The NEDD8 Conjugation Pathway and Its Relevance in Cancer Biology and Therapy. *Genes Cancer*. 2010;1(7):708-716. doi:10.1177/1947601910382898

193. Faull S V., Lau AMC, Martens C, et al. Structural basis of Cullin 2 RING E3 ligase regulation by the COP9 signalosome. *Nat Commun*. 2019;10(1):1-13. doi:10.1038/s41467-019-11772-y

194. Shen L nan, Liu H, Dong C, Xirodimas D, Naismith JH, Hay RT. Structural basis of NEDD8 ubiquitin discrimination by the deNEDDylating enzyme NEDP1. *EMBO J*. 2005;24(7):1341-1351. doi:10.1038/sj.emboj.7600628

195. Chan Y, Yoon J, Wu JT, et al. DEN1 deneddylates non-cullin proteins in vivo. *J Cell Sci*. 2008;121(19):3218-3223. doi:10.1242/jcs.030445

196. Hori T, Osaka F, Chiba T, et al. Covalent modification of all members of human cullin family proteins by NEDD8. *Oncogene*. 1999;18(48):6829-6834. doi:10.1038/sj.onc.1203093

197. Merlet J, Burger J, Gomes JEE, Pintard L. Regulation of cullin-RING E3 ubiquitin-ligases by neddylation and dimerization. *Cell Mol Life Sci*. 2009;66(11-12):1924-1938. doi:10.1007/s00018-009-8712-7

198. Sarikas A, Hartmann T, Pan ZQ. The cullin protein family. *Genome Biol*. 2011;12(4):220. doi:10.1186/gb-2011-12-4-220

199. Chunshui Zhou, Volker Seibert, Rory Geyer, Edward Rhee, Svetlana Lyapina, Greg Cope RJD and DAw. The fission yeast COP9/signalosome is involved in cullin modification by ubiquitin-related Ned8p. *BMC Biochem*. 2001;2(7):1-11. doi:1472-2091-2-7

200. Bennett EJ, Rush J, Gygi SP, Harper JW. Dynamics of Cullin-RING Ubiquitin Ligase Network Revealed by Systematic Quantitative Proteomics. *Cell*. 2010;143(6):951-965. doi:10.1016/j.cell.2010.11.017

201. Enchev RI, Schulman BA, Peter M. Protein neddylation: Beyond cullin-RING ligases. *Nat Rev Mol Cell Biol*. 2015;16(1):30-44. doi:10.1038/nrm3919

202. Strickland EC, Geer MA, Hong J, Fitzgerald MC. False-Positive Rate Determination of Protein Target Discovery using a Covalent Modification- and Mass Spectrometry-Based Proteomics Platform. *J Am Soc Mass Spectrom*. 2014;25(1):132-140. doi:10.1007/s13361-013-0754-2

203. Huang DT, Ayrault O, Hunt HW, et al. E2-RING Expansion of the NEDD8 Cascade Confers Specificity to Cullin Modification. *Mol Cell*. 2009;33(4):483-495. doi:10.1016/j.molcel.2009.01.011

204. Santonico E. Old and New Concepts in Ubiquitin and NEDD8 Recognition. *Biomolecules*. 2020;10(4):566. doi:10.3390/biom10040566

205. Li S, Fang W, Cui Y, et al. Neddylation promotes protein translocation between the cytoplasm and nucleus. *Biochem Biophys Res Commun*. 2020;529(4):991-997. doi:10.1016/j.bbrc.2020.07.012

206. Sadayappan S, Gilbert RJ. The potential role of neddylation in pre- and postnatal cardiac remodeling. *Am J Physiol Circ Physiol*. 2019;317(2):H276-H278. doi:10.1152/ajpheart.00260.2019

207. Maghames CM, Lobato-Gil S, Perrin A, et al. NEDDylation promotes nuclear protein aggregation and protects the Ubiquitin Proteasome System upon proteotoxic stress. *Nat Commun*. 2018;9(1):4376. doi:10.1038/s41467-018-06365-0

208. Shi CS, Kuo KL, Lin WC, et al. Neddylation inhibitor, MLN4924 suppresses angiogenesis in huvecs and solid cancers: in vitro and in vivo study. *Am J Cancer Res*. 2020;10(3):953-964. http://www.ncbi.nlm.nih.gov/pubmed/32266102

209. Zhang Y, Hu MY, Qiao CX, et al. Cloning and functional identification of a novel BCA3 splice. *Genet Mol Res*. 2014;13(4):10648-10656. doi:10.4238/2014.December.18.7

210. Gao F, Cheng J, Shi T, Yeh ETH. Neddylation of a breast cancer-associated protein recruits a class III histone deacetylase that represses NFκB-dependent transcription. *Nat Cell Biol*. 2006;8(10):1171-1177. doi:10.1038/ncb1483

211. Oved S, Mosesson Y, Zwang Y, et al. Conjugation to Nedd8 Instigates Ubiquitylation and Down-regulation of Activated Receptor Tyrosine Kinases. *J Biol Chem*. 2006;281(31):21640-21651. doi:10.1074/jbc.M513034200

212. Samatar AA, Wang L, Mirza A, Koseoglu S, Liu S, Kumar CC. Transforming Growth Factor-β2 Is a Transcriptional Target for Akt/Protein Kinase B via Forkhead Transcription Factor. *J Biol Chem*. 2002;277(31):28118-28126. doi:10.1074/jbc.M203686200

213. Zuo W, Huang F, Chiang YJ, et al. c-Cbl-Mediated Neddylation Antagonizes Ubiquitination and Degradation of the TGF-β Type II Receptor. *Mol Cell*. 2013;49(3):499-510. doi:10.1016/j.molcel.2012.12.002

214. Syed V. TGF-β Signaling in Cancer. *J Cell Biochem*. 2016;117(6):1279-1287. doi:10.1002/jcb.25496

215. Hafner A, Bulyk ML, Jambhekar A, Lahav G. The multiple mechanisms that regulate p53 activity and cell fate. *Nat Rev Mol Cell Biol*. 2019;20(4):199-210. doi:10.1038/s41580-019-0110-x

216. Abida WM, Nikolaev A, Zhao W, Zhang W, Gu W. FBXO11 promotes the neddylation of p53 and inhibits its transcriptional activity. *J Biol Chem*. 2007;282(3):1797-1804. doi:10.1074/jbc.M609001200

217. Brooks CL, Gu W. p53 regulation by ubiquitin. *FEBS Lett*. 2011;585(18):2803-2809. doi:10.1016/j.febslet.2011.05.022

218. Conforti F, Sayan AE, Sreekumar R, Sayan BS. Regulation of p73 activity by post-translational modifications. *Cell Death Dis*. 2012;3(3):e285-e285. doi:10.1038/cddis.2012.27

219. Chen Y, Liu W, Naumovski L, Neve RL. ASPP2 inhibits APP-BP1-mediated

NEDD8 conjugation to cullin-1 and decreases APP-BP1-induced cell proliferation and neuronal apoptosis. *J Neurochem*. 2003;85(3):801-809. doi:10.1046/j.1471-4159.2003.01727.x

220. Aoki I, Higuchi M, Gotoh Y. NEDDylation controls the target specificity of E2F1 and apoptosis induction. *Oncogene*. 2013;32:3954-3964. doi:10.1038/onc.2012.428

221. Embade N, Fernández-Ramos D, Varela-Rey M, et al. Murine Double Minute 2 Regulates Hu Antigen R Stability in Human Liver and Colon Cancer Through NEDDylation. Published online 2011. doi:10.1002/hep.24795

222. Zhou Q, Li H, Li Y, et al. Inhibiting neddylation modification alters mitochondrial morphology and reprograms energy metabolism in cancer cells. *JCI insight*. 2019;4(4). doi:10.1172/jci.insight.121582

223. Zhou Q, Zheng Y, Sun Y. Neddylation regulation of mitochondrial structure and functions. *Cell Biosci*. 2021;11(1):55. doi:10.1186/s13578-021-00569-6

224. Choo YS, Vogler G, Wang D, et al. Regulation of parkin and PINK1 by neddylation. *Hum Mol Genet*. 2012;21(11):2514-2523. doi:10.1093/hmg/dds070

225. Hellwig-Bürgel T, Stiehl DP, Wagner AE, Metzen E, Jelkmann W. Review: Hypoxia-Inducible Factor-1 (HIF-1): A Novel Transcription Factor in Immune Reactions. *J Interf Cytokine Res*. 2005;25(6):297-310. doi:10.1089/jir.2005.25.297

226. Park JB, Seo J, Park JW, Chun YS. Neddylation blockade induces HIF-1α driven cancer cell migration via upregulation of ZEB1. *Sci Rep*. 2020;10(1):18210. doi:10.1038/s41598-020-75286-0

227. Vogl AM, Brockmann MM, Giusti SA, et al. Neddylation inhibition impairs spine development, destabilizes synapses and deteriorates cognition. *Nat Neurosci*. 2015;18(2):239-251. doi:10.1038/nn.3912

228. Hong BH, Ha S, Joo Y, et al. Amyloid precursor protein binding protein-1 knockdown reduces neuronal differentiation in fetal neural stem cells. *Neuroreport*. 2012;23(2):61-66. doi:10.1097/WNR.0b013e32834e7d4f

229. Vogl AM, Phu L, Becerra R, et al. Global site-specific neddylation profiling reveals that NEDDylated cofilin regulates actin dynamics. *Nat Struct Mol Biol*. 2020;27(2):210-220. doi:10.1038/s41594-019-0370-3

230. Scudder SL, Patrick GN. Synaptic structure and function are altered by the neddylation inhibitor MLN4924. *Mol Cell Neurosci*. 2015;65:52-57. doi:10.1016/j.mcn.2015.02.010

231. Brockmann MM, Döngi M, Einsfelder U, Körber N, Refojo D, Stein V. Neddylation regulates excitatory synaptic transmission and plasticity. *Sci Rep*.

2019;9(1):17935. doi:10.1038/s41598-019-54182-2

232. Chen YZ. APP induces neuronal apoptosis through APP-BP1-mediated downregulation of β-catenin. *Apoptosis*. 2004;9(4):415-422. doi:10.1023/B:APPT.0000031447.05354.9f

233. Laifenfeld D, Patzek LJ, McPhie DL, et al. Rab5 Mediates an Amyloid Precursor Protein Signaling Pathway That Leads to Apoptosis. *J Neurosci*. 2007;27(27):7141-7153. doi:10.1523/JNEUROSCI.4599-06.2007

234. Chen Y, Bodles AM, McPhie DL, Neve RL, Mrak RE, Griffin WST. APP-BP1 inhibits Abeta42 levels by interacting with Presenilin-1. *Mol Neurodegener*. 2007;2:3. doi:10.1186/1750-132

235. Zhang L, Jing H, Li H, et al. Neddylation is critical to cortical development by regulating Wnt/β-catenin signaling. *Proc Natl Acad Sci*. 2020;117(42):26448-26459. doi:10.1073/pnas.2005395117

236. Costantini F, Shakya R. GDNF/Ret signaling and the development of the kidney. *BioEssays*. 2006;28(2):117-127. doi:10.1002/bies.20357

237. Qiu X, Wei R, Li Y, et al. NEDL2 regulates enteric nervous system and kidney development in its Nedd8 ligase activity-dependent manner. *Oncotarget*. 2016;7(21):31440-31453. doi:10.18632/oncotarget.8951

238. Cabal-Herrera AM, Tassanakijpanich N, Salcedo-Arellano MJ, Hagerman RJ. Fragile X-Associated Tremor/Ataxia Syndrome (FXTAS): Pathophysiology and Clinical Implications. *Int J Mol Sci*. 2020;21(12):4391. doi:10.3390/ijms21124391

239. Lin Y, Xue J, Deng J, et al. Neddylation activity modulates the neurodegeneration associated with fragile X associated tremor/ataxia syndrome (FXTAS) through regulating Sima. *Neurobiol Dis*. 2020;143:105013. doi:10.1016/j.nbd.2020.105013

240. Nikoletopoulou V, Papandreou ME, Tavernarakis N. Autophagy in the physiology and pathology of the central nervous system. *Cell Death Differ*. 2015;22(3):398-407. doi:10.1038/cdd.2014.204

241. Lieberman OJ, Sulzer D. The Synaptic Autophagy Cycle. *J Mol Biol*. 2020;432(8):2589-2604. doi:10.1016/j.jmb.2019.12.028

242. Feltri ML, D'Antonio M, Previtali S, Fasolini M, Messing A, Wrabetz L. P0-Cre transgenic mice for inactivation of adhesion molecules in Schwann cells. *Ann N Y Acad Sci*. 1999;883:116-123. http://www.ncbi.nlm.nih.gov/pubmed/10586237

243. Wiśniewski JR, Zougman A, Nagaraj N, Mann M. Universal sample preparation method for proteome analysis. *Nat Methods*. 2009;6(5):359-362. doi:10.1038/nmeth.1322

244. KAJIGAYA H, ISHIBASHI T, HAYASHI A, YAMAGUCHI Y, BABA H. Concentration of neddylation-related molecules in paranodal myelin of the peripheral nervous system. *Proc Japan Acad Ser B*. 2016;92(2):56-68. doi:10.2183/pjab.92.56

245. Iruarrizaga-Lejarreta M, Varela-Rey M, Lozano JJ, et al. The RNA-Binding Protein Human Antigen R Controls Global Changes in Gene Expression during Schwann Cell Development. *J Neurosci*. 2012;32(14):4944-4958. doi:10.1523/JNEUROSCI.5868-11.2012

246. Soucy TA, Smith PG, Milhollen MA, et al. An inhibitor of NEDD8-activating enzyme as a new approach to treat cancer. *Nature*. 2009;458(7239):732-736. doi:10.1038/nature07884

247. Wei W, Jin J, Schlisio S, Harper JW, Kaelin WG. The v-Jun point mutation allows c-Jun to escape GSK3-dependent recognition and destruction by the Fbw7 ubiquitin ligase. *Cancer Cell*. 2005;8(1):25-33. doi:10.1016/j.ccr.2005.06.005

248. Fuentes L, Lebenkoff S, White K, et al. YAP and TAZ control peripheral myelination and the expression of laminin receptors in Schwann cells. *Nat Neurosci*. 2016;93(4):292-297. doi:10.1038/nn.4316.YAP

249. Grove M, Kim H, Santerre M, et al. YAP/TAZ initiate and maintain Schwann cell myelination. *Elife*. 2017;6:1-27. doi:10.7554/eLife.20982

250. Fernando RN, Cotter L, Perrin-Tricaud C, et al. Optimal myelin elongation relies on YAP activation by axonal growth and inhibition by Crb3/Hippo pathway. *Nat Commun*. 2016;7(1):12186. doi:10.1038/ncomms12186

251. Poitelon Y, Lopez-Anido C, Catignas K, et al. YAP and TAZ control peripheral myelination and the expression of laminin receptors in Schwann cells. *Nat Neurosci*. 2016;19(7):879-887. doi:10.1038/nn.4316

252. Lopez-Anido C, Poitelon Y, Gopinath C, et al. Tead1 regulates the expression of Peripheral Myelin Protein 22 during Schwann cell development. *Hum Mol Genet*. Published online June 10, 2016:ddw158. doi:10.1093/hmg/ddw158

253. Deng Y, Wu LMN, Bai S, et al. A reciprocal regulatory loop between TAZ/YAP and G-protein Gαs regulates Schwann cell proliferation and myelination. *Nat Commun*. 2017;8(1):15161. doi:10.1038/ncomms15161

254. Norrmén C, Suter U. Akt/mTOR signalling in myelination. *Biochem Soc Trans*. 2013;41(4):944-950. doi:10.1042/BST20130046

255. Shahrizaila N, Lehmann HC, Kuwabara S. Guillain-Barré syndrome. *Lancet*. 2021;397(10280):1214-1228. doi:10.1016/S0140-6736(21)00517-1

256. Jessen KR, Mirsky R. The origin and development of glial cells in peripheral nerves. *Nat Rev Neurosci*. 2005;6(9):671-682. doi:10.1038/nrn1746

257. Yu Q, Sun Y. Targeting protein neddylation to inactivate cullin-ring ligases by gossypol: A lucky hit or a new start? *Drug Des Devel Ther*. 2021;15:1-8. doi:10.2147/DDDT.S286373

258. Naik SK, Lam EWF, Parija M, et al. NEDDylation negatively regulates ERRβ expression to promote breast cancer tumorigenesis and progression. *Cell Death Dis*. 2020;11(8):703. doi:10.1038/s41419-020-02838-7

259. Zhao Y, Sun Y. *Cullin-RING Ligases as Attractive Anti-Cancer Targets*. Vol 19.; 2013.

260. Jessen KR, Mirsky R, Lloyd AC. Schwann Cells: Development and Role in Nerve Repair. *Cold Spring Harb Perspect Biol*. 2015;7(7):a020487. doi:10.1101/cshperspect.a020487

261. Stolt CC, Wegner M. Schwann cells and their transcriptional network: Evolution of key regulators of peripheral myelination. *Brain Res*. 2016;1641:101-110. doi:10.1016/j.brainres.2015.09.025

262. Zou J, Ma W, Li J, et al. Neddylation mediates ventricular chamber maturation through repression of Hippo signaling. *Proc Natl Acad Sci*. 2018;115(17):E4101-E4110. doi:10.1073/pnas.1719309115

263. Figlia G, Norrmén C, Pereira JA, Gerber D, Suter U. Dual function of the PI3K-Akt-MTORC1 axis in myelination of the peripheral nervous system. *Elife*. 2017;6:1-27. doi:10.7554/eLife.29241

264. Ishii A, Furusho M, Bansal R. Mek/ <scp>ERK1</scp> / <scp>2-MAPK</scp> and <scp>PI3K</scp> /Akt/ <scp>mTOR</scp> signaling plays both independent and cooperative roles in Schwann cell differentiation, myelination and dysmyelination. *Glia*. 2021;69(10):2429-2446. doi:10.1002/glia.24049

265. Decker L. Peripheral Myelin Maintenance Is a Dynamic Process Requiring Constant Krox20 Expression. *J Neurosci*. 2006;26(38):9771-9779. doi:10.1523/JNEUROSCI.0716-06.2006

266. Bremer M, Fröb F, Kichko T, et al. Sox10 is required for Schwann-cell homeostasis and myelin maintenance in the adult peripheral nerve. *Glia*. 2011;59(7):1022-1032. doi:10.1002/glia.21173

9 SUPPLEMENTARY

RNA seq Data

Gene Name	Gene Abbreviations	Accession code	-Log p-value WT_KO	q-value WT_KO	KO/WT Ratio
BTB/POZ domain-containing protein KCTD16	Kctd16	Q5DTY9	11,460	0,00000	25,820
Sulfiredoxin-1	Srxn1	Q9D975	6,653	0,00025	14,035
Glutathione S-transferase A3	Gsta3	P30115	6,564	0,00022	13,728
Collagen alpha-2(XI) chain	Col11a2	Q64739	4,109	0,00092	12,049
UDP-glucuronosyltransferase 1-6	Ugt1a6	Q64435	4,540	0,00070	10,708
Bone marrow proteoglycan	Prg2	Q61878	5,855	0,00021	9,677
NAD(P)H dehydrogenase [quinone] 1	Nqo1	Q64669	7,433	0,00050	8,493
Glia-derived nexin	Serpine2	Q07235	5,345	0,00029	8,211
MORF4 family-associated protein 1	Mrfap1	Q9CQL7	5,847	0,00020	7,473
Molybdenum cofactor sulfurase	Mocos	Q14CH1	5,324	0,00034	7,195
Alcohol dehydrogenase class 4 mu/sigma chain	Adh7	Q64437	3,725	0,00174	6,916
Calmodulin-like protein 3	Calml3	Q9D6P8	2,315	0,01690	6,910
Glycerol-3-phosphate acyltransferase 1 mitochondrial	Gpam	Q61586	5,262	0,00033	6,484
TPR and ankyrin repeat-containing protein 1	Trank1	Q8BV79	2,409	0,01463	6,025
Glutamate--cysteine ligase regulatory subunit	Gclm	O09172	7,564	0,00057	5,618
Serine/threonine-protein phosphatase 2A 65 kDa regulatory subunit A beta isoform	Ppp2r1b	Q7TNP2	5,823	0,00019	5,547
Transient receptor potential cation channel subfamily V member 3	Trpv3	Q8K424	3,455	0,00263	5,370
60S ribosomal protein L22-like 1	Rpl22l1	Q9D7S7	2,555	0,01109	5,259
Torsin-1A-interacting protein 2 isoform IFRG15	Tor1aip2	Q9ER81	4,038	0,00099	5,258
Cyclin-dependent kinase 4	Cdk4	P30285	3,332	0,00317	5,240
Nuclear cap-binding protein subunit 1	Ncbp1	Q3UYV9	4,503	0,00067	5,084
Tubulin-specific chaperone cofactor E-like protein	Tbcel	Q8C5W3	2,876	0,00635	5,017
Sodium bicarbonate cotransporter 3	Slc4a7	Q8BTY2	3,242	0,00346	4,974
Pannexin-1	Panx1	Q9JIP4	3,897	0,00125	4,915
Mortality factor 4-like protein 1	Morf4l1	P60762	4,230	0,00084	4,873
Eukaryotic translation initiation factor 2-alpha kinase 3	Eif2ak3	Q9Z2B5	4,249	0,00085	4,870
Ribonucleoside-diphosphate reductase large subunit	Rrm1	P07742	4,676	0,00056	4,859
Eosinophil cationic protein 2	Ear2	P97425	4,749	0,00059	4,793
SWI/SNF-related matrix-associated actin-dependent regulator of chromatin subfamily D member 2	Smarcd2	Q99JR8	3,915	0,00119	4,776
Transmembrane protease serine 11F	Tmprss11f	Q8BHM9	2,811	0,00699	4,769
Flavin reductase (NADPH)	Blvrb	Q923D2	6,199	0,00030	4,718
Testis-expressed sequence 15 protein	Tex15	F8VPN2	2,194	0,02017	4,636
ADP-ribosyl cyclase/cyclic ADP-ribose hydrolase 1	Cd38	P56528	3,357	0,00308	4,629
Protein KRBA1	Krba1	Q6NXZ1	2,415	0,01439	4,593
Heme oxygenase 1	Hmox1	P14901	5,402	0,00030	4,561
Signal peptide CUB and EGF-like domain-containing protein 1	Scube1	Q6NZL8	4,146	0,00088	4,548
Nischarin	Nisch	Q80TM9	6,412	0,00019	4,490
EF-hand domain-containing protein D2	Efhd2	Q9D8Y0	2,866	0,00644	4,466
Galectin-3-binding protein	Lgals3bp	Q07797	5,331	0,00035	4,443
Angiopoietin-related protein 2	Angptl2	Q9R045	3,600	0,00211	4,394
Oxysterol-binding protein-related protein 8	Osbpl8	B9EJ86	1,975	0,03017	4,357
Armadillo repeat-containing X-linked protein 3	Armcx3	Q8BHS6	4,382	0,00082	4,302
Amine oxidase [flavin-containing] B	Maob	Q8BW75	3,003	0,00487	4,189
F-box only protein 38	Fbxo38	Q8BMI0	3,525	0,00231	4,141
Aldose reductase-related protein 2	Akr1b8	P45377	6,333	0,00033	4,098
Pleiotrophin	Ptn	P63089	3,715	0,00177	4,088
Thioredoxin reductase 1 cytoplasmic	Txnrd1	Q9JMH6	8,431	0,00000	4,085
Serine/threonine-protein kinase MARK1	Mark1	Q8VHJ5	3,183	0,00386	4,084
Mannose-1-phosphate guanyltransferase alpha	Gmppa	Q922H4	2,195	0,02024	4,054
40S ribosomal protein S27-like	Rps27l	Q6ZWY3	3,181	0,00389	4,009
Arylsulfatase B	Arsb	P50429	4,161	0,00091	3,984
Neuronal cell adhesion molecule	Nrcam	Q810U4	3,431	0,00275	3,980
Complement component C9	C9	P06683	4,709	0,00060	3,958
Acyl-coenzyme A thioesterase 10 mitochondrial	Acot10	Q32MW3	3,940	0,00116	3,953
Alstrom syndrome protein 1 homolog	Alms1	Q8K4E0	3,151	0,00397	3,902
E3 ubiquitin/ISG15 ligase TRIM25	Trim25	Q61510	1,735	0,04569	3,833
La-related protein 4B	Larp4b	Q6A0A2	2,282	0,01780	3,815
G1/S-specific cyclin-D1	Ccnd1	P25322	1,960	0,03073	3,813
Zinc finger CCCH domain-containing protein 15	Zc3h15	Q3TIV5	4,771	0,00054	3,767
F-box/WD repeat-containing protein 11	Fbxw11	Q5SRY7	4,843	0,00046	3,736
Epoxide hydrolase 1	Ephx1	Q9D379	5,529	0,00024	3,718

Gene Name	Gene Abbreviations	Accession code	-Log p-value WT_KO	q-value WT_KO	KO/WT Ratio
FAD synthase	Flad1	Q8R123	2,577	0,01070	3,691
Carbonyl reductase [NADPH] 3	Cbr3	Q8K354	4,273	0,00081	3,677
Thrombomodulin	Thbd	P15306	2,174	0,02084	3,672
Adenylate cyclase type 1	Adcy1	O88444	2,377	0,01550	3,641
Kinesin-like protein KIF3B	Kif3b	Q61771	2,059	0,02591	3,634
Cyclin-dependent kinase 2	Cdk2	P97377	4,018	0,00099	3,622
Eosinophil peroxidase	Epx	P49290	3,060	0,00452	3,597
Nuclear pore glycoprotein p62	Nup62	Q63850	2,315	0,01695	3,569
Dynamin-binding protein	Dnmbp	Q6TXD4	3,685	0,00191	3,495
HEAT repeat-containing protein 3	Heatr3	Q8BQM4	3,275	0,00332	3,484
Putative Polycomb group protein ASXL1	Asxl1	P59598	3,209	0,00363	3,480
Ankyrin repeat domain-containing protein 27	Ankrd27	Q3UMR0	3,030	0,00462	3,426
Integrin alpha-3	Itga3	Q62470	3,394	0,00293	3,391
Zinc finger SWIM domain-containing protein 8	Zswim8	Q3UHH1	2,478	0,01291	3,370
Glutathione S-transferase Mu 1	Gstm1	P10649	6,232	0,00031	3,359
Guanylate-binding protein 4	Gbp4	Q61107	3,007	0,00483	3,339
Formin-like protein 3	Fmnl3	Q6ZPF4	3,325	0,00315	3,323
GDNF family receptor alpha-1	Gfra1	P97785	5,842	0,00019	3,273
Nibrin	Nbn	Q9R207	2,779	0,00763	3,252
Coiled-coil domain-containing protein 181	Ccdc181	Q80ZU5	4,511	0,00067	3,237
Nuclear factor NF-kappa-B p100 subunit	Nfkb2	Q9WTK5	2,041	0,02650	3,223
40S ribosomal protein S29	Rps29	P62274	2,473	0,01302	3,214
Short transient receptor potential channel 4-associated protein	Trpc4ap	Q9JLV2	2,603	0,01024	3,211
Alpha-ketoglutarate-dependent dioxygenase FTO	Fto	Q8BGW1	6,029	0,00026	3,189
Arachidonate 15-lipoxygenase	Alox15	P39654	4,042	0,00097	3,183
SUN domain-containing protein 1	Sun1	Q9D666	1,765	0,04326	3,181
Zinc transporter SLC39A7	Slc39a7	Q31125	2,059	0,02597	3,171
Rho GTPase-activating protein 42	Arhgap42	B2RQE8	1,717	0,04723	3,167
Tyrosine-protein kinase receptor UFO	Axl	Q00993	4,414	0,00072	3,136
DDB1- and CUL4-associated factor 8	Dcaf8	Q8N7N5	2,455	0,01352	3,086
Glutathione reductase mitochondrial	Gsr	P47791	6,325	0,00032	3,073
Oligoribonuclease mitochondrial	Rexo2	Q9D8S4	2,315	0,01698	3,065
Exostosin-like 3	Extl3	Q9WVL6	2,348	0,01630	3,060
Proton-coupled amino acid transporter 2	Slc36a2	Q8BHK3	2,634	0,00964	3,050
Coiled-coil domain-containing protein 51	Ccdc51	Q3URS9	5,943	0,00023	3,039
R3H domain-containing protein 2	R3hdm2	Q80TM6	1,710	0,04777	3,029
Centrosomal protein of 170 kDa protein B	Cep170b	Q80U49	2,416	0,01439	3,017
Lysophosphatidylcholine acyltransferase 1	Lpcat1	Q3TFD2	2,440	0,01378	2,986
Glutaredoxin-related protein 5 mitochondrial	Glrx5	Q80Y14	6,174	0,00029	2,975
Dual specificity mitogen-activated protein kinase kinase 3	Map2k3	O09110	2,289	0,01775	2,970
Cytochrome c oxidase subunit 7C mitochondrial	Cox7c	P17665	2,069	0,02547	2,955
Aldehyde dehydrogenase dimeric NADP-preferring	Aldh3a1	P47739	2,541	0,01144	2,954
Trans-Golgi network integral membrane protein 1	Tgoln1	Q62313	2,950	0,00537	2,943
Sorting nexin-16	Snx16	Q8C080	2,227	0,01949	2,936
Histone deacetylase complex subunit SAP18	Sap18	O55128	2,627	0,00983	2,926
Exportin-T	Xpot	Q9CRT8	2,032	0,02698	2,922
Inactive serine/threonine-protein kinase PLK5	Plk5	Q4FZD7	2,022	0,02748	2,908
Importin-11	Ipo11	Q8K2V6	2,513	0,01208	2,876
Rho GTPase-activating protein 11A	Arhgap11a	Q80Y19	1,841	0,03795	2,866
Tetratricopeptide repeat protein 9A	Ttc9	Q3V038	3,567	0,00219	2,863
U3 small nucleolar RNA-associated protein 6 homolog	Utp6	Q8VCY6	2,842	0,00660	2,861
FERM domain-containing protein 4B	Frmd4b	Q920B0	3,734	0,00172	2,855
SWI/SNF complex subunit SMARCC1	Smarcc1	P97496	2,733	0,00812	2,855
Kinesin-like protein KIF1C	Kif1c	O35071	2,971	0,00510	2,838
PDZ and LIM domain protein 5	Pdlim5	Q8CI51	4,713	0,00061	2,835
CD97 antigen	Cd97	Q9Z0M6	3,041	0,00461	2,829
Interferon-induced transmembrane protein 3	Ifitm3	Q9CQW9	2,362	0,01594	2,821
Epidermal growth factor-like protein 8	Egfl8	Q6GUQ1	2,268	0,01811	2,802
Pirin	Pir	Q9D711	3,485	0,00252	2,790
EMILIN-1	Emilin1	Q99K41	3,884	0,00126	2,786
Grainyhead-like protein 1 homolog	Grhl1	Q921D9	2,872	0,00645	2,783
Mortality factor 4-like protein 2	Morf4l2	Q9R0Q4	2,077	0,02538	2,781
Rho guanine nucleotide exchange factor 3	Arhgef3	Q91X46	1,745	0,04494	2,772
Fibrillin-2	Fbn2	Q61555	7,374	0,00040	2,757
Procollagen-lysine 2-oxoglutarate 5-dioxygenase 2	Plod2	Q9R0B9	3,653	0,00195	2,742
Kelch-like protein 22	Klhl22	Q99JN2	1,721	0,04681	2,729

Gene Name	Gene Abbreviations	Accession code	-Log p-value WT_KO	q-value WT_KO	KO/WT Ratio
BAG family molecular chaperone regulator 1	Bag1	Q60739	3,868	0,00135	2,721
Liprin-alpha-2	Ppfia2	Q8BSS9	2,218	0,01978	2,716
Serpin B8	Serpinb8	O08800	2,418	0,01440	2,716
Glutathione S-transferase P 1	Gstp1	P19157	6,883	0,00029	2,708
GDNF-inducible zinc finger protein 1	Gzf1	Q4VBD9	3,104	0,00422	2,705
ATP-binding cassette sub-family A member 6	Abca6	Q8K441	1,846	0,03767	2,697
Protein PML	Pml	Q60953	3,663	0,00197	2,695
Haloacid dehalogenase-like hydrolase domain-containing protein 3	Hdhd3	Q9CYW4	2,985	0,00504	2,675
DNA mismatch repair protein Msh6	Msh6	P54276	3,151	0,00399	2,668
Cytochrome c oxidase subunit 6C	Cox6c	Q9CPQ1	3,622	0,00203	2,668
AF4/FMR2 family member 2	Aff2	O55112	1,907	0,03379	2,655
Microsomal glutathione S-transferase 1	Mgst1	Q91VS7	2,583	0,01061	2,652
Protein canopy homolog 3	Cnpy3	Q9DAU1	2,957	0,00527	2,649
Rho-related GTP-binding protein RhoJ	Rhoj	Q9ER71	1,993	0,02911	2,639
Protein IMPACT	Impact	O55091	1,974	0,03022	2,628
Dynein light chain Tctex-type 1	Dynlt1	P51807	2,417	0,01438	2,610
Lysyl oxidase homolog 2	Loxl2	P58022	2,297	0,01753	2,608
1-aminocyclopropane-1-carboxylate synthase-like protein 1	Accs	A2AIG8	1,689	0,05004	2,594
DNA replication licensing factor MCM5	Mcm5	P49718	3,737	0,00173	2,570
Integrin beta-2	Itgb2	P11835	4,151	0,00090	2,569
Carboxypeptidase E	C	Q00493	1,751	0,04449	2,568
Ciliary neurotrophic factor receptor subunit alpha	Cntfr	O88507	1,747	0,04475	2,568
Inosine-5'-monophosphate dehydrogenase 2	Impdh2	P24547	5,419	0,00030	2,554
Collagen alpha-1(XVIII) chain	Col18a1	P39061	6,601	0,00024	2,533
NADP-dependent malic enzyme mitochondrial	Me3	Q8BMF3	3,599	0,00214	2,532
Androglobin	Adgb	G3UZ78	1,749	0,04454	2,531
Cohesin subunit SA-1	Stag1	Q9D3E6	1,823	0,03940	2,526
Translocation protein SEC63 homolog	Sec63	Q8VHE0	2,138	0,02233	2,525
Cullin-associated NEDD8-dissociated protein 2	Cand2	Q6ZQ73	3,565	0,00218	2,506
Breast cancer anti-estrogen resistance protein 3	Bcar3	Q9QZK2	1,840	0,03797	2,503
Matrix metalloproteinase-14	Mmp14	P53690	3,659	0,00196	2,502
Ethanolamine kinase 1	Etnk1	Q9D4V0	3,189	0,00380	2,499
Influenza virus NS1A-binding protein homolog	Ivns1abp	Q920Q8	3,361	0,00306	2,489
Peptidyl-prolyl cis-trans isomerase FKBP11	Fkbp11	Q9D1M7	2,821	0,00685	2,474
N-acetylneuraminate lyase	Npl	Q9DCJ9	3,607	0,00206	2,472
Structural maintenance of chromosomes flexible hinge domain-containing protein 1	Smchd1	Q6P5D8	1,978	0,03001	2,469
Sphingomyelin synthase-related protein 1	Samd8	Q9DA37	3,075	0,00447	2,468
Sphingomyelin phosphodiesterase 2	Smpd2	O70572	2,257	0,01848	2,459
F-box/WD repeat-containing protein 8	Fbxw8	Q8BIA4	2,265	0,01820	2,458
Dipeptidyl peptidase 1	Ctsc	P97821	2,994	0,00492	2,454
Teneurin-3	Tenm3	Q9WTS6	2,736	0,00812	2,439
Volume-regulated anion channel subunit LRRC8A	Lrrc8a	Q80WG5	3,665	0,00198	2,438
Tyrosine-protein phosphatase non-receptor type 12	Ptpn12	P35831	2,105	0,02420	2,438
Protein MAATS1	Maats1	Q8BRC6	3,317	0,00317	2,437
Adipocyte enhancer-binding protein 1	Aebp1	Q640N1	4,362	0,00082	2,435
Transforming growth factor beta-1-induced transcript 1 protein	Tgfb1i1	Q62219	3,690	0,00188	2,434
BRISC and BRCA1-A complex member 1	Babam1	Q3UI43	3,245	0,00349	2,427
Constitutive coactivator of PPAR-gamma-like protein 2	Fam120c	Q8C3F2	2,115	0,02375	2,419
Plasma alpha-L-fucosidase	Fuca2	Q99KR8	4,534	0,00069	2,413
Trinucleotide repeat-containing gene 18 protein	Tnrc18	Q80WC3	2,553	0,01124	2,413
Serum paraoxonase/lactonase 3	Pon3	Q62087	2,699	0,00865	2,399
Growth arrest-specific protein 2	Gas2	P11862	4,831	0,00045	2,397
Transferrin receptor protein 1	Tfrc	Q62351	3,471	0,00260	2,392
Fucose mutarotase	Fuom	Q8R2K1	3,520	0,00233	2,388
Peroxisomal biogenesis factor 3	x3	Q9QXY9	2,445	0,01366	2,386
5'-AMP-activated protein kinase subunit gamma-2	Prkag2	Q91WG5	2,867	0,00647	2,382
DNA-directed RNA polymerase III subunit RPC9	Crcp	O35427	3,530	0,00231	2,377
Uncharacterized protein C17orf62 homolog	1 SV	Q3TYS2	1,763	0,04332	2,370
CD44 antigen	Cd44	P15379	6,682	0,00027	2,353
Phospholipase DDHD1	Ddhd1	Q80YA3	2,778	0,00761	2,347
Exportin-5	Xpo5	Q924C1	4,047	0,00095	2,343
Apolipoprotein E	Apoe	P08226	3,383	0,00293	2,342
Transmembrane protein 205	Tmem205	Q91XE8	2,089	0,02498	2,337
Ninein-like protein	Ninl	Q6ZQ12	2,653	0,00924	2,335
Aftiphilin	Aftph	Q80WT5	2,504	0,01233	2,335

Gene Name	Gene Abbreviations	Accession code	-Log p-value WT_KO	q-value WT_KO	KO/WT Ratio
Transmembrane protein 43	Tmem43	Q9DBS1	4,839	0,00046	2,331
Endoplasmic reticulum aminopeptidase 1	Erap1	Q9EQH2	3,307	0,00318	2,324
PDZ and LIM domain protein 7	Pdlim7	Q3TJD7	2,067	0,02560	2,318
Collagen triple helix repeat-containing protein 1	Cthrc1	Q9D1D6	1,855	0,03706	2,314
Activating signal cointegrator 1 complex subunit 2	Ascc2	Q91WR3	1,937	0,03220	2,314
Tyrosine-protein phosphatase non-receptor type 9	Ptpn9	O35239	1,933	0,03240	2,312
Down syndrome cell adhesion molecule homolog	Dscam	Q9ERC8	1,965	0,03067	2,309
Receptor tyrosine-protein kinase erbB-2	Erbb2	P70424	3,151	0,00396	2,308
S-formylglutathione hydrolase	Esd	Q9R0P3	4,395	0,00075	2,306
Ubiquitin-associated protein 2	Ubap2	Q91VX2	3,679	0,00194	2,299
GDH/6PGL endoplasmic bifunctional protein	H6pd	Q8CFX1	2,867	0,00645	2,297
CST complex subunit STN1	Obfc1	Q8K2X3	2,031	0,02705	2,297
Signal peptidase complex subunit 2	Spcs2	Q9CYN2	2,514	0,01211	2,290
Stromal interaction molecule 1	Stim1	P70302	4,040	0,00099	2,282
Chromobox protein homolog 3	Cbx3	P23198	2,455	0,01350	2,282
Sequestosome-1	Sqstm1	Q64337	4,284	0,00083	2,278
Armadillo repeat-containing X-linked protein 2	Armcx2	Q6A058	2,074	0,02542	2,274
Mitogen-activated protein kinase kinase kinase 10	Map3k10	Q66L42	2,194	0,02017	2,265
Endoplasmic reticulum-Golgi intermediate compartment protein 1	Ergic1	Q9DC16	1,812	0,04010	2,260
Apoptosis-associated speck-like protein containing a CARD	Pycard	Q9EPB4	2,196	0,02032	2,251
Calcium/calmodulin-dependent protein kinase kinase 1	Camkk1	Q8VBY2	1,776	0,04246	2,250
Thrombospondin-1	Thbs1	P35441	2,584	0,01059	2,248
ER membrane protein complex subunit 8	Emc8	O70378	4,098	0,00093	2,246
RNA-binding protein 25	Rbm25	B2RY56	2,197	0,02036	2,243
H-2 class I histocompatibility antigen K-K alpha chain	H2-K1	P04223	2,157	0,02161	2,241
Neural cell adhesion molecule L1-like protein	Chl1	P70232	3,495	0,00248	2,236
Nesprin-3	Syne3	Q4FZC9	2,002	0,02869	2,235
General transcription factor 3C polypeptide 1	Gtf3c1	Q8K284	1,708	0,04788	2,235
Myb-binding protein 1A	Mybbp1a	Q7TPV4	3,605	0,00207	2,233
Mitogen-activated protein kinase kinase kinase MLK4	Mlk4	Q8VDG6	2,101	0,02429	2,231
PITH domain-containing protein 1	Pithd1	Q8BWR2	2,655	0,00921	2,221
Protein 4.1	Epb41	P48193	1,987	0,02938	2,214
Lysosomal alpha-mannosidase	Man2b1	O09159	3,781	0,00157	2,213
Unconventional myosin-VIIa	Myo7a	P97479	3,132	0,00405	2,210
DNA replication licensing factor MCM2	Mcm2	P97310	3,190	0,00382	2,208
Protein VPRBP	Vprbp	Q80TR8	2,159	0,02150	2,201
cAMP-dependent protein kinase catalytic subunit beta	Prkacb	P68181	2,196	0,02035	2,193
Zinc transporter ZIP12	Slc39a12	Q5FWH7	3,396	0,00289	2,187
Pre-mRNA-processing-splicing factor 8	Prpf8	Q99PV0	2,153	0,02178	2,186
Craniofacial development protein 1	Cfdp1	O88271	2,322	0,01693	2,183
N-acetylgalactosamine kinase	Galk2	Q68FH4	4,731	0,00062	2,180
Cingulin-like protein 1	Cgnl1	Q6AW69	1,940	0,03206	2,177
Cathepsin B	Ctsb	P10605	3,058	0,00450	2,172
Signal peptidase complex catalytic subunit SEC11A	Sec11a	Q9R0P6	3,639	0,00199	2,164
Nuclear pore complex protein Nup160	Nup160	Q9Z0W3	2,078	0,02536	2,160
Apolipoprotein D	Apod	P51910	2,861	0,00651	2,159
DNA replication licensing factor MCM4	Mcm4	P49717	4,005	0,00101	2,153
Serine/threonine-protein kinase WNK4	Wnk4	Q80UE6	2,135	0,02246	2,149
Ephrin type-A receptor 2	Epha2	Q03145	2,260	0,01839	2,138
Endoplasmic reticulum lectin 1	Erlec1	Q8VEH8	3,385	0,00294	2,137
Nestin	Nes	Q6P5H2	3,233	0,00350	2,134
DNA-directed RNA polymerase III subunit RPC4	Polr3d	Q91WD1	1,998	0,02890	2,134
Sorting nexin-3	Snx3	O70492	2,707	0,00857	2,130
Peroxiredoxin-6	Prdx6	O08709	5,747	0,00017	2,122
Bone sialoprotein 2	Ibsp	Q61711	2,052	0,02621	2,116
Phosphoserine phosphatase	Psph	Q99LS3	1,886	0,03520	2,115
Septin-10	sept-10	Q8C650	3,520	0,00234	2,111
DnaJ homolog subfamily C member 8	Dnajc8	Q6NZB0	1,796	0,04149	2,109
ATP-binding cassette sub-family F member 3	Abcf3	Q8K268	2,662	0,00906	2,109
Sphingosine-1-phosphate lyase 1	Sgpl1	Q8R0X7	3,759	0,00175	2,107
Protein TASOR	Fam208a	Q69ZR9	1,848	0,03751	2,097
Egl nine homolog 1	Egln1	Q91YE3	1,722	0,04670	2,092
U4/U6.U5 tri-snRNP-associated protein 2	Usp39	Q3TIX9	1,742	0,04523	2,086
ADP-ribosylation factor-binding protein GGA2	Gga2	Q6P5E6	2,669	0,00904	2,081
Large neutral amino acids transporter small subunit 1	Slc7a5	Q9Z127	1,795	0,04153	2,079
Glutamate--cysteine ligase catalytic subunit	Gclc	P97494	7,389	0,00044	2,071

Gene Name	Gene Abbreviations	Accession code	-Log p-value WT_KO	q-value WT_KO	KO/WT Ratio
Phosphatidylserine synthase 1	Ptdss1	Q99LH2	2,238	0,01913	2,070
U4/U6 small nuclear ribonucleoprotein Prp31	Prpf31	Q8CCF0	2,730	0,00816	2,067
Pre-mRNA-processing factor 40 homolog A	Prpf40a	Q9R1C7	3,990	0,00099	2,066
DNA damage-binding protein 1	Ddb1	Q3U1J4	3,490	0,00249	2,060
Peptidyl-prolyl cis-trans isomerase G	Ppig	A2AR02	1,862	0,03671	2,057
Rho guanine nucleotide exchange factor 9	Arhgef9	Q3UTH8	3,932	0,00115	2,051
Peroxiredoxin-1	Prdx1	P35700	3,153	0,00400	2,049
Exosome complex component RRP43	Exosc8	Q9D753	2,526	0,01175	2,048
Proteasome activator complex subunit 3	Psme3	P61290	1,995	0,02910	2,041
HEAT repeat-containing protein 5B	Heatr5b	Q8C547	1,713	0,04759	2,041
Thymidylate synthase	Tyms	P07607	2,087	0,02505	2,040
GRIP and coiled-coil domain-containing protein 1	Gcc1	Q9D4H2	3,032	0,00461	2,029
Phosphoribosyl pyrophosphate synthase-associated protein 1	Prpsap1	Q9D0M1	1,991	0,02922	2,029
Vam6/Vps39-like protein	Vps39	Q8R5L3	4,227	0,00083	2,024
Protein SMG7	Smg7	Q5RJH6	2,059	0,02595	2,023
EF-hand domain-containing protein D1	Efhd1	Q9D4J1	5,350	0,00029	2,017
C-Jun-amino-terminal kinase-interacting protein 1	Mapk8ip1	Q9WVI9	2,457	0,01344	2,015
Proteasome activator complex subunit 4	Psme4	Q5SSW2	2,234	0,01916	2,012
Centrosomal protein kizuna	Kiz	Q3UXL4	3,570	0,00218	2,009
Tyrosine-protein phosphatase non-receptor type substrate 1	Sirpa	P97797	2,199	0,02032	2,008
Secretory carrier-associated membrane protein 2	Scamp2	Q9ERN0	3,400	0,00290	2,005
LEM domain-containing protein 2	Lemd2	Q6DVA0	1,714	0,04755	2,005
Cleft lip and palate transmembrane protein 1 homolog	Clptm1	Q8VBZ3	2,929	0,00557	2,001
DNA mismatch repair protein Msh2	Msh2	P43247	2,213	0,02002	2,000
FUN14 domain-containing protein 1	Fundc1	Q9DB70	2,321	0,01690	1,996
72 kDa type IV collagenase	Mmp2	P33434	2,828	0,00680	1,994
Dedicator of cytokinesis protein 7	Dock7	Q8R1A4	2,597	0,01041	1,991
mRNA cap guanine-N7 methyltransferase	Rnmt	Q9D0L8	2,670	0,00906	1,987
Platelet-derived growth factor receptor beta	Pdgfrb	P05622	1,710	0,04779	1,985
Membrane-associated progesterone receptor component 1	Pgrmc1	O55022	3,183	0,00387	1,982
Proliferating cell nuclear antigen	Pcna	P17918	2,448	0,01364	1,982
Proteasome subunit beta type-8	Psmb8	P28063	1,837	0,03804	1,980
Kinesin-like protein KIF1B	Kif1b	Q60575	2,537	0,01151	1,974
Signal-induced proliferation-associated protein 1	Sipa1	P46062	1,737	0,04558	1,970
Anaphase-promoting complex subunit 5	Anapc5	Q8BTZ4	2,288	0,01779	1,957
Ribosome biogenesis protein WDR12	Wdr12	Q9JJA4	2,737	0,00813	1,957
Transcriptional coactivator YAP1	Yap1	P46938	2,401	0,01470	1,953
Src substrate cortactin	Cttn	Q60598	2,811	0,00701	1,945
Histone H2A type 2-B	Hist2h2ab	Q64522	2,257	0,01847	1,942
Type 2 phosphatidylinositol 4 5-bisphosphate 4-phosphatase	Tmem55a	Q9CZX7	1,934	0,03235	1,942
Integral membrane protein 2B	Itm2b	O89051	2,188	0,02023	1,942
Transcription factor TFIIIB component B'' homolog	Bdp1	Q571C7	2,320	0,01688	1,937
1 4-alpha-glucan-branching enzyme	Gbe1	Q9D6Y9	2,950	0,00537	1,937
Complement C1r-A subcomponent	C1ra	Q8CG16	3,386	0,00295	1,937
Solute carrier family 12 member 9	Slc12a9	Q99MR3	2,428	0,01408	1,935
UDP-glucose 6-dehydrogenase	Ugdh	O70475	3,327	0,00316	1,930
Ubiquitin conjugation factor E4 B	Ube4b	Q9ES00	4,060	0,00096	1,924
Elongator complex protein 3	Elp3	Q9CZX0	1,800	0,04123	1,924
Ubiquitin fusion degradation protein 1 homolog	Ufd1l	P70362	2,190	0,02021	1,923
DNA topoisomerase 2-beta	Top2b	Q64511	2,125	0,02314	1,922
Protein arginine N-methyltransferase 1	Prmt1	Q9JIF0	4,593	0,00062	1,921
Thrombospondin-2	Thbs2	Q03350	4,109	0,00091	1,920
FACT complex subunit SSRP1	Ssrp1	Q08943	3,482	0,00256	1,919
Tumor necrosis factor alpha-induced protein 8	Tnfaip8	Q921Z5	3,009	0,00481	1,917
Ceramide synthase 1	Cers1	P27545	2,078	0,02537	1,917
CD166 antigen	Alcam	Q61490	5,740	0,00017	1,915
Transgelin	Tagln	P37804	2,241	0,01901	1,911
N-acetylglucosamine-6-sulfatase	Gns	Q8BFR4	3,317	0,00318	1,910
Nuclear factor NF-kappa-B p105 subunit	Nfkb1	P25799	3,350	0,00306	1,908
Calcium-binding mitochondrial carrier protein SCaMC-2	Slc25a25	A2ASZ8	1,964	0,03059	1,908
Serine/threonine-protein kinase PAK 1	Pak1	O88643	1,844	0,03774	1,906
Apolipoprotein B-100	Apob	E9Q414	1,755	0,04396	1,906
Protocadherin gamma-A4	Pcdhga4	Q91XY4	1,725	0,04649	1,901
Iron-responsive element-binding protein 2	Ireb2	Q811J3	2,091	0,02486	1,900
Galectin-1	Lgals1	P16045	2,258	0,01844	1,899
Programmed cell death protein 4	Pdcd4	Q61823	2,912	0,00579	1,879

Gene Name	Gene Abbreviations	Accession code	-Log p-value WT_KO	q-value WT_KO	KO/WT Ratio
Nucleoporin GLE1	Gle1	Q8R322	1,972	0,03037	1,873
Hydroxymethylglutaryl-CoA synthase mitochondrial	Hmgcs2	P54869	3,145	0,00404	1,869
Ubiquilin-2	Ubqln2	Q9QZM0	2,275	0,01804	1,869
REST corepressor 2	Rcor2	Q8C796	2,252	0,01860	1,866
Cullin-3	Cul3	Q9JLV5	3,417	0,00280	1,859
Selenoprotein N	Sepn1	D3Z2R5	3,694	0,00186	1,858
G patch domain-containing protein 1	Gpatch1	Q9DBM1	2,668	0,00904	1,855
Microtubule-associated serine/threonine-protein kinase 2	Mast2	Q60592	2,059	0,02595	1,854
Ubiquitin carboxyl-terminal hydrolase 8	Usp8	Q80U87	2,736	0,00814	1,854
Protein ERGIC-53	Lman1	Q9D0F3	2,888	0,00608	1,852
Calponin-2	Cnn2	Q08093	2,269	0,01812	1,850
Exosome complex exonuclease RRP42	Exosc7	Q9D0M0	2,536	0,01151	1,846
Nucleolar protein 58	Nop58	Q6DFW4	2,233	0,01919	1,846
DnaJ homolog subfamily B member 11	Dnajb11	Q99KV1	3,043	0,00461	1,843
4F2 cell-surface antigen heavy chain	Slc3a2	P10852	5,846	0,00020	1,843
Acyl-CoA synthetase family member 3 mitochondrial	Acsf3	Q3URE1	2,447	0,01364	1,842
Collagen alpha-1(XII) chain	Col12a1	Q60847	4,661	0,00060	1,842
Protein DEK	Dek	Q7TNV0	3,616	0,00203	1,834
Phospholipid transfer protein	Pltp	P55065	1,930	0,03255	1,832
UDP-N-acetylhexosamine pyrophosphorylase-like protein 1	Uap1l1	Q3TW96	4,475	0,00066	1,831
Proteasome-associated protein ECM29 homolog	Ecm29	Q6PDI5	2,283	0,01783	1,826
Neuromodulin	Gap43	P06837	2,010	0,02807	1,823
Golgi integral membrane protein 4	Golim4	Q8BXA1	2,102	0,02428	1,817
Protein unc-45 homolog A	Unc45a	Q99KD5	1,751	0,04446	1,815
Serine palmitoyltransferase 2	Sptlc2	P97363	1,918	0,03316	1,814
Transaldolase	Taldo1	Q93092	5,223	0,00039	1,810
U5 small nuclear ribonucleoprotein 200 kDa helicase	Snrnp200	Q6P4T2	2,403	0,01471	1,808
Cyclin-dependent kinase 6	Cdk6	Q64261	1,758	0,04387	1,806
Phospholipase D4	Pld4	Q8BG07	2,170	0,02100	1,804
Solute carrier family 12 member 2	Slc12a2	P55012	4,420	0,00069	1,803
6-phosphogluconate dehydrogenase decarboxylating	Pgd	Q9DCD0	4,891	0,00041	1,803
Leucine zipper transcription factor-like protein 1	Lztfl1	Q9JHQ5	1,794	0,04167	1,803
tRNA (cytosine(34)-C(5))-methyltransferase	Nsun2	Q1HFZ0	2,424	0,01416	1,802
Metalloreductase STEAP4	Steap4	Q923B6	2,339	0,01650	1,800
DNA replication licensing factor MCM3	Mcm3	P25206	4,200	0,00085	1,799
Signal transducer and activator of transcription 3	Stat3	P42227	4,139	0,00088	1,799
Cap-specific mRNA (nucleoside-2'-O-)-methyltransferase 1	Cmtr1	Q9DBC3	3,632	0,00200	1,798
REST corepressor 1	Rcor1	Q8CFE3	1,709	0,04790	1,795
SLAIN motif-containing protein 2	Slain2	Q8CI08	3,555	0,00217	1,795
Ubiquitin-protein ligase E3C	Ube3c	Q80U95	2,013	0,02787	1,793
Thioredoxin-related transmembrane protein 4	Tmx4	Q8C0L0	2,769	0,00769	1,792
cAMP-dependent protein kinase type I-alpha regulatory subunit	Prkar1a	Q9DBC7	2,226	0,01946	1,792
Lysosomal alpha-glucosidase	Gaa	P70699	1,777	0,04250	1,791
Protein sidekick-1	Sdk1	Q3UH53	4,000	0,00100	1,791
Plexin-D1	Plxnd1	Q3UH93	2,139	0,02237	1,790
NADP-dependent malic enzyme	Me1	P06801	5,264	0,00034	1,787
Shootin-1	Shtn1	Q8K2Q9	1,852	0,03724	1,786
Kin of IRRE-like protein 1	Kirrel	Q80W68	2,401	0,01468	1,786
Myotubularin-related protein 3	Mtmr3	Q8K296	2,316	0,01697	1,783
Thrombospondin-4	Thbs4	Q9Z1T2	4,260	0,00082	1,780
Heterogeneous nuclear ribonucleoprotein A1	Hnrnpa1	P49312	3,405	0,00284	1,773
Disintegrin and metalloproteinase domain-containing protein 9	Adam9	Q61072	2,777	0,00759	1,772
Regulator of chromosome condensation	Rcc1	Q8VE37	3,621	0,00202	1,772
RNA-binding protein 26	Rbm26	Q6NZN0	1,867	0,03646	1,772
Ras-related protein M-Ras	Mras	O08989	3,280	0,00330	1,771
ADP-ribosylation factor-like protein 8B	Arl8b	Q9CQW2	3,373	0,00297	1,768
Cyclin-dependent kinase inhibitor 1B	Cdkn1b	P46414	2,202	0,02026	1,767
Splicing factor 3B subunit 1	Sf3b1	Q99NB9	2,763	0,00779	1,766
Meiosis arrest female protein 1	Marf1	Q8BJ34	2,848	0,00656	1,766
Uncharacterized protein C1orf87 homolog	Gm12695	A2AGB2	1,909	0,03374	1,755
Dynein light chain 2 cytoplasmic	Dynll2	Q9D0M5	1,865	0,03652	1,754
Histone-lysine N-methyltransferase KMT5B	Kmt5b	Q3U8K7	2,663	0,00904	1,750
Myc box-dependent-interacting protein 1	Bin1	O08539	2,633	0,00969	1,749
Calcitonin gene-related peptide 1	Calca	Q99JA0	1,688	0,04999	1,746
Dedicator of cytokinesis protein 1	Dock1	Q8BUR4	4,150	0,00090	1,745
Glutathione peroxidase 3	Gpx3	P46412	2,513	0,01211	1,738

Gene Name	Gene Abbreviations	Accession code	-Log p-value WT_KO	q-value WT_KO	KO/WT Ratio
Synaptosomal-associated protein 23	Snap23	O09044	1,964	0,03060	1,733
Vacuolar protein sorting-associated protein 41 homolog	Vps41	Q5KU39	1,963	0,03058	1,728
Cation channel sperm-associated protein 2	Catsr2	A2ARP9	1,972	0,03035	1,726
Aldehyde oxidase 1	Aox1	O54754	2,099	0,02446	1,724
Prostaglandin reductase 1	Ptgr1	Q91YR9	3,297	0,00318	1,722
Deoxynucleoside triphosphate triphosphohydrolase SAMHD1	Samhd1	Q60710	2,209	0,02009	1,722
AP-1 complex subunit sigma-1A	Ap1s1	P61967	1,793	0,04170	1,721
Translocon-associated protein subunit alpha	Ssr1	Q9CY50	3,035	0,00464	1,707
Monoacylglycerol lipase ABHD12	Abhd12	Q99LR1	2,342	0,01652	1,706
Tumor suppressor candidate 5 homolog	Tusc5	Q8C838	1,988	0,02928	1,706
Beta-arrestin-2	Arrb2	Q91YI4	1,726	0,04648	1,705
Lymphocyte-specific protein 1	Lsp1	P19973	2,023	0,02745	1,700
Pre-mRNA-splicing factor ATP-dependent RNA helicase DHX15	Dhx15	O35286	3,033	0,00463	1,695
Switch-associated protein 70	Swap70	Q6A028	2,406	0,01466	1,694
Eukaryotic translation initiation factor 3 subunit I	Eif3i	Q9QZD9	1,909	0,03376	1,692
DNA-directed RNA polymerase II subunit RPB4	Polr2d	Q9D7M8	1,711	0,04767	1,690
Prolyl 3-hydroxylase 3	P3h3	Q8CG70	2,610	0,01011	1,687
Actin-related protein 2/3 complex subunit 2	Arpc2	Q9CVB6	2,566	0,01085	1,687
Histone deacetylase 2	Hdac2	P70288	1,735	0,04566	1,686
Thioredoxin	Txn	P10639	1,801	0,04117	1,683
Phosphotriesterase-related protein	Pter	Q60866	1,799	0,04126	1,681
Baculoviral IAP repeat-containing protein 6	Birc6	O88738	2,219	0,01979	1,679
Nuclear pore complex protein Nup98-Nup96	Nup98	Q6PFD9	3,347	0,00308	1,677
Nuclear pore complex protein Nup107	Nup107	Q8BH74	2,450	0,01354	1,674
Protein transport protein Sec23B	Sec23b	Q9D662	3,890	0,00124	1,673
Engulfment and cell motility protein 2	Elmo2	Q8BHL5	3,354	0,00307	1,673
26S proteasome non-ATPase regulatory subunit 3	Psmd3	P14685	2,492	0,01265	1,673
P2X purinoceptor 7	P2rx7	Q9Z1M0	2,337	0,01649	1,668
Retinoblastoma-binding protein 5	Rbbp5	Q8BX09	2,019	0,02770	1,668
Pleiotropic regulator 1	Plrg1	Q922V4	2,647	0,00939	1,667
Biglycan	Bgn	P28653	4,170	0,00093	1,665
S-phase kinase-associated protein 1	Skp1	Q9WTX5	2,216	0,01984	1,664
Nuclear pore complex protein Nup93	Nup93	Q8BJ71	2,018	0,02771	1,660
Ski-like protein	Skil	Q60665	3,036	0,00464	1,659
40S ribosomal protein S15	Rps15	P62843	1,968	0,03044	1,658
Tyrosine-protein kinase JAK1	Jak1	P52332	2,870	0,00648	1,658
Lysine-specific demethylase 2B	Kdm2b	Q6P1G2	2,595	0,01041	1,656
Cullin-1	Cul1	Q9WTX6	3,170	0,00395	1,650
VPS10 domain-containing receptor SorCS2	Sorcs2	Q9EPR5	4,804	0,00056	1,650
Cysteine--tRNA ligase cytoplasmic	Cars	Q9ER72	2,195	0,02027	1,650
Ras GTPase-activating protein 3	Rasa3	Q60790	2,897	0,00596	1,647
Pro-cathepsin H	Ctsh	P49935	1,932	0,03244	1,647
ATP-dependent RNA helicase DHX36	Dhx36	Q8VHK9	2,282	0,01783	1,647
Sorting nexin-12	Snx12	O70493	1,860	0,03677	1,646
Reticulocalbin-3	Rcn3	Q8BH97	2,770	0,00771	1,643
Legumain	Lgmn	O89017	3,177	0,00390	1,641
Endonuclease/exonuclease/phosphatase family domain-containing protein 1	Eepd1	Q3TGW2	1,869	0,03639	1,641
Carnitine O-palmitoyltransferase 1 liver isoform	Cpt1a	P97742	2,040	0,02651	1,640
Monofunctional C1-tetrahydrofolate synthase mitochondrial	Mthfd1l	Q3V3R1	3,021	0,00469	1,638
Phosphatidylinositol 4-kinase alpha	Pi4ka	E9Q3L2	1,713	0,04762	1,637
Ubiquitin carboxyl-terminal hydrolase 47	Usp47	Q8BY87	3,672	0,00196	1,637
Chromodomain-helicase-DNA-binding protein 4	Chd4	Q6PDQ2	1,765	0,04328	1,635
DnaJ homolog subfamily C member 7	Dnajc7	Q9QYI3	1,790	0,04179	1,634
Cytoglobin	Cygb	Q9CX80	4,148	0,00089	1,633
Kinectin	Ktn1	Q61595	3,237	0,00347	1,632
DNA polymerase delta subunit 2	Pold2	O35654	2,284	0,01787	1,632
Cathepsin D	Ctsd	P18242	5,746	0,00017	1,631
Glucose-6-phosphate 1-dehydrogenase X	G6pdx	Q00612	4,303	0,00081	1,630
La-related protein 1	Larp1	Q6ZQ58	3,547	0,00225	1,628
NADH dehydrogenase [ubiquinone] 1 beta subcomplex subunit 7	Ndufb7	Q9CR61	2,038	0,02654	1,626
Elongator complex protein 4	Elp4	Q9ER73	2,042	0,02661	1,625
Anamorsin	Ciapin1	Q8WTY4	2,123	0,02333	1,625
Epidermal growth factor receptor	Egfr	Q01279	3,105	0,00423	1,622
Hydroxysteroid dehydrogenase-like protein 2	Hsdl2	Q2TPA8	2,082	0,02518	1,620
ATP-binding cassette sub-family D member 3	Abcd3	P55096	1,714	0,04757	1,619

Gene Name	Gene Abbreviations	Accession code	-Log p-value WT_KO	q-value WT_KO	KO/WT Ratio
Cytoplasmic FMR1-interacting protein 1	Cyfip1	Q7TMB8	3,275	0,00330	1,612
Cytochrome c oxidase subunit 5A mitochondrial	Cox5a	P12787	1,882	0,03547	1,608
Serine/threonine-protein kinase PLK3	Plk3	Q60806	2,598	0,01039	1,606
Transthyretin	Ttr	P07309	1,723	0,04667	1,606
Nucleobindin-2	Nucb2	P81117	1,845	0,03774	1,604
40S ribosomal protein S17	Rps17	P63276	2,472	0,01301	1,602
Peroxisomal NADH pyrophosphatase NUDT12	Nudt12	Q9DCN1	1,699	0,04892	1,600
A-kinase anchor protein 2	Akap2	O54931	2,948	0,00538	1,599
Conserved oligomeric Golgi complex subunit 3	Cog3	Q8CI04	1,758	0,04387	1,596
Superoxide dismutase [Cu-Zn]	Sod1	P08228	1,726	0,04651	1,595
Lysosome membrane protein 2	Scarb2	O35114	2,515	0,01208	1,595
Proteasome subunit beta type-1	Psmb1	O09061	1,735	0,04566	1,593
U6 snRNA-associated Sm-like protein LSm2	Lsm2	O35900	2,277	0,01802	1,593
Golgi resident protein GCP60	Acbd3	Q8BMP6	2,666	0,00902	1,587
Alpha-1 3/1 6-mannosyltransferase ALG2	Alg2	Q9DBE8	3,794	0,00154	1,584
Stonin-1	Ston1	Q8CDJ8	4,649	0,00060	1,584
EGF-containing fibulin-like extracellular matrix protein 2	Efemp2	Q9WVJ9	1,883	0,03541	1,582
Protein FAM188A	Fam188a	Q9CV28	1,921	0,03294	1,578
Plasminogen activator inhibitor 1 RNA-binding protein	Serbp1	Q9CY58	2,379	0,01545	1,574
AP-3 complex subunit beta-1	Ap3b1	Q9Z1T1	2,283	0,01784	1,568
Dynactin subunit 3	Dctn3	Q9Z0Y1	3,220	0,00363	1,568
DnaJ homolog subfamily B member 4	Dnajb4	Q9D832	3,122	0,00408	1,568
cGMP-inhibited 3' 5'-cyclic phosphodiesterase B	Pde3b	Q61409	1,947	0,03162	1,565
ADP-ribosylation factor-like protein 2	Arl2	Q9D0J4	2,183	0,02038	1,565
Cell surface glycoprotein MUC18	Mcam	Q8R2Y2	3,950	0,00111	1,560
40S ribosomal protein S27	Rps27	Q6ZWU9	2,235	0,01919	1,557
Heterogeneous nuclear ribonucleoprotein H	Hnrnph1	O35737	1,994	0,02907	1,556
ATP-dependent RNA helicase DDX42	Ddx42	Q810A7	2,042	0,02663	1,549
Eukaryotic translation initiation factor 3 subunit C	Eif3c	Q8R1B4	1,998	0,02893	1,548
Kelch-like protein 26	Klhl26	Q8BGY4	2,338	0,01650	1,547
Acidic leucine-rich nuclear phosphoprotein 32 family member E	Anp32e	P97822	4,206	0,00083	1,546
Methylosome subunit pICln	Clns1a	Q61189	2,205	0,02019	1,544
Platelet-activating factor acetylhydrolase 2 cytoplasmic	Pafah2	Q8VDG7	2,283	0,01782	1,543
Vinexin	Sorbs3	Q9R1Z8	3,133	0,00407	1,540
Collagen alpha-1(XXVIII) chain	Col28a1	Q2UY11	3,832	0,00149	1,538
Inverted formin-2	Inf2	Q0GNC1	2,388	0,01509	1,537
Proliferation-associated protein 2G4	Pa2g4	P50580	2,319	0,01688	1,537
WD40 repeat-containing protein SMU1	Smu1	Q3UKJ7	2,082	0,02518	1,532
U6 snRNA-associated Sm-like protein LSm4	Lsm4	Q9QXA5	2,569	0,01081	1,532
Phosphoribosylformylglycinamidine synthase	Pfas	Q5SUR0	2,152	0,02178	1,532
Tubby protein	Tub	P50586	1,828	0,03886	1,528
Brain acid soluble protein 1	Basp1	Q91XV3	3,498	0,00245	1,525
BRI3-binding protein	Bri3bp	Q8BXV2	2,747	0,00798	1,525
Ras-related protein Rab-4B	Rab4b	Q91ZR1	2,071	0,02543	1,524
Protein Shroom2	Shroom2	A2ALU4	3,480	0,00255	1,523
Splicing factor U2AF 65 kDa subunit	U2af2	P26369	3,462	0,00263	1,523
CDGSH iron-sulfur domain-containing protein 2	Cisd2	Q9CQB5	2,836	0,00666	1,523
Bifunctional polynucleotide phosphatase/kinase	Pnkp	Q9JLV6	2,044	0,02651	1,523
Rho-related GTP-binding protein RhoC	Rhoc	Q62159	2,014	0,02785	1,522
Ubiquilin-1	Ubqln1	Q8R317	1,699	0,04890	1,522
Protein LSM14 homolog A	Lsm14a	Q8K2F8	4,177	0,00087	1,519
Lamin-B2	Lmnb2	P21619	2,637	0,00965	1,519
High mobility group protein B2	Hmgb2	P30681	2,181	0,02042	1,518
Septin-5	sept-05	Q9Z2Q6	1,872	0,03620	1,517
Secretogranin-2	Scg2	Q03517	2,076	0,02540	1,516
Tumor necrosis factor receptor superfamily member 16	Ngfr	Q9Z0W1	3,350	0,00306	1,515
Myosin-8	Myh8	P13542	2,017	0,02767	1,513
Submandibular gland protein C	Muc19	Q6JHY2	2,269	0,01813	1,510
Protein phosphatase 1F	Ppm1f	Q8CGA0	1,813	0,03996	1,510
Transcription elongation factor B polypeptide 1	Tceb1	P83940	1,777	0,04249	1,509
Proteasome subunit beta type-4	Psmb4	P99026	2,252	0,01857	1,508
Calreticulin	Calr	P14211	1,693	0,04970	1,506
Glypican-3	Gpc3	Q8CFZ4	1,811	0,04006	1,505
Mitochondrial import receptor subunit TOM34	Tomm34	Q9CYG7	3,169	0,00393	1,504
Zinc finger CCHC domain-containing protein 7	Zcchc7	B1AX39	1,897	0,03431	1,502
Eukaryotic translation initiation factor 3 subunit L	Eif3l	Q8QZY1	3,062	0,00455	1,502

Gene Name	Gene Abbreviations	Accession code	-Log p-value WT_KO	q-value WT_KO	KO/WT Ratio
1-acylglycerol-3-phosphate O-acyltransferase ABHD5	Abhd5	Q9DBL9	2,754	0,00792	0,500
Glutamate receptor ionotropic delta-1	Grid1	Q61627	2,026	0,02724	0,499
ProteinCP1	Oscp1	Q8BHW2	1,774	0,04249	0,496
Cubilin	Cubn	Q9JLB4	1,904	0,03409	0,495
Arf-GAP domain and FG repeat-containing protein 2	Agfg2	Q80WC7	2,259	0,01844	0,491
Cytosolic 5'-nucleotidase 1A	Nt5c1a	A3KFX0	2,013	0,02784	0,490
Retinol dehydrogenase 7	Rdh7	O88451	2,974	0,00509	0,489
Keratin type II cytoskeletal 2 epidermal	Krt2	Q3TTY5	2,030	0,02709	0,487
3-hydroxy-3-methylglutaryl-coenzyme A reductase	Hmgcr	Q01237	1,911	0,03361	0,486
Rho guanine nucleotide exchange factor 10	Arhgef10	Q8C033	2,200	0,02033	0,485
Protein capicua homolog	Cic	Q924A2	1,724	0,04666	0,485
Integrin alpha-6	Itga6	Q61739	5,772	0,00018	0,484
Dr1-associated corepressor	Drap1	Q9D6N5	1,904	0,03405	0,483
Glycerol-3-phosphate dehydrogenase [NAD(+)] cytoplasmic	Gpd1	P13707	5,820	0,00018	0,481
Glypican-6	Gpc6	Q9R087	1,704	0,04838	0,480
CD99 antigen-like protein 2	Cd99l2	Q8BIF0	2,244	0,01892	0,479
Selenoprotein O	Selo	Q9DBC0	2,705	0,00864	0,479
Tapasin	Tapbp	Q9R233	2,018	0,02769	0,479
DNA-binding protein RFX6	Rfx6	Q8C7R7	2,286	0,01785	0,478
Pleckstrin homology domain-containing family A member 4	Plekha4	Q8VC98	4,266	0,00084	0,478
Membrane primary amine oxidase	Aoc3	O70423	2,317	0,01697	0,477
Secreted frizzled-related protein 5	Sfrp5	Q9WU66	2,119	0,02356	0,475
Elongation of very long chain fatty acids protein 6	Elovl6	Q920L5	1,976	0,03010	0,473
Cytoplasmic phosphatidylinositol transfer protein 1	Pitpnc1	Q8K4R4	1,866	0,03652	0,472
D-beta-hydroxybutyrate dehydrogenase mitochondrial	Bdh1	Q80XN0	6,561	0,00021	0,472
WD repeat-containing protein 7	Wdr7	Q920I9	2,148	0,02187	0,469
RNA-binding protein 28	Rbm28	Q8CGC6	2,206	0,02017	0,469
SH3 domain-containing protein 21	Sh3d21	Q7TSG5	1,857	0,03687	0,466
SLIT and NTRK-like protein 5	Slitrk5	Q810B7	2,699	0,00866	0,465
Transmembrane gamma-carboxyglutamic acid protein 3	Prrg3	Q6PAQ9	2,705	0,00862	0,465
NEDD8-activating enzyme E1 catalytic subunit	Uba3	Q8C878	5,956	0,00024	0,464
DDB1- and CUL4-associated factor 5	Dcaf5	Q80T85	2,160	0,02153	0,463
Protein-methionine sulfoxide oxidase MICAL3	Mical3	Q8CJ19	3,369	0,00299	0,460
Histidine triad nucleotide-binding protein 3	Hint3	Q9CPS6	2,925	0,00561	0,458
Mitochondrial inner membrane protein OXA1L	Oxa1l	Q8BGA9	2,374	0,01550	0,453
Phosphoglycerate mutase 2	Pgam2	O70250	1,809	0,04027	0,448
Rho GTPase-activating protein 29	Arhgap29	Q8CGF1	1,757	0,04385	0,448
Coiled-coil domain-containing protein 85A	Ccdc85a	Q5SP85	2,355	0,01610	0,446
DENN domain-containing protein 3	Dennd3	A2RT67	1,842	0,03784	0,445
Integrin beta-4	Itgb4	A2A863	8,713	0,00000	0,441
Prolyl 4-hydroxylase subunit alpha-3	P4ha3	Q6W3F0	2,717	0,00839	0,440
Dystrophin-related protein 2	Drp2	Q05AA6	5,925	0,00022	0,440
YjeF N-terminal domain-containing protein 3	Yjefn3	F6W8I0	3,116	0,00415	0,440
Histone H1.0	H1f0	P10922	2,439	0,01377	0,439
Centromere protein C	Cenpc	P49452	2,053	0,02615	0,437
Insulin-like growth factor 1 receptor	Igf1r	Q60751	2,545	0,01139	0,434
Transmembrane protein 131	Tmem131	O70472	2,262	0,01835	0,433
HRAS-like suppressor 3	Pla2g16	Q8R3U1	2,819	0,00687	0,432
Mevalonate kinase	Mvk	Q9R008	5,094	0,00038	0,430
E3 SUMO-protein ligase CBX4	Cbx4	O55187	1,865	0,03652	0,428
Unconventional myosin-Id	Myo1d	Q5SYD0	5,536	0,00024	0,427
Isopentenyl-diphosphate Delta-isomerase 1	Idi1	P58044	4,940	0,00042	0,427
NEDD8-activating enzyme E1 regulatory subunit	Nae1	Q8VBW6	6,453	0,00020	0,426
Acetoacetyl-CoA synthetase	Aacs	Q9D2R0	5,071	0,00038	0,425
Fibromodulin	Fmod	P50608	2,408	0,01462	0,424
RIB43A-like with coiled-coils protein 1	Ribc1	Q9D0B8	2,901	0,00593	0,423
Protein shisa-4	Shisa4	Q8CA71	2,628	0,00983	0,422
Phosphatidylinositol 3 4 5-trisphosphate-dependent Rac exchanger 2 protein	Prex2	Q3LAC4	2,224	0,01963	0,421
Calpain-12	Capn12	Q9ER56	2,671	0,00907	0,417
Golgi reassembly-stacking protein 1	Gorasp1	Q91X51	1,990	0,02923	0,416
Keratin type II cytoskeletal 2 oral	Krt76	Q3UV17	1,742	0,04527	0,411
Ig mu chain C region	Ighm	P01872	3,455	0,00262	0,408
3-keto-steroid reductase	Hsd17b7	O88736	5,989	0,00024	0,404
Large tegument protein deneddylase	M48	A8E1C4	4,294	0,00084	0,402
CCAAT/enhancer-binding protein zeta	Cebpz	P53569	3,596	0,00213	0,402

Gene Name	Gene Abbreviations	Accession code	-Log p-value WT_KO	q-value WT_KO	KO/WT Ratio
AP-3 complex subunit mu-2	Ap3m2	Q8R2R9	2,844	0,00658	0,399
Leucine-rich repeat LGI family member 3	Lgi3	Q8K406	6,407	0,00018	0,397
Probable ribonuclease ZC3H12C	Zc3h12c	Q5DTV4	2,831	0,00680	0,396
Probable ATP-dependent RNA helicase DDX58	Ddx58	Q6Q899	1,819	0,03971	0,396
N6-adenosine-methyltransferase subunit METTL3	Mettl3	Q8C3P7	2,857	0,00656	0,392
Major facilitator superfamily domain-containing protein 1	Mfsd1	Q9DC37	2,049	0,02628	0,388
Fatty acid desaturase 1	Fads1	Q920L1	2,331	0,01666	0,383
Collagen alpha-6(VI) chain	Col6a6	Q8C6K9	4,694	0,00059	0,382
Zinc finger SWIM domain-containing protein 4	Zswim4	Q8C7B8	2,466	0,01320	0,380
Tyrosine-protein kinase Tec	Tec	P24604	2,791	0,00740	0,371
Centrosomal protein of 164 kDa	Cep164	Q5DU05	3,172	0,00396	0,366
Kelch-like protein 10	Klhl10	Q9D5V2	5,929	0,00022	0,366
Terminal uridylyltransferase 7	Zcchc6	Q5BLK4	3,178	0,00389	0,366
Serine/threonine-protein kinase SIK3	Sik3	Q6P4S6	3,310	0,00316	0,361
Lanosterol 14-alpha demethylase	Cyp51a1	Q8K0C4	4,610	0,00063	0,361
Secretory carrier-associated membrane protein 5	Scamp5	Q9JKD3	1,845	0,03773	0,361
Angiogenic factor with G patch and FHA domains 1	Aggf1	Q7TN31	2,105	0,02418	0,359
Probable palmitoyltransferase ZDHHC4	Zdhhc4	Q9D6H5	4,706	0,00059	0,355
Squalene monooxygenase	Sqle	P52019	3,052	0,00456	0,354
2' 3'-cyclic-nucleotide 3'-phosphodiesterase	Cnp	P16330	8,807	0,00000	0,352
Zinc finger protein 292	Zfp292	Q9Z2U2	2,748	0,00800	0,344
WD repeat-containing protein mio	Mios	Q8VE19	3,590	0,00212	0,344
Transcription factor HIVEP2	Hivep2	Q3UHF7	1,797	0,04150	0,344
Chromodomain-helicase-DNA-binding protein 5	Chd5	A2A8L1	2,635	0,00965	0,338
Isoprenoid synthase domain-containing protein	Ispd	Q5RJG7	5,113	0,00039	0,333
Plasmolipin	Pllp	Q9DCU2	2,159	0,02151	0,331
Echinoderm microtubule-associated protein-like 3	Eml3	Q8VC03	3,523	0,00232	0,330
Regulatory solute carrier protein family 1 member 1	Rsc1a1	Q9ER99	2,094	0,02478	0,328
TLR4 interactor with leucine rich repeats	Tril	Q9DBY4	2,724	0,00824	0,323
Solute carrier organic anion transporter family member 3A1	Slco3a1	Q8R3L5	1,831	0,03862	0,312
Bromodomain testis-specific protein	Brdt	Q91Y44	2,615	0,01005	0,310
Angiomotin	Amot	Q8VHG2	2,176	0,02074	0,310
Squalene synthase	Fdft1	P53798	8,908	0,00000	0,309
Platelet glycoprotein 4	Cd36	Q08857	2,237	0,01912	0,307
Folliculin-interacting protein 1	Fnip1	Q68FD7	2,980	0,00504	0,307
Poly(rC)-binding protein 4	Pcbp4	P57724	2,055	0,02611	0,306
U4/U6 small nuclear ribonucleoprotein Prp3	Prpf3	Q922U1	3,242	0,00347	0,305
Sulfotransferase 1A1	Sult1a1	P52840	5,463	0,00023	0,304
Nucleolar transcription factor 1	Ubtf	P25976	3,921	0,00117	0,293
Dermatopontin	Dpt	Q9QZZ6	2,258	0,01842	0,289
Solute carrier family 22 member 16	Slc22a16	Q497L8	1,812	0,04007	0,282
Protein-arginine deiminase type-2	Padi2	Q08642	2,776	0,00759	0,272
Fatty acyl-CoA reductase 1	Far1	Q922J9	4,971	0,00042	0,270
Chromodomain-helicase-DNA-binding protein 8	Chd8	Q09XV5	3,648	0,00196	0,263
SNW domain-containing protein 1	Snw1	Q9CSN1	3,217	0,00364	0,262
MRG/MORF4L-binding protein	Mrgbp	Q9DAT2	3,709	0,00178	0,261
Lanosterol synthase	Lss	Q8BLN5	7,290	0,00036	0,260
Pleckstrin homology-like domain family B member 2	Phldb2	Q8K1N2	2,849	0,00658	0,258
Arf-GAP with coiled-coil ANK repeat and PH domain-containing protein 1	Acap1	Q8K2H4	3,025	0,00467	0,256
Coiled-coil domain-containing protein 90B mitochondrial	Ccdc90b	Q8C3X2	2,366	0,01580	0,254
Ferritin heavy chain	Fth1	P09528	5,887	0,00021	0,252
Exophilin-5	Exph5	Q0VAV2	2,327	0,01675	0,249
ABI gene family member 3	Abi3	Q8BYZ1	4,629	0,00059	0,242
Zinc finger protein 40	Hivep1	Q03172	4,530	0,00068	0,237
Rho GTPase-activating protein 32	Arhgap32	Q811P8	4,078	0,00093	0,207
Cytosolic carboxypeptidase 3	Agbl3	Q8CDP0	2,055	0,02615	0,172
Hydroxymethylglutaryl-CoA synthase cytoplasmic	Hmgcs1	Q8JZK9	8,199	0,00000	0,171
Kinesin-like protein KIF18A	Kif18a	Q91WD7	4,793	0,00055	0,159
Filaggrin (Fragment)	Flg	P11088	7,059	0,00033	0,151
Probable helicase senataxin	Setx	A2AKX3	2,315	0,01692	0,140

Supplementary table 1. Raw data from RNAseq experiment in NAE1 cKO mice. Transcriptome profiles were obtained from P7 sciatic nerves from control (n = 4) and NAE1 cKO (n = 4) mice.

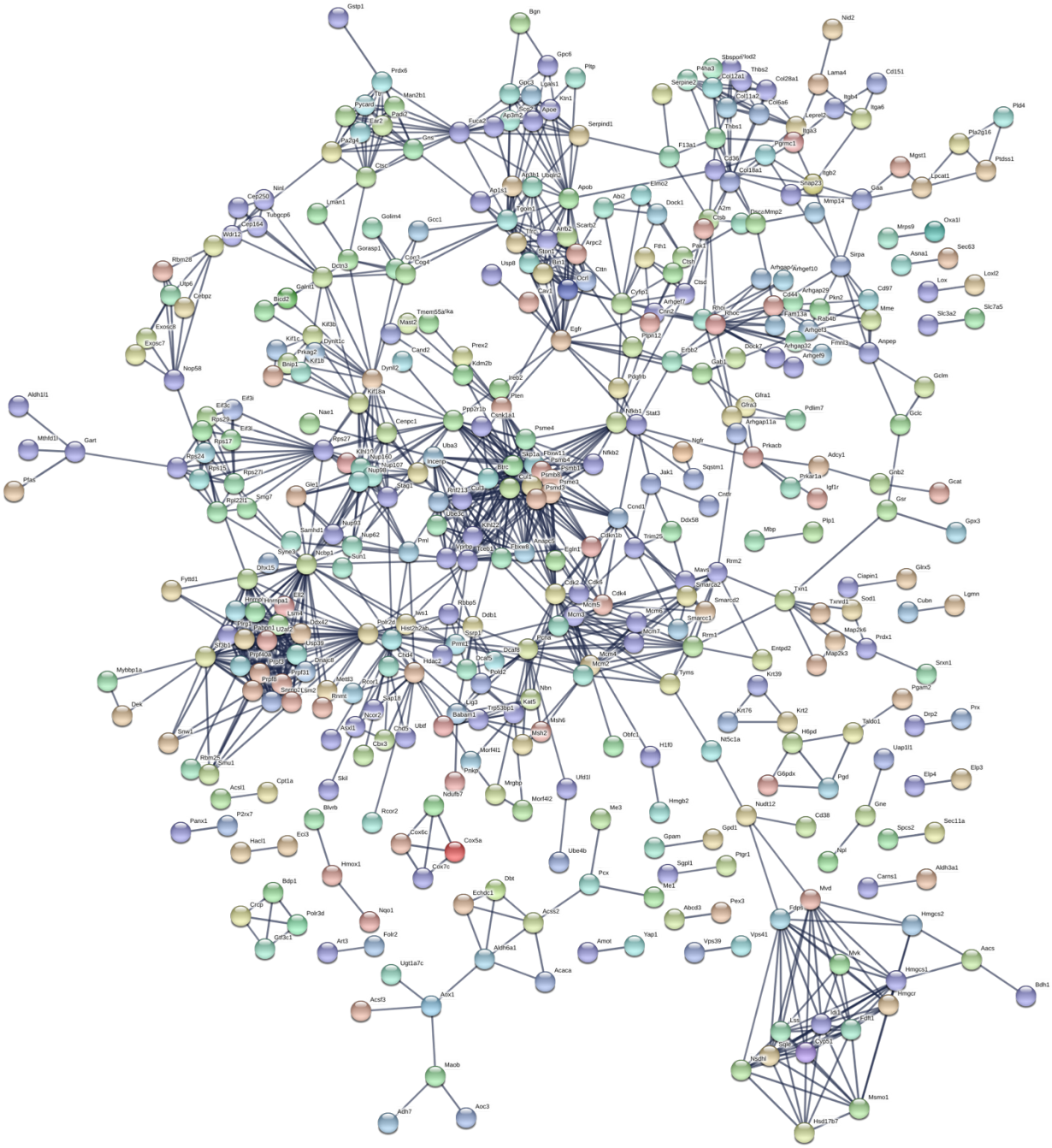

Supplementary figure 1. Neddylation inhibition induces large sale changes in proteomic profiles
Representation of the upregulated and downregulated genes obtained in the RNAseq data using the STRING software. The parameters used were: Full string network, evidence network edges, all interaction sources active, required interaction 0.4 minimum. Highlighted zones of the interactome show the main affected cellular functions or pathways. In a red circle were highlighted EGFR and Nae1.

10 ACKNOWLEDGEMENTS

Desde muy joven soñé con poder llegar a ser científico y poder aportar algún conocimiento nuevo a la ciencia para agradecerle de alguna forma a la humanidad el que haya tenido la oportunidad de venir a este mundo. Siempre me ha apasionado la ciencia y por eso me siento tremendamente alegre de poder haber colaborado en la medida de lo posible a seguir sumando con esta tesis de neurociencias sobre la neddylación en Schwann cells.

Pero solo ha sido posible que haya llegado hasta aquí gracias a muchísima gente a la que he tenido la suerte de conocer a lo largo de los años. Este es el verdadero premio que me llevo después de llevar investigando casi 7 años.

Esto no es una ceremonia de los Goya ni nada parecido, así que con la aprobación o no de quien lea esta tesis, voy a enumerar con bastante detalle toda la gente a la que le debo estar aquí y haber podido realizar esta tesis.

En primer lugar, le agradezco enormemente a mi director de tesis **Ashwin Woodhoo** haberme dado la oportunidad de trabajar en la investigación de las células de Schwann y haberme enseñado tanto durante estos 4 años que he vivido en Bilbao. Ha sido una experiencia muy enriquecedora, me ha permitido madurar como investigador y progresar mucho personalmente.

No habría podido acceder a la beca FPI con la que he podido realizar mi tesis si no hubiese sido por la experiencia que adquirí en diferentes laboratorios antes de venir "al Norte". Le doy las gracias por ello **Rafael Delgado** del 12 de Octubre de Madrid y especialmente a la que fue mi directora de TFM durante el Master **Covadonga Alonso**. Gracias a los dos pude iniciarme en la investigación y llegar a Bilbao con las ganas y la experiencia necesaria para empezar la tesis con buen pie.

1. Cic bioGUNE

1.1 AW Lab

Fui muy afortunado porque no conociendo a nadie en Bilbao, desde la primera semana se me abrieron las puerta a conocer gente maravillosa, y por supuesto al primer grupo que conocí fue al "Dream Team" de la neurociencia, el AW Lab. No tengo palabras para describir lo mucho que le debo a **Encarni Pérez**: Me llevaste a conocer Bilbao desde la primera semana, compartimos festivales y momentazos y siempre me has ayudado en el lab según surgían complicaciones. Muchísimas gracias Encarni, milaesker txalpedun. La crack de los WB, la que nunca descansa y siempre da el 100% dentro y fuera del lab, se echarán de menos los vermús, tus fiestecillas de terraceo y el echarte la bronca por conducir con el móvil **Marta Palomo** ☺, de todo corazón te deseo lo mejor en Viena. Poco después llegó mi archienemigo pero indudable compañero **Adrían Barreira** que siempre es capaz de sacarte unas risas y que complementa perfectamente mi carácter random e improvisado con su profesionalidad y organización. Muchísimas gracias por todos los momentos de "escenas de matrimonio" que hemos compartido juntos Mili.
En el gran 2019 se unió al grupo la Mundialista y "Robocop" **Laura Vila**, amante del amarillo y de que le cocinen, a la cual le debo 1001 croquetas por todos los ánimos y apoyo que me ha dado estos últimos años de tesis.
Finalmente completó este dream team la llegada temporal de **Rosa Angela**, talentosa luchadora italiana a la cual le deseo lo mejor en su PhD y el fichaje de **Leire Moreno**, con la que disfruté mucho trabajando codo con codo el poco tiempo que pudimos compartir en el lab. Eskerriak

asko por haberme ayudado con las Schwann cells y estar siempre ahí para darme consejillos para escribir la tesis.

1.2 Anguitos.

Tener un equipo tan bueno a mi lado ha sido una ventaja para hacer los largos experimentos algo más amenos, pero mucho mejor áun ha sido contar con la compañía en las poyatas del siguiente pasillo al loco grupo de los Anguitos (**Aize , Ana**, **Ainhoa**, **Ainitze , Diego**, **Estibaliz**, **Héctor**, **Ianire , Itzi , Julen Leti A**, **Leti S** y **Miguel**). El frikismo, ánimo y energía que desbordan ha sido siempre mejor que la cafeína y los gritos de "Anguitos paquete o Asgüitos paquete" conseguían quitarle seriedad a cualquier mal momento. Muchas gracias por haber estado siempre ahí apoyando los "Chandal days", los "Socialgunes", los "Hallowenes", las decoraciones de Navidad y llenar nuestro laboratorio de un aire algo más alegre. Gracias a la fofo reina **Ana y** su escudero **Carlos** por las quedadas frikis de cine y debates de Marvel o Start Wars. Un abrazo enorme a **H y Reina Madre** por siempre dar apoyo con sus expertos consejos para la escritura de la tesis, otro a **Estiti** por su ayuda y los viajecillos en coche a Deusto. Se nota el DNA vírico del madrileño **Diego Barriales** porque siempre hemos tenido la mejor química posible. Mazo gracias por ayudarme siempre en la organización de eventos birriles / bioguneros y por todos los consejos sobre como "montar" la tesis. Mando un agradecimiento especial al jefazo **Juan Anguita** porque en los días buenos transmite muy buen rollo y en los no tan buenos te recuerda que nunca hay que perder la profesionalidad.

1.3. AP Lab

Justo al final de la tesis he tenido el placer de poder compartir laboratorio con el grupo de **Asís Palazón**, al que agradezco enormemente haberme aceptado como parte de su equipo y haberme dado los medios y la oportunidad de seguir con mi Proyecto. Además esto me ha permitido conocer a otra fan de las plantitas y gominolas como es **So Young Lee**, al fichaje estrella de "La terreta" y los single-cells **Paloma**, al que "tiene su cajón como una despensa" **Asier Antoñana**, a "el chico que vive en el P2" **Borja**, al basketlover pero "solo ACB" **Ale**, a la que "manejaba un citómetro desde los 4 años" **Leire** y al resto del maravilloso equipo de AP Lab (**Ander de Blas**, **Ander**, **Ana**, **Laura Vila** otra vez y **Adrían Barreira** otra vez (te quejarás...)).

1.4 Otros Laboratorios

Durante estos 4 años también he tenido el placer de compartir tiempo con otros laboratorios del bioGUNE, especialmente con el laboratorio de Metabolómica. He pasado muchas horas de revelador con **Rubén**, **Marina** y **Naroa** y les agradezco la energía y alegría que me han transmitido cuando las bandas de los westerns no salían. Gracias **Robin** por todos los consejos sobre cómo manejar bien la tabla en Isla y "la Salvaje", espero que te vaya genial, "Samurai surfer".

Grazie Sara y Chiara por todos los grandes momentos que hemos compartido juntos: cenas, playeo y noches en el Stage. Hicisteis de 2018 un año "Erasmus no Erasmus" inmejorable. Ha sido un placer conoceros y compartir tantas historias, espero que os vaya genial lo que os quede por *"el Norte"* ☺

1.5 Animalario

Y hablando de pasar horas en salas cerradas y claustrofóbicas… Mi tesis ha sido más bien eso que hacía cuando no estaba en el Animalario. Han sido años ahí abajo y habría perdido la cabeza

si no fuera por el gran equipo que han montado. **Arantxa**, **Iker, Itzi** , **Nahia**, **Virginia** y muchísimas gracias por ayudarme a ser algo más ordenado con los animales y haberme echado broncas necesarias cuando no mandaba los servicios. Gracias también por haber hecho más amenas las horas en el zulo y estar siempre para echar una mano.

1.6 Comité de Empresa y Comisión de igualdad.

Como no podía ser de otra forma y no contento con únicamente dedicarme a la tesis, también tuve el placer de formar parte del Comité de Empresa junto con **Cora, Ana Aransay, Encarni, Itziar M, Itziar F , Vidal, Inma y Onintza** así como de la Comisión de Igualdad (**Arkaitz, Mada, Itziar F, Adriana y Bea**). Muchas gracias a todxs por haberme permitido formar parte de estos grupos para mejorar la situación laboral de todxs en el bioGUNE y haber tenido tanta paciencia conmigo en las reuniones. Conseguimos dar pequeños pasos para mejorar la situación en el bioGUNE y estoy seguro de que seguiréis luchando para seguir avanzando en ello en los próximos años.

2. UPV /EHU y Achucarro

En la tesis hay de todo, pero lo que también ha tenido esta han sido viajes en coche a la UPV. Prácticamente casi el único uso que le he dado a ese cacharro rojo que dejaba siempre tirado en el parking del bioGUNE ¿Y para qué? Para aprender de electro microscopía de la mano de **Svein** y colaborar con **Laura, Carlos e Izaskun**. Os mando un saludo enorme a los cuatro y muchos ánimos para acabar la tesis a **Irene** por estar ahí siempre debatiendo sobre los episodios del Conquis. Le agradezco también a **Amanda Sierra** el haberme dado buenos consejos e ideas durante estos años sobre como desarrollar el proyecto que ha sido esta tesis.

3. Deusto Team

Durante estos 4 años en Bilbao he conocido a muchísima gente que me ha alegrado los días en estos tiempos tan complicados y que ha hecho de la tesis un periodo un poquito menos estresante. En primer lugar quiero agradecerles al **Deusto Team** por haber sido siempre una fuente de planazos, debates, risas y buenos momentos. *Grazie Mille* **Alice** por corregirme cuando me equivoco, haberme ayudado a ser mejor persona y haber estado siempre a mi lado estos cuatro años, contigo empezó todo ;). El dúo de Otero siempre me ha acompañado en los veves y en las canchas, *eskerrik* **Mikel y Miguel** por todos los buenos momentos y liadas que hemos compartido desde que llegasteis. Habéis conseguido que me haya sentido como en casa en Bilbao y que me haya hecho fan de levantar hierros en el "Templo"
Eskerrik (porque sé que está muy bien dicho) a **Leire** por todas las tardes de juegos y por la muy agradecida sinceridad que te caracteriza, espero que encuentres un buen curro que te guste en la privada y que luego nos coloques por enchufe a todos ahí XD.

Y si hubo *dúo de Deusto* también hubo *dúo de Indautxu* (**Jana y Laura**). Gràcies por siempre intentar (por beneficio propio también) hacer quedadas por vuestro barrio y poder ir a por mi glorioso milhojas de idiazábal. Gracias otra vez por transmitir un rollo tan positivo en el grupo y por siempre haberme apoyado en los malos momentos.

Un abrazo enorme a los dos desaparecidos que no estaban casi nunca pero que de vez en cuando se apuntaban y se agradecía mucho, ya fuera por los debates interesantes (**Orhi**) o por los consejos de Burpees y memes (**Unai**).

David, Maider, María llegaron más tarde pero han sido muy buenxs fichajes para el grupo, me habría gustado compartir más momentos con el príncipe de Santand-Air y sus compis pero bueno… al menos nos llevamos un "buen recuerdo inmunológico" del Alta fit…
Tarde también se fundó el Veggie Team (**Sara** y **Richi**) que tantas alegrías culinarias y de entretenimiento me han dado siempre. Muchas gracias por tantas partidas inolvidables y tantos "Ni guás". Mucho ánimo con los agradecidos vecinos que con tan buenos ojos ven tu sesiones de batería **Richi**.

Y en último lugar quiero agradecer a la Germana que se nos fue hace tiempo de Deusto pero ni Alice ni yo la olvidaremos nunca, *viele danke* **Maxi** por todos los buenos momentos que compartimos compartiendo música juntos, tanto en el salón como en el BBK.

4. Bilbao.

Viele Danke Philipp y Giacomo por las grandes noches de bailoteo que me disteis con o sin Agua de Valencia de por medio y por haber inventado el concepto de "Día Tranki" que podía significar acabar un día *random* a las 5 de la mañana en el Mystik.

En parte fue muy fácil adaptarme a mi nueva vida en Bilbao cuando llegué por el gran trabajo que realizaban **Lucia**, **Miguel**, **Iliaria** y **Valentin** organizando planes, cenas y fiestas ya fuera por casco viejo o en el propio Guggenheim. ¡Gracias a todos!

Gracias **Inma y Alfredo** por haberme enseñado tanto sobre la situación Italiana, haber planificado cafés científicos y debates así como haber sido un ejemplo en la lucha social.

En último lugar me gustaría agradecer a **Rober** haber estado siempre IN para todos los planes los primeros años y haberme transmitido tan buen rollo. Espero que te vaya genial con la escritura.

5. Madrid

Yo siempre he solido presentarme como alguien raro pero sobretodo, de todos lados. En mi vida he podido visitar y vivir en diferentes ciudades y pueblos, pero sin duda una ciudad que guardaré siempre con un cariño especial es Madrid. Nací allí pero fue llegar al mundo y ya me llevaron a vivir a mi amada "Terreta". Sin embargo, pude volver a Capital City dos años al acabar la carrera y allí no solo disfruté como loco de concierto en concierto, sino que conocí a gente de la que nunca querré separarme.

En el master tuve una suerte increíble de hacer migas desde el principio con **Irene T**, **Lucía** y **Arantxa** para después incluir en el equipo a la **Lider Castro** (Victoria) y **Diego Afro**. Hubo noches increíbles, buenos momentos, festivales e incluso maratones de cine inolvidables. Gracias a todos por haber hecho de apenas 2 años en Madrid una experiencia tan genial. *Never forget the Space Monkeys' nights*.

El último que llegó a mi corazón en ese tiempo fue **Juan Diego Riveros Zalamea**. Como me suele caracterizar, establezco vínculos con personas increíbles justo cuando les queda poco tiempo a mi lado. En este caso afortunadamente seguimos manteniendo el contacto y finalmente saltó el charco volando de Bogotá a Bilbao para hacer la tesis aquí. Pudimos así retomar una amistad increíble que espero que ni 6000km puedan romper. Hermano, espero que acabes la tesis genial porque mereces eso y **TODO**.

5.1 Hospital 12 de Octubre

Madrid no solo fue jolgorio y estudiar, también pude iniciarme en la investigación en el 12 de Octubre, donde pude reencontrarme con **Irene T** y quejarme una y mil veces de que no funcionaban las maxis y las PCRs. Has pasado mil y un apuros pero te levantas cada día y das siempre lo mejor. TXAPELDUN con 9 mayúsculas. Por allí también estaban **Marcos**, al que le deseo mucha felicidad en su nueva etapa en el hospi y con su nueva familia; **Octavio**, **Alhena**, **Miguel** y resto del equipazo con los que pude disfrutar de la capital en todo su esplendor y las 1001 noches de mi amado Space Monkeys...
Del 12 de Octubre también me llevé lecciones incalculables. **Alma** y **Joanna** me enseñaron muchísimo no solo sobre como ser un mejor investigador, sino también como ser mejor persona, y desde entonces esa crack Polaca ha sido siempre mi modelo a seguir profesionalmente cuando pienso en que tipo de investigador me gustaría ser.

5.2 INIA

Antes del bioGUNE vino el 12 de Octubre y antes del hospital vino el INIA. Ahí tuve mucha suerte de que **Covadonga Alonso** me diera la oportunidad de hacer las practicas del Máster en su labo y que pudiera conocer a **Inma**, **Lucía** y **Miguel** pasando largas horas purificando virus de peste porcina y anotando las frases célebres que iban surgiendo en el cuaderno. Fue donde empezó todo y gracias a ellos fue de la mejor manera posible.

6. Valencia

6.1 Universidad de Valencia

Y de la capital pasamos a Valencia, "la Terreta" donde empecé mis pasos en la ciencia. La carrera fue larga e intensa pero la verdad es que desde el principio tuve la suerte de tener varios profesorxs que me marcaron mucho y gracias a los cuales llegué a la conclusión de que mi futuro era iniciarme en la investigación y hacer el doctorado. Aprendí mucho de **Paco Pérez** (Pacops), **Juli Peretó** (al que también agradezco la organización e invitación a su congreso de biología molecular) y de **Isabel Fariñas**, la cual transmitía un amor por la ciencia en sus clases que te embriagaba e inspiraba.

Eso es lo que me llevo de las clases en sí en Bioquímica, pero lo mejor de la carrera obviamente fue coincidir con gente tan friki como yo que también amaban la bioquímica, Marvel y muchas más movidas. El grupo de **los Cipotes** se formó durante segundo curso y pese a las mil distancias y charcos que nos han separado, hemos seguido manteniendo la llama de los comentarios con segundas y los "yayihostels" varios. **Toni**, gracias por servirme de fuente de inspiración demostrando que con trabajo duro y dedicación se puede no solo brillar en el campo o en las aulas, sino donde quieras y en todo lo que te propongas. Os deseo lo mejor a ti y a **Brock** (y al trasto de Bubu) en Barna. **Camila**, han sido muchos años sin poder más que compartir whatsapps y skypes con mi camarada vegetariana pero siempre que vuelves nos alegras la vida aunque sea por un par de horas. **Álvaro**, espero que puedas vivir muy bien ya como doctor con Isis y que la bendición del dios emperador te lleve lejos. **Ainara**, compañera de neuroscience, espero que después de la currada que te has pegado de confocal puedas tener una etapa post doctoral más relajada, porque te la has ganado de sobra.
Sonia, han sido años complicados, ha habido muchos reveses pero has demostrado que eres una guerrera y que puedes contra todo. Me alegro de que le hayas dado la vuelta a la tortilla y

solo deseo que dure mucho tiempo y puedas ser lo más feliz posible. Cuenta conmigo siempre que haya un maratón LoR o Star Wars .
Saiz. No tengo palabras para agradecerte todo el apoyo que siempre me has dado durante tanto tiempo. Solo puedo decir que espero que allá donde te lleve tu camino sepas que siempre tendrás a los cipotes de tu lado y todas las playlist que hagan falta para cada momento.

El *burjapiso*… que buenos recuerdos. Ese equipo infalible de **Samuel, Rubén y Carlos** que fue evolucionando con el tiempo. Se os ha echado mucho de menos desde entonces y os deseo lo mejor en esta etapa post doctoral (predoctoral para Carlos). Nunca se olvidarán las partidas de Mario Kart terribles ni los partidazos de padel en la Uni.

6.2 Universidad de la Vida

Y como no, también tengo que agradecerle el haber podido llegar aquí a "**La droga**", sin ella no habría nunca llegado tan lejos y su apoyo constante y punch que da poder verles y compartir ratos con ellxs no tiene precio. No me creo la suerte de haber coincidido con vosotros y haber mantenido esta amistad tantos años. Sois totalmente "*Mel de romer*".
"La droga" (**Fabra**, **Valero**, **Sergio**, **Inma**, **Débora, Ignacio**, **Faerna**, **Marieta, Vicent**, **Andrea**, **Maria**, **Josele**, **Jose**, **Meritxell** y **Claudia**).

7. Alicante

Vicky, me alegro muchísimo de que pudiésemos reencontrarnos hace 11 años y recordaré siempre con mucho cariño todas las veces que hemos podido vernos pese a los caminos tan diferentes que hemos seguido. A ver si conseguimos seguir en contacto ya que tu amistad es de esas que nunca nunca querría perder.

Muchas gracias al equipo de Chumbawamba (**Rubén**, **Adán**, **Josema** y **Vero**) por todos los "Octoberfest" patrocinados por el Corte Inglés de los que disfrutamos antes de que me hiciera vegetariano XD.
Javi, BRO, espero que os vaya genial a Judit y a ti en vuestra nueva etapa y nunca olvidéis que TAKEDWN siempre tendrá a Take-Taketo en su ala izquierda para cuando le necesite.

8. Familia

En estos agradecimientos guardo un abrazo especial para aquellas personas que me marcaron tanto de pequeño, amigos de mis padres como **Mazón**, **Claudia**, **Ted** , **Maite** y **Arturo** que siempre guardaré en mi corazón. Especialmente a **Claudia**, que me enseñó a amar el piano y que me demostró que con esfuerzo y perseverancia llegan los reconocimientos al trabajo duro. Gracias por esa lección y tus preciosas canciones, profe.

Y si he llegado hasta aquí es porque el apoyo familiar que he tenido siempre ha sido el mejor, les doy mil gracias a mis primos y tíos por siempre haberme dado su energía, comprensión y cariño cuando he podido estar con ellos. Mi hermana **Alba** siempre ha sido un ejemplo de trabajo duro y perseverancia para mí y la quiero lo que no está escrito.
Mis padres han sido mi referente en la vida y si he llegado tan lejos es porque me han estado apoyando siempre, me han permitido descubrir sitios increíbles y siempre se han preocupado por instruir mi mente. Si soy científico es porque ellos sembraron la semilla de la curiosidad en mi mente y siempre la han alimentado con libros y más libros. Mila esker Ama eta Aita, esta tesis os la dedico a vosotros.

In this acknowledgement section I can't leave out the person who has helped me to find happiness during these complicated years. **Helen Springer** is one of the best people I know in the world and I can´t find the words to write about how much I love her and how happy I am about sharing my life with her. Thanks Hon for being always there when I need a little bit of your positivity.

Y en último lugar quiero dejar a las dos personas que más han influenciado mi carrera, uno bien desde el principio y el otro en ese momento clave (bachillerato) donde casi todxs (o la mayoría) tomamos la dura decisión que marca (no siempre pero casi) nuestro futuro académico y profesional. Mi profesor de Biología en el Bachillerato **Tono Berti** me impactó como pocas cosas en la vida, porque me supo transmitir como pocas personas la pasión por la ciencia, por descubrir, ser crítico e investigar allá donde hay incógnitas e incertidumbre. Sus clases fueron una fuente de inspiración y gracias a ellas tuve claro que mi futuro sería la Bioquímica.
En último lugar quiero dar las gracias a mi abuelo **Manuel Caro**. No pudo ver como llegaba aquí, ni pudo verme acabar la carrera ni Máster, pero si le debo a alguien que siga ilusionándome con cada pequeña nueva cosa que aprendo de la vida y de la ciencia, es a él. "Tendrás un microscopio antes que un telescopio" me decía… y no se equivocó…

"El mayor espectáculo del mundo es la vida" Manuel Caro.